Title
The role of myotubularin in cellular morphogenesis

Author
Juan, Joseph

Publication Date
2009

Peer reviewed|Thesis/dissertation

UNIVERSITY OF CALIFORNIA, SAN DIEGO

The Role of *Myotubularin* in Cellular Morphogenesis

A thesis submitted in partial satisfaction of the

requirements for the degree Master of Science

in

Biology

by

Joseph Juan

Committee in charge:

Professor Amy Kiger, Chair
Professor Ethan Bier
Professor Richard Firtel

2009

The Thesis of Joseph Juan is approved, and it is acceptable in quality and form for publication on microfilm and electronically:

_____

_____

_____
Chair

University of California, San Diego

2009

TABLE OF CONTENTS

LIST OF FIGURES AND TABLES

LIST OF FIGURES

LIST OF TABLES

ACKNOWLEDGEMENTS

I thank Amy Kiger for her guidance, insight, and support and for allowing me to participate in this project as a member of her lab; Inés Ribeiro, Michaella Velichkova, Pavan Kadandale, and Steve Jean for their assistance, training, and advice; and Kiger lab for aiding in the progress of my work and for the enjoyable experience this entire time. I also thank my family, friends, and colleagues for their encouragement throughout this entire process and their continued support.

ABSTRACT OF THE THESIS

The Role of *Myotubularin* in Cellular Morphogenesis

by

Joseph Juan

Master of Science in Biology

University of California, San Diego, 2009

Professor Amy Kiger, Chair

Cellular morphogenesis is an important process crucial for the proper function of nearly all cells. Cell shape change is a dynamic and highly regulated process and requires the strict spatial control of numerous cellular processes including cytoskeletal remodeling and membrane trafficking. Phosphoinositide phosphates (PIPs) provide one means of spatiotemporally regulating specific cell morphogenesis-related processes through their recruitment of specific PIP-binding effector proteins. One PIP regulator, *myotubularin* [a predicted PI(3)P and PI(3,5)P_2 phosphatase] was identified as a gene essential for the ecdysone

hormone-induced cellular elongation of Kc cells. To gain a better understanding of the *in vivo* mechanisms through which *mtm*-dependent phosphoinositide regulation provides the spatial information necessary for the proper execution of morphogenetic programs, the role of *mtm* in the morphogenesis of the *Drosophila* blood cells (hemocytes) was investigated. In this report, I verify previous *in vitro* studies in our lab implicating *mtm* in protrusion formation and proper endolysosomal membrane homeostasis, *in vivo*. Using *Drosophila* hemocytes, I also examine the relationship between *mtm*-dependent processes to cellular morphogenesis.

Our work points toward a model in which *mtm*, through the strict spatiotemporal regulation of class II PI 3-kinase (*Pi3K68D*)-synthesized PI(3)P pools, regulates the recruitment and activity of specific PIP binding effector proteins such as *Spir* to then mediate specific cellular events such as cytoskeletal remodeling and endolysosomal membrane trafficking to control cellular morphogenesis. This study therefore provides greater insight into the mechanisms through which phosphoinositides regulate and integrate multiple cellular processes to mediate changes in cell shape.

INTRODUCTION

The function of almost all cells is intertwined with their ability to attain and modify specific morphologies. This essential ability to undergo cellular morphogenesis is a complex event involving the regulated integration of membrane remodeling, protein trafficking, and cytoskeletal rearrangements. Therefore, whether it be the extension of a neuron to a distant synapse, the migration of a macrophage to a site of infection, or the formation of an elongated muscle fiber, the ability of a cell to integrate multiple cellular processes to modify its shape lies at the core of each cell's specialized functions. To better understand cellular morphogenesis, a screen was conducted to identify genes required for an induced cell shape change in *Drosophila* Kc cells. A complete block in the formation of protrusions following RNAi depletion identified a gene essential for the cellular morphogenesis of Kc cells, *myotubularin* (*mtm*).

Mutations in specific members of the myotubularin (MTM) family of lipid phosphatases have been linked to two distinct human diseases: Charcot-Marie-Tooth disease type 4B (CMT4B) and X-linked myotubular myopathy (XLMTM). CMT4B is a disease affecting Schwann cells which leads to a peripheral neuropathy marked by demyelination of the neurons, myelin outfoldings, and slowed nerve conduction velocity. These defects in Schwann cells then result in weakness and atrophy of peripheral muscles (Bolino et al., 2004; Tanaka and Hirokawa, 2002). The two types of CMT4B (CMT4B1 and CMT4B2) are caused by mutations in myotubularin-related protein 2 (MTMR2) and MTMR13,

respectively. XLMTM is a centronuclear myopathy characterized by low muscle tone and centrally localized nuclei in muscles. Mutations in the *MTM1* gene have been implicated in causing XLMTM (Bolino et al., 2000; Buj-Bello et al., 2002; Laporte et al., 1996; Robinson et al., 2008). It is thought that CMT4B and XLMTM are diseases which arise in Schwann cells and muscle fibers due to the unique and complicated structures of these tissues and the enormous reliance of these tissues' functions on their specific cell shape and morphogenesis (Suter, 2007). Schwann cells must undergo cell shape changes to produce elaborate protrusions called myelin sheaths which insulate neurons to maintain normal nerve conduction velocity (Tanaka and Hirokawa, 2002). Likewise, normal muscle function is highly dependent on the maintenance of its morphology and internal myofibril architecture (Buj-Bello et al., 2002). The elaborate structure of the Schwann cells and muscle fibers along with the requirement for *mtm* in the creation of Kc cell protrusions makes it plausible that the human diseases CMT4B and XLMTM are the product of dysfunctional cellular morphogenesis. By understanding the role of *mtm* in cellular morphogenesis we may gain insight into the exact cellular and molecular bases for these two human diseases.

Myotubularin has been implicated in phosphoinositidylinositol phosphtate (PIP) metabolism and regulation. It is believed that the contributions of *mtm* to the execution and regulation of multiple cellular processes leading to cellular morphogenesis occurs through *mtm*'s spatiotemporal regulation of specific phosphoinositide pools. Phosphatidylinositol (PtdIns) constitutes only about 15%

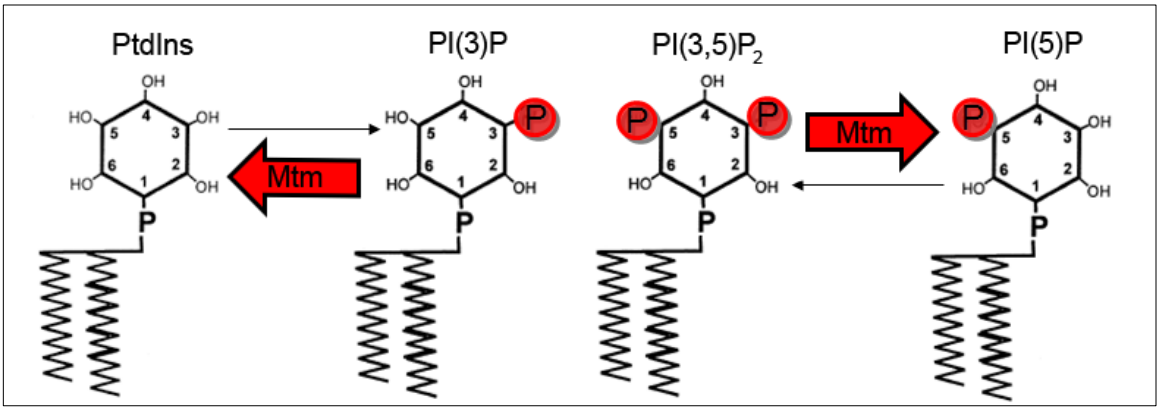

Figure 1: Regulation of phosphatidylinositol phosphates by *mtm*

Phosphatidyinositols (PtdIns) can be phosphorylated at the D3, D4, or D5 positions (left) to produce seven different phosphoinositide species. *In vitro*, *mtm* has been demonstrated to dephosphorylate PI(3)P and PI(3,5)P_2 at the D3 position to produce PtdIns and PI(5)P, respectively.

of the total phospholipids within a eukaryotic cell while its phosphorylated forms, the PIPs, are ten times less abundant. Yet the PIPs are indispensable for their many cellular roles (Di Paolo and De Camilli, 2006). Phosphorylation of the inositol ring of phosphatidylinositol (PtdIns) at the D3, D4, or D5 positions either alone or in combination produce seven different inositol phospholipids which then recruit specific interactors containing phosphoinositide binding domains (Lemmon, 2003) (Fig. 1). Specific processes are executed upon the recruitment of specific proteins to defined cellular membranes. Through the recruitment of various effector proteins to sites of PIP accumulation, PIPs influence a diverse set of functions including membrane trafficking, cytoskeletal remodeling, and organelle identity (Behnia and Munro, 2005; Nicot and Laporte, 2008; Oikawa et al., 2004). Interconversions between phosphoinositide species can occur very quickly via phosphorylation or dephosphorylation and this process is highly

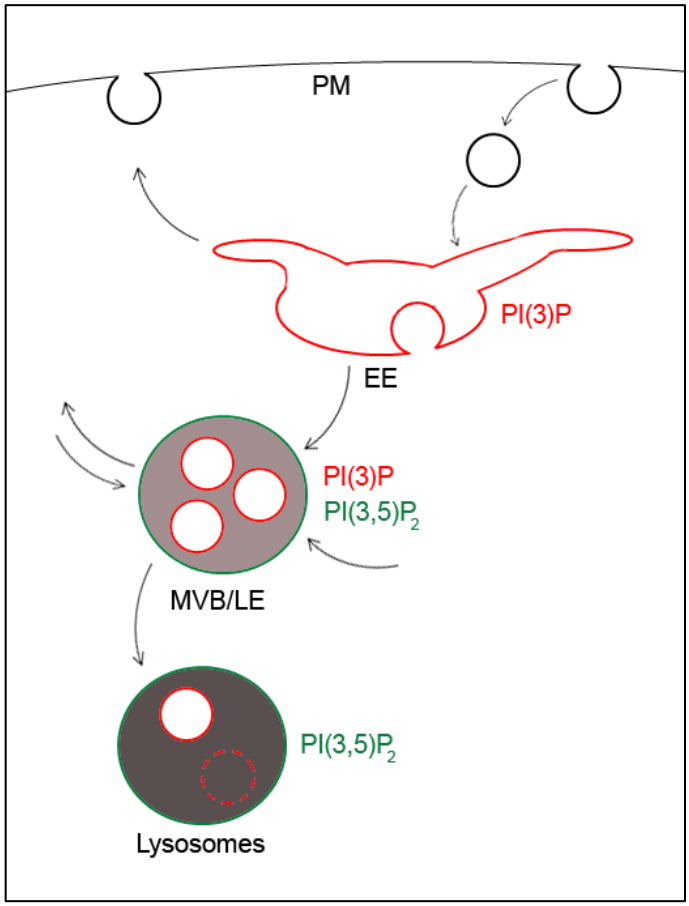

Figure 2: Phosphoinositides in the endolysosomal pathway

PI(3)P is localized to the early endosomes (EE) as well as the intralumenal vesicles of multivesicular bodies (MVB), while $PI(3,5)P_2$ localizes to the late endosomes and lysosomes.

regulated by PIP kinases and phosphatases. This ability to quickly phosphorylate or dephosphorylate the PIPs to up or downregulate specific PIP species make these lipid second messengers ideal regulators of various cellular processes requiring strict spatiotemporal control. The importance of phosphoinositides for proper cellular function is emphasized by the fact that mutations in many PIP regulators (including the *myotubularin* family of lipid phosphatases) lead to a number of human diseases (Bolino et al., 2000; Laporte et al., 1996).

While the *in vitro* substrates of the MTM proteins have been clearly identified, their *in vivo* cellular functions, their regulation, and how *mtm* loss-of-function lead to CMT4B and XLMTM remain largely unresolved (Cao et al., 2008). Initially identified as a protein tyrosine phosphatases (PTP), myotubularin and its related proteins were later shown to preferentially bind and dephosphorylate the phosphoinositides phosphatidylinositol 3-phosphate (PI(3)P) and phosphatidylinositol 3,5-bisphosphate ($PI(3,5)P_2$) at the D3 position (Laporte et al., 1996; Taylor et al., 2000; Walker et al., 2001) (Fig. 1). These PIPs play critical roles in endolysosomal trafficking and therefore one possibility regarding *mtm*'s regulation of cellular morphogenesis is that cell shape change is a secondary consequence of *mtm*'s primary regulation of membrane trafficking and remodeling through the endolysosomal pathway (Fig. 2). Endosomes are highly dynamic organelles that sit at the crossroads of many membrane and protein trafficking events. A multitude of cellular processes could therefore be regulated through the regulation of endosome dynamics. PI(3)P, a substrate for MTM proteins, localizes to the early endosomes and the intralumenal vesicles of multivesicular late endosomes and is responsible for recruiting specific FYVE-(for conserved in Fab1, YGLO23, Vps27, and EEA1; a PI(3)P zinc finger binding domain) containing effector proteins to these compartments (Gaullier et al., 1998). Upon recruitment, these PI(3)P binding proteins mediate early endosome functions including endosome fusion and membrane invagination. PI(3)P production on the early endosomes is mediated by the type III PI 3-kinase

complex hVps34/hVps15 which phosphorylates PI into PI(3)P (Gillooly et al., 2000). PI(3,5)P_2 localizes to the multivesicular late endosomes and is produced by the phosphorylation of PI(3)P at the D5 position by the PI(3)P 5-kinase Fab1/PIKfyve (Gary et al., 1998). PI(3,5)P_2 is necessary for protein sorting into intralumenal vesicles, retrograde trafficking from the endolysosomal pathway, and control of lysosomal size and acidification (Odorizzi et al., 1998; Rutherford et al., 2006; Yamamoto et al., 1995). Because the identities and properties of organelles are defined by the presence of specific phosphoinositides in conjunction with resident proteins, it is proposed that specific MTM proteins regulate the function of endocytic compartments by controlling the presence and localized levels of PI(3)P and PI(3,5)P_2 (Behnia and Munro, 2005). Through this regulation of endocytic trafficking and dynamics, MTM proteins are therefore poised to regulate and integrate a number of cellular processes involved in cellular morphogenesis. In support of the role for MTM in endocytic trafficking, studies demonstrated that myotubularin overexpression (resulting in PI(3)P depletion) produced an accumulation of enlarged vesicles, defective invagination into multivesicular bodies, and impaired late endosome-to-lysosome trafficking (Tsujita et al., 2004). Depletion of MTM1 in mammalian cells (resulting in an increase in PI(3)P levels) and depletion of MTMR2 (resulting in an increase in PI(3,5)P_2 levels) also resulted in defects at different phases of the endolysosomal trafficking pathway. Loss of MTM1 led to early endosome-to-late endosome trafficking defects, while loss of MTMR2 led to defects in late-endosome-to-

lysosome trafficking. These results suggested that the different MTM family members not only target different PIP subpools, but also potentially play non-overlappping roles in the cell (Cao et al., 2008). The differences between MTM1 and MTMR2 in regards to the regulation of the endolysosomal membrane trafficking pathway may also explain the distinct pathologies caused by mutations in each MTM family member. Given the central role for PI(3)P and PI(3,5)P_2 in the endolysosomal pathway, mutations in the MTMs may lead to their associated neuropathies and centronuclear myopathies via the misregulation of distinct membrane trafficking and remodeling events in Schwann cells and muscles (Nicot and Laporte, 2008).

While the role of the MTM proteins is to turnover specific pools of PI(3)P and PI(3,5)P_2, the PI 3-kinases (PI3Ks) serve to produce pools of PI(3)P and therefore act as antagonists to MTM activity. By understanding the cellular roles of the PI3Ks, we may be able to identify and better understand the cellular roles for *mtm* function. There are three classes of PI 3-kinases and each produce a distinct PIP subpool. Class I PI 3-kinases mainly use PI(4,5)P_2 to produce PI(3,4,5)P_3, while class II and class III PI 3-kinases phosphorylate the D3 position of PI to synthesize PI(3)P (Lindmo and Stenmark, 2006; Stewart et al., 2003). The PI3Ks are thought to regulate cellular processes through the localized production of these specific PIP subpools which then recruit FYVE and Phox-homology domain-containing proteins to specific subcellular sites. Along with the requirement for PI 3-kinase-dependent PI(3)P production in membrane

trafficking, autophagy, and the endolysosomal pathway, PI 3-kinase activity also controls numerous other processes relying primarily on cytoskeletal remodeling (including macropinocytosis and regulated exocytosis) (Blommaart et al., 1997; Clague et al., 1995; Ito et al., 2002; Stephens et al., 2002). As antagonists of PI 3-kinase activity, the Mtm proteins could potentially play crucial roles in cytoskeletal reorganization by directly opposing PI3K activity and abolishing the potential binding targets for various PI(3)P binding proteins. Earlier studies reaffirm this notion that cytoskeletal remodeling (along with various other cellular processes) requires the functional and finely balanced interactions between the MTMs and PI3Ks. As mentioned earlier, in *Drosophila melanogaster*, RNAi-mediated knockdown of *mtm* in Kc cells disrupted their ability to undergo ecdysone induced elongation, a process highly dependent on the remodeling of the cytoskeletal architecture. Subsequently, when the class II PI 3-kinase *Pi3K68D* was also knocked down in these *mtm* deficient cells their ability to elongate was restored (Kiger, unpublished data). Previous work suggests that along with their antagonistic effects on one another, the myotubularins and PI 3-kinases also directly regulate one another's activities. In mammals, the myotubularins MTM1 and MTMR2 directly bind the class III PI 3-kinase complex hVPS15/hVPS34 via hVPS15 (Cao et al., 2008). Because myotubularin binding of the hVPS15/hVPS34 complex inhibited both MTMR2 phosphatase activity as well as hVPS15/hVPS34 binding to the activating Rab GTPases, it is believed that such interactions cause a mutual inactivation of both MTM1 and hVPS34 to

provide strict spatiotemporal control of PI(3)P levels (Cao et al., 2008). It is therefore apparent that the mechanisms through which MTM-PI3K interactions contribute to the strict spatiotemporal regulation of PI(3)P, and how this ultimately controls cell morphogenesis, warrant further study.

Along with the regulatory interactions between MTM and the PI 3-kinases, other means of MTM regulation are also possible. For example, the catalytically active members of the myotubularin family have been shown to interact with the catalytically inactive members. As a member of the protein tyrosine phosphatase (PTP) superfamily, the myotubularin family of lipid 3-phosphatases is unique in that six out of its 14 members contain amino acid substitutions which render them catalytically inactive pseudophosphatases (Clague and Lorenzo, 2005). Though unable to directly dephosphorylate PI(3)P or PI(3,5)P_2, the binding of these inactive proteins to the active myotubularins still mediate essential functions within the cell. For example, through the measurement of the turnover of their respective substrates, the active phosphatases MTMR7 and MTMR2 were shown to be stimulated by their interactions with the catalytically inactive myotubularins MTMR9 and MTMR5/MTMR13, respectively (Berger et al., 2006; Kim et al., 2003; Lorenzo et al., 2006). Mutations in the inactive protein MTMR13 lead to a similar disease as that caused by mutations in the active MTMR2 protein (CMT4B2 and CMT4B1 respectively), further suggesting the importance of the pseudophosphatases in regulating the active myotubularins (Robinson et al., 2008). Discovering the spatiotemporal details of active phosphatase regulation by

the inactive myotubularins will therefore be important in determining how the myotubularins influence cell shape via membrane and cytoskeletal remodeling.

While many studies examining the cellular roles of the myotubularin proteins have been performed in yeast and mice, *Drosophila melanogaster* provides yet another powerful and relevant model organism in elucidating the functions of myotubularin and its related proteins. The *Drosophila* system provides a variety of advantages to studying *mtm* function, including its use as a powerful genetic tool, the reduced complexity of its myotubularin family of proteins in comparison to vertebrate systems, and the ability to look at the contributions of *mtm*-regulated cellular morphogenesis to tissue function. A number of cell lines and in vivo tissues (including muscles, neurons, and blood cells) of *Drosophila* rely heavily on cytoskeletal, membrane, and protein trafficking and remodeling for their function and therefore provide potentially useful systems for studying the contributions of *Mtm* to cellular morphogenesis**.** In particular, *Drosophila* blood cells, otherwise known as hemocytes, are a useful cell type to utilize when investigating the contributions of *mtm* function to cellular morphogenesis. Hemocytes are composed of three functionally distinct cell lineages. The largest blood cell population, comprising of 95% of the circulating hemocytes, are the plasmatocytes. The remaining 5% of the circulating blood cells are composed of the crystal cells. The third cell lineage, the lamellocytes, differentiates from the same progenitor cells but appear only during metamorphosis and in response to specific immune challenges (Crozatier et al.,

2004; Lanot et al., 2001). Plasmatocytes most closely resemble the monocyte/granulocyte lineage in vertebrates and act as dedicated phagocytes of the innate immune system (Hartenstein, 2006; Meister and Lagueux, 2003). To perform its duties, this cell lineage relies heavily on cell morphogenesis and proper endolysosomal trafficking. Along with the need to migrate to sites of infection and wounding, these cells must also dispose of microorganisms and apoptotic cells via a process of attachment, engulfment, and subsequent lysosomal degradation (Aderem and Underhill, 1999; Meister and Lagueux, 2003; Ramet et al., 2002). These cells also play a role in tissue remodeling during pupation, as the hemocytes differentiate into pupal macrophages upon ecdysone stimulation and are then responsible for the histolysis and phagocytosis of larval tissues (Lanot et al., 2001). When the plasmatocytes meet an invader it cannot engulf, it sends signals to the prohemocytes in the lymph glands which then differentiate into the lamellocytes. Like the plasmatocytes, the roles of the lamellocytes cells also depend significantly on their ability to undergo changes in cell shape as they must migrate to parasitization sites and encapsulate large size invaders (Schulz et al., 2004). Therefore, the different hemocyte lineages can serve as important models for studying the contributions of MTM to various cellular activities.

Cell morphology and morphogenesis are crucial to the proper function of nearly all cells. The contributions of phosphoinositides and its regulators (and in particular, the contributions of the myotubularin family of lipid phosphatases) to

cellular processes involved in cellular morphogenesis are therefore of great importance in deciphering not only the mechanism behind such events but also in understanding how defects in PIP regulation lead to various diseases. Through our work in *Drosophila*, our results suggest that through the regulation of specific PI(3)P pools (produced by the class II PI 3-kinase, *Pi3K68D*), *mtm* plays a critical role in regulating cellular morphogenesis, and in particular, the ability of a cell to make a protrusion. Our data suggests that membrane homeostasis and cytoskeletal remodeling are two important factors affected by Mtm activity during the formation of cell protrusions. The regulation of PI(3)P pools by *mtm* is believed to spatiotemporally regulate the recruitment of specific effector proteins (such as the actin nucleator *Spir*) which then serve to not only carry out membrane trafficking and cytoskeletal remodeling, but also integrate these processes to mediate and maintain changes in cell shape. Our work also sheds light on how *mtm* activity may be regulated. The catalytically inactive myotubularin related protein, *Sbf*, seems to positively regulate *mtm* functions important for cellular remodeling. These results therefore shed light onto the networks regulated by *mtm* to mediate cellular morphogenesis.

MATERIALS AND METHODS

Vector construction

mtm cDNA was amplified by PCR (sense primer: 5'-CAC CAT GGA TCC CTC CGC G-3', antisense primer: 5'-GTG CAT AGG CGA GGC CAG A-3') from the *UAS-mtm:GFP* construct and cloned into the pENTR/D-TOPO entry vector (Invitrogen), and subcloned by an LR recombination reaction into Gateway destination vectors pTGW-1075 (for creation of the UAS-GFP:Mtm construct), pTW1129-mCherry (*UAS-mCherry:mtm* construct), pTWM-1108 (*UAS-mtm:6xmyc*), and pTFW-1115 (*UAS-3xFLAG:mtm*). After the LR reaction, the plasmids were transformed into TOP10 competent cells via the heat shock method. Transgenic cells were screened on LB agar plates containing 50 µg/µl ampicillin. After overnight incubation at 37°C, single colonies were picked from their respective plates and expanded in LB broth (Miller's) containing 50 µg/µl ampicillin placed on a shaker overnight at 37°C. Plasmid DNA was then purified using the QIAGEN Plasmid Maxi Kit and stored at -20°C.

Cell lysis for protein sample preparation/Western Blot

Cells were pelleted via centrifugation and resuspended in RIPA lysis buffer containing a 1:100 dilution of a protease inhibitor cocktail (Sigma). Crude cell extracts were run through NuPage 4-12% Bis-Tris-Gel (Invitrogen) per manufacturer's instructions. The gels were transferred to PVDF membrane

(Invitrogen) using a Trans-Blot SD semi-dry transfer cell (BioRad). The Western blots were blocked with 1XPBS containing 5% milk and 0.1% Tween-20 for 1 hour at room temperature with shaking. The membranes were washed free of milk with 0.1% Tween-20-PBS for 6 minutes with buffer changes every 2 minutes. Each antibody solution was individually diluted, rabbit anti-GFP polyclonal (eBioscience) 1:4000; mouse anti-FLAG monoclonal (Sigma) 1:600; or mouse anti-Myc (Sigma) 1:10,000 into 0.1% Tween-20-PBS, added to the appropriate membranes, and incubated for 3 hours at room temperature with shaking. Membranes were washed with 0.1% Tween-20-PBS for 30 minutes with buffer changes every 5 minutes. Secondary antibodies, anti-rabbit HRP (Invitrogen) and anti-mouse HRP (Invitrogen), were then individually diluted 1:10,000 into 0.1% Tween-20-PBS. Diluted secondary antibodies were then added to the appropriate membranes and incubated for 1 hour at room temperature with shaking. Membranes were washed again for 30 minutes with 0.1% Tween-20-PBS with buffer changes every 5 minutes. The Supersignal West Pico Chemiluminescent Substrates (Thermo Scientific) were prepared by mixing one part of the Luminol/Enhancer Solution and one part of the Stable Peroxide Solution. The membranes were incubated with the substrates for 1 minute and placed in plastic sheet protectors prior to exposure to Kodak Scientific Imaging Film (Kodak) for 30 and 60 second exposures.

Cell culture and transfection

Drosophila Kc cells were cultured in Schnedier's *Drosophila* Medium containing 10% Fetal Bovine Serum and 1% of Penicillin/Streptomyocin in an incubator at 24°C. Cells were grown in 25 cm^2 tissue culture flasks (FALCON; Becton Dickinson) and routinely passaged every 2-3 days when cells reached confluency. Approximately 1 day prior to transfection, Kc cells were plated onto a 96-well plate at a density of 750,000 cells/well for fluorescence microscopy, and onto a 24-well plate at a density of 1,000,000 cells/well for protein sample preparations. Transfection of the *metallothionein-GAL4* driver along with the UAS-constructs of interest (including the *UAS-GFP:mtm*, *UAS-mCherry:mtm*, *UAS-mtm:6xmyc*, *UAS-3xFLAG:mtm*, *UAS-mCherry:Sbf*, *UAS-mCherry:2xFYVE*, *UAS-GFP:Atg18*, *UAS-GFP:Rab5*, *UAS-Rab7:GFP*, and *UAS-LAMP:GFP* constructs) were performed with the Effectene Transfection Reagent (QIAGEN) per manufacturer's instructions.

Ecdysone treatment and induction of UAS-transgene expression

To induce cellular elongation, transfected cells were incubated with a final concentration of 1 nM 20-hydroxyecdysone (Sigma) diluted into Schnedier's Drosophila Medium containing 10% Fetal Bovine Serum and 1% of Penicillin/Streptomyocin for approximately 4 hours and 24 hours prior to live imaging. To induce the *metallothionein-GAL4* driver, transfected cells were

incubated with a 0.75 mM final concentration of $CuSO_4$ diluted into complete media for approximately 18 hours prior to live imaging.

Staining of Kc cells

For visualization of lysosomes in live Kc cells, transfected cells were washed for 5 minutes with LysoTracker Red DND-99 (Invitrogen) and Hoechst 33342 (Molecular Probes) diluted 1:7,500 and 1:1000, respectively, into complete media. Cells were then washed with and subsequently kept in 100 µl of complete media and visualized using fluorescence microscopy. Digital images were taken at 63X with the Zeiss Axiovert 200 microscope controlled by the AxioVision program. Photoshop and ImageJ were used for digital editing.

Live fluorescence microscopy of Kc cells

After approximately 18 hours of $CuSO_4$-induced transgene expression, live transfected Kc cells in 96-well plates were imaged at 63X with the Zeiss Axiovert 200 microscope controlled by the AxioVision program. Photoshop and ImageJ were used for digital editing.

Molecular characterization of candidate *mtm* excision alleles

Genomic DNA was isolated from about 30 anesthetized flies for each genotype (*mtm* excision allele mutants and wild-type) by grinding flies in 200 µl of a buffer composed of 100 mM Tris-HCl (pH 7.5), 100 mM EDTA, 100 mM NaCl, 0.5%

SDS. A 800 µl solution composed of 1 part 5M KAc, and 2.5 parts 6M LiCl stock was then added to the ground fly mixture. Mixtures were spun down and the resulting supernatant was collected. 300 µl of isopropanol was then added to 500 µl of supernatant to precipitate the genomic DNA. Genomic DNA isolated from *mtm* excision allele mutants as well as wild-type flies were then used for PCR analysis using 1 µl of genomic DNA. The following primers were used in various combinations to determine the presence or absence of various genomic regions near and within the *mtm* gene (Table 1).

Table 1: Primers for the detection of genomic regions within various *mtm* alleles

Primer #	Primer Sequence (5' - 3')
382	CAG GTG GTT CAG ATA CAT GCC
383	CGT GTT GCA GAG GAA GGT G
37	GTA CTC TAG ACT ATT AGT GCA TAG GCG AGG C
27	GTA CTC TAG ACT TAC CAT AAC CAA CTA CCG TCT G
29	GTA CTC TAG ACT TAC CAT AAC CAA CTA CCG TCT G
142	CAC CCA AGG CTC TGC TCC CAC AAT
248	CGC AGA ACG CTG AAT AAA TG

Primers used to identify the presence or absence of genomic regions within candidate *mtm* excision alleles are provided. Both forward and reverse primers are given from 5' to 3'.

Drosophila stocks and crosses

Crosses producing *mtm* null mutants were grown at 25°C, while UAS/GAL4 combinations were grown at 29°C to maximize GAL4-driven expression. Predicted null trans-heterozygous mutants were generated by crossing the $mtm^{\Delta 77}$/*CyOActGFP*, $mtm^{\Delta 210}$/*CyOActGFP*, *or* $mtm^{z2\text{-}4747}$/*CyOActGFP* stocks.

Mutant and wild-type larvae were identified through the absence and presence of GFP, respectively. For expression of *mtm* fusion proteins the *UAS-Cherry:mtm*, *UAS-GFP:mtm*, and *UAS-mtm:GFP* stocks were used. For expression of RNAi hairpins the [*UAS-IR*$^{mtm\ 3.1}$], [*UAS-IR*$^{mtm\ 3.1}$; *UAS-IR*$^{mtm\ 3.5}$], [*UAS-IR*^{Sbf}], *and* [*UAS-IR*^{Sbf}, *UAS-IR*$^{mtm\ 3.5}$] stocks were utilized. For co-expression of the *mtm* fusion protein and RNAi hairpin, the [*UAS-IR*$^{mtm\ 3.1}$, *UAS-mtm:GFP*] stock was used. For expression of the PI(3)P binding reporter, the [*Cg-GAL4/UAS-Cherry:2xFYVE*] stock was utilized. The [*UAS-lacZ*] line was used as a control. The GAL4 driver lines used included [*Cg-GAL4*], [*Pxn-GAL4*], [*Cg-GAL4*, *UAS-EGFP*], and [*Pxn-GAL4*, *UAS-EGFP*].

Stocks and crosses were grown in glass vials containing standard cornmeal (agar, cornmeal, sugar, yeast, de-ionized water, propionic acid, methylparaben, 95% ethanol, and yeast sprinkles).

Characterization of animal viability/lethal phase

For trans-heterozygous *mtm* null mutants, first instar larvae were collected from egg-laying chambers on grape juice agar plates one day after embryo laying. Larvae were then transferred to fresh grape plates supplemented with yeast paste where they were allowed to develop at 25°C. The number of live larvae were counted each day up to 12 days after embryo laying.

For RNAi hairpin-expressing mutants, fly crosses set up to produce wild-type and mutant animals were incubated at 25°C in glass vials containing

standard cornmeal for 12 hours to allow for sufficient egg laying. Following this incubation period, parents were flipped out and animals were allowed to develop in the cornmeal-containing vials. The number of animals reaching either the pupal, pharate, or adult stages were subsequently counted for each wild-type and mutant genotype.

Visualization of hemocyte distribution in live flies

To visualize hemocyte patterns in live adult flies, flies containing GFP-expressing hemocytes were immobilized by placing carbon dioxide-anesthetized flies onto a layer of vacuum grease on glass slides. The ventral side of immobilized flies were imaged using fluorescence microscopy. Digital images were taken at 5X with a Leica DM16000 inverted microscope controlled by the Volocity program. Photoshop was used for digital editing.

Hemocyte viability assay

Hemocytes were bled from three to four third instar larvae four days after embryo laying into 80-100 ul of phosphate buffered saline (PBS) and allowed to attach to a glass cover slip for 1 hour at 25°C. Cell viability was then determined using the Live/Dead Assay for Cell Viability kit (Invitrogen). Hemocytes were incubated in a phosphate buffered saline (PBS) solution containing Calcein AM diluted to a final concentration of 2 μM and Ethidium homodimer-1 diluted to a final concentration of 4 μM for 20 minutes. Cells were then washed with PBS for 5 minutes and

imaged at 63X with the Zeiss Axiovert 200 microscope controlled by the AxioVision program.

Imaging of spread hemocytes

For visualization of live hemocytes expressing various UAS-controlled constructs, hemocytes were bled from three to four wandering third instar larvae four days after embryo laying into 80-100 µl of Schnedier's Drosophila Medium containing 10% Fetal Bovine Serum and 1% of Penicillin/Streptomyocin and allowed to attach to a glass cover slip for 1 hour at 25°C. To visualize DNA, cells were incubated with Hoechst 33342 (Molecular Probes) diluted 1:1000 in complete media for 10 minutes. Cells were then washed with fresh complete media and were visualized using fluorescence microscopy. Digital images were taken either at 63X with the Zeiss Axiovert 200 microscope controlled by the AxioVision program or at 60X with the Olympus DSU Spinning Disc Confocal controlled by the SlideBook software. Photoshop and ImageJ were used for digital editing. For time-lapse imaging, the Olympus Spinning Disc Confocal microscope controlled by the SlideBook software was used. ImageJ was again utilized for digital editing and production of time-lapse movies.

For visualization of lysosomes in live hemocytes, hemocytes were bled from three to four wandering third instar larvae four days after embryo laying (AEL) into 80-100 µl of complete media for 1 hour at 25°C. Cells were washed for 5 minutes with LysoTracker Red DND-99 (Invitrogen) and Hoechst 33342

(Molecular Probes) both diluted 1:1000 into complete media. Cells were then washed with and subsequently kept in 80-100 µl of complete media and visualized using fluorescence microscopy. Digital images were taken at 60X with the FV1000 Spectral Deconvolution Confocal microscope controlled by the Fluoview program. Photoshop and ImageJ were used for digital editing. For time-lapse imaging, the Olympus Spinning Disc Confocal microscope controlled by the SlideBook software was used. ImageJ was again utilized for digital editing and production of time-lapse movies.

For F-actin and microtubule visualization, hemocytes were bled from three to four wandering third instar larvae four days after embryo laying (AEL) into 80-100 µl of phosphate buffered saline (PBS) and allowed to attach to a glass cover slip for 1 hour at 25°C. Cells were then fixed for 10 minutes with 3.7% paraformaldehyde-PBS, followed by two 5-minute washings with PBST (PBS containing 0.1% of Triton X-100), and finally a 10 minute incubation with PBSTB (3% bovine serum albumin (BSA)-PBS containing 0.1% of Triton X-100). The cells were then stained overnight at 4°C with Alexa Fluor 546 phalloidin (Molecular Probes) (1:1000), mouse anti-α-tubulin (Sigma) (1:500), and Alexa Fluor 647 goat anti-mouse IgG (Molecular Probes) (1:1000) diluted in PBSTB (3% BSA, 1% Triton X-100). Cells were then washed with PBS for 10 minutes, PBS containing a 1:1000 dilution of DAPI for 10 minutes, and then with PBS twice for 10 minutes. Hemocytes were kept in PBS and visualized using

fluorescence microscopy. Digital images were taken either at 63X with either the Zeiss Axiovert 200 microscope controlled by the AxioVision program.

For F-actin visualization alone, hemocytes were bled from three to four wandering third instar larvae four days after embryo laying (AEL) into 80-100 µl of phosphate buffered saline (PBS) and allowed to attach to a glass cover slip for 1 hour at 25°C. Cells were then fixed for 10 minutes with 3.7% paraformaldehyde-PBS, followed by two 5-minute washings with PBST (PBS containing 0.1% of Triton X-100), and finally a 10 minute incubation with PBSTB (3% bovine serum albumin (BSA)-PBS containing 0.1% of Triton X-100). The cells were then stained overnight at 4°C with Alexa Fluor 546 phalloidin (or Alexa Fluor 488 phalloidin) (Molecular Probes) diluted 1:1000 in PBSTB (3% BSA, 1% Triton X-100). Following this, cells were washed with PBST for 10 minutes, then with PBS containing a 1:1000 dilution of DAPI for 10 minutes, and then with PBS twice for 10 minutes. Hemocytes were kept in PBS and visualized using fluorescence microscopy. Digital images were taken either at 63X with either the Zeiss Axiovert 200 microscope controlled by the AxioVision program or at 60X with the Olympus Spinning Disc Confocal controlled by the SlideBook software. Photoshop and ImageJ were used for digital editing.

RESULTS

MTM IN HEMOCYTE FUNCTION AND MORPHOLOGY

Initial work in our lab demonstrated a requirement for *mtm* in cellular morphogenesis in cell cultures. *Mtm* RNAi abrogated the ability of Kc cell cultures to undergo ecdysone hormone-induced cellular elongation. Therefore, we sought to determine whether *mtm* loss of function could also affect morphogenetic events in the analogous cell types in *Drosophila*. We sought to determine whether *mtm* was required for the proper execution of morphology-based hemocyte functions, and if so, to use this *in vivo* system to tease apart the specific cellular processes and mechanisms that underlie an *mtm* role in *the* regulation of cell shape change.

Molecular characterization of candidate *mtm* excision alleles

Previously, candidate white-eyed P(w-) *mtm* excision alleles were produced via transposase-induced mobilization of the P{EPgy2}CG9117$^{[EY15305]}$ Pw+ element adjacent to the *mtm* gene. To confirm and molecularly characterize deletions within the *mtm* gene, lesions were mapped by PCR analysis of genomic DNA isolated from homozygous mutant larvae (for *mtm*$^{\Delta 77}$ and *mtm*$^{\Delta 210}$; identified through their lack of GFP-expressing balancers). Using various primers, the presence or absence of specific DNA-matched sequences to the primers were determined for each genotype (Fig. 3). PCR results indicated the deletion of a region ~1200-2100 bps in length, spanning both the *mtm* and *CG9117* genes and

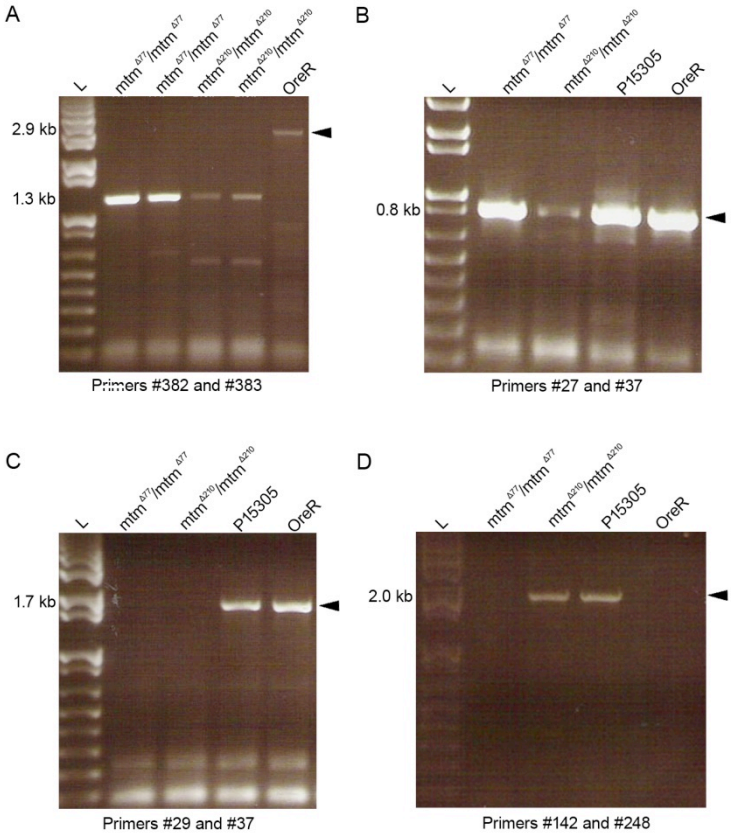

Figure 3: Detection of genomic deletions within the candidate *mtm* excision alleles

PCR amplification of DNA sequences throughout the *mtm* gene of candidate alleles produced through transposon-mediated mutagenesis. Amplification of a genomic region spanning the (**A**) *mtm* and *CG31640* genes; (**B**) 3' end of *mtm*, (**C**) majority of the *mtm* gene beginning at the 5' end, (**D**) and the P{EPgy2}CG9117[EY15305] P element and the *CG31640* gene. The sizes of the amplified DNA fragments are indicated to the side of each figure. Arrowheads indicate the expected PCR product sizes.

the majority of the Pw+ element for the $mtm^{\Delta 210}$ allele (Fig. 4). However, we were unable to determine the exact extent of the deletion as PCR reactions failed to produce a sequencible amplicon. For the $mtm^{\Delta 77}$ candidate allele, sequencing of an amplicon spanning the *mtm* region identified the deletion of a 1,716 bp region that removed half of the *mtm* gene from the 5' end and the entire and *CG9117* gene (primers #382 and #383) (Fig. 4). Both *mtm* excision alleles delete the

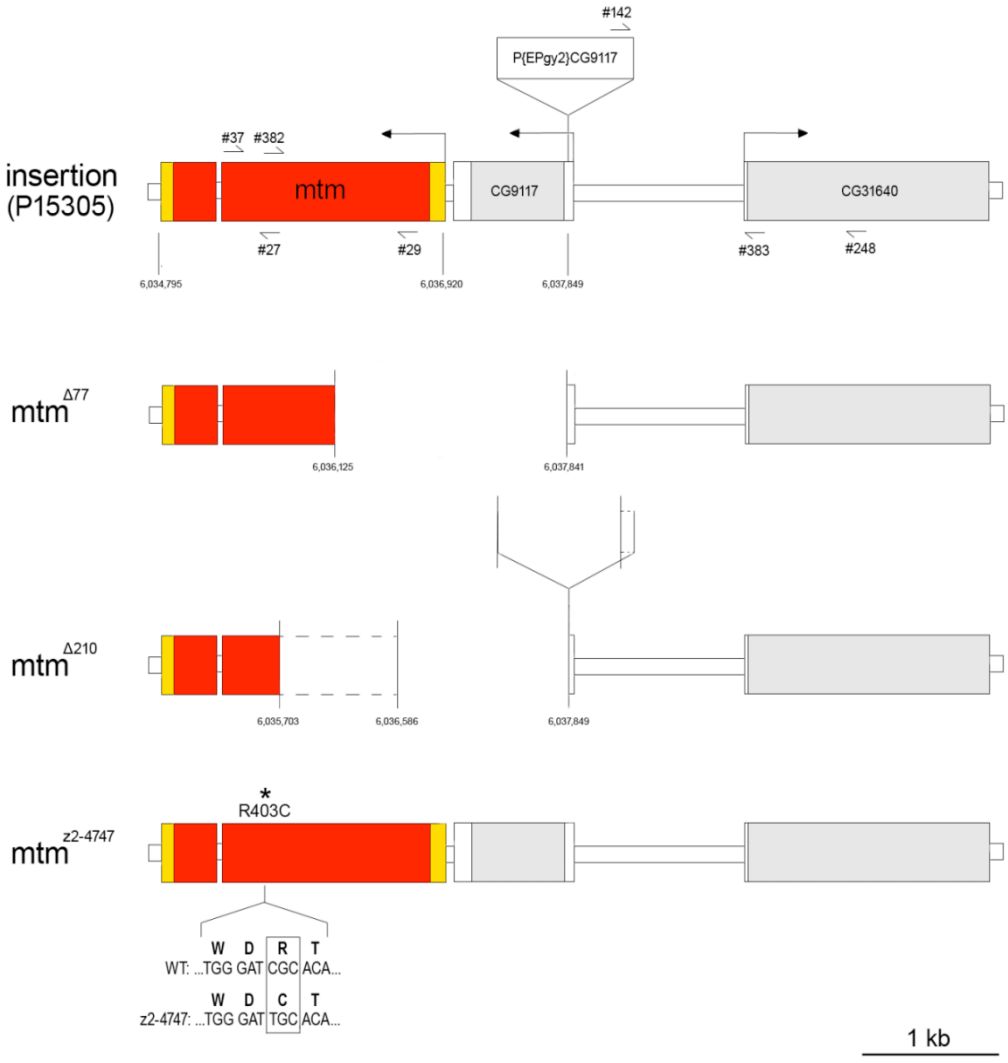

Figure 4: Genomic maps of *mtm* mutant alleles

Location of primers for PCR analysis of candidate *mtm* excision alleles (top). Extent of the deletions in the $mtm^{\Delta 77}$ and $mtm^{\Delta 210}$ excision alleles as determined by sequence analysis. Location of the missense mutation in the $mtm^{z2\text{-}4747}$ TILLING allele (bottom).

promoter, transcription start, and first half coding region for *mtm*, as well as the 3' region of the adjacent *CG9117* gene.

Along with these *mtm* excision alleles, we also acquired an allele with an *mtm* point mutation in the predicted catalytic site ($mtm^{z2\text{-}4747}$), identified by TILLING (Targeting Induced Local Lesions in Genomes) of a collection of

chemically mutagenized second chromosomes for use in loss of function experiments. In addition, we generated UAS-controlled *mtm* hairpin transgenes (UAS-IR^{mtm}) for RNAi-mediated *mtm* depletion in targeted tissues.

Mtm is an essential gene for *Drosophila* viability

To determine the developmental requirements for *mtm* function, the viability of homozygous *mtm* excision allele (*mtm*$^{\Delta 77}$ and *mtm*$^{\Delta 210}$) mutants were determined. Homozygous genomic mutants were smaller in size than their wild-type siblings, took longer to reach pupation, and exhibited lethality throughout late third-instar larval and early pupal stages (and those that did reach the pupal stage died shortly following head eversion) (Fig. 5, Table 2). To determine whether the lethality seen with the homozygous *mtm* mutants were due to *mtm* loss of function, the *mtm* excision alleles were used *in trans* with the point-mutated allele. Similar to the *mtm* homozygous excision mutants, the trans-heterozygous *mtm* mutants were also smaller in size than age-matched siblings, delayed in reaching pupation, and lethal at the late third-instar larval and early pupalstages (Table 2). These results, along with confirming a functional requirement for *mtm* in fly viability, confirm the strength and specificity of the *mtm*$^{z2\text{-}4747}$ allele and suggest that all alleles are functional nulls.

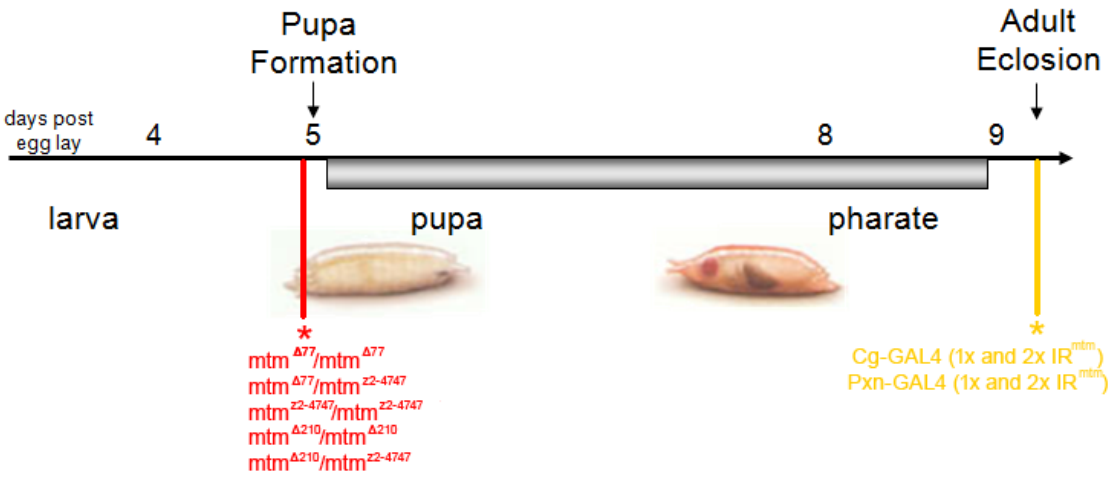

Figure 5: Lethal phase of the *mtm* mutants

The lethal phase for each mutant is indicated above. The *mtm* null mutants die at an earlier stage than animals expressing *mtm* RNAi in their hemocytes.

Hemocyte-specific Mtm loss of function results in lethality at eclosion

Given that *mtm* RNAi cell morphology phenotypes were discovered in Kc cell cultures, a hemocyte-derived cell line, we asked whether *mtm* knockdown specifically in an analogous *in vivo* tissue would show similar requirements for cellular morphogenesis. To induce an RNAi effect specifically in *Drosophila* hemocytes, hemocyte-specific GAL4 drivers were used to drive expression of a UAS-controlled transgene containing inverted repeats of the *mtm* gene resulting in the production of RNAi hairpins. This *mtm* RNAi hairpin producing transgene had been tested previously for specificity and efficiency, as expression of a wild-type *mtm* cDNA was able to rescue the lethality caused by IR^{mtm} expression. Interestingly, *mtm* RNAi hairpin expression induced with hemocyte drivers, Pxn

Table 2: *Mtm* homozygous and transheterozygous mutants are lethal at the late third-instar larvae and early pupal stages

Genotype	Phenotype	Comments
$mtm^{\Delta 77}$	Lethal	Late third-instar larval and pupal stage after head eversion.
$mtm^{\Delta 210}$	Lethal	Late third-instar larval and pupal stage after head eversion.
$mtm^{z2\text{-}4747}$	Lethal	Late third-instar larval and pupal stage after head eversion.
$mtm^{\Delta 77}/mtm^{\Delta 210}$	Lethal	Late third-instar larval and pupal stage after head eversion.
$mtm^{\Delta 77}/mtm^{z2\text{-}4747}$	Lethal	Late third-instar larval and pupal stage after head eversion.
$mtm^{\Delta 210}/mtm^{z2\text{-}4747}$	Lethal	Late third-instar larval and pupal stage after head eversion.

Lethal phase of various *mtm* homozygous and transheterozygous mutants.

GAL4 or Cg-GAL4, resulted in lethality at the pharate adult stage (Table 3). The majority of the hairpin RNAi-expressing animals died during mid-eclosion. Flies that died at the mid-eclosion stage often managed to extract their heads and upper thoraces from their pupal cases, but usually had their distal leg segments pinned to the inside of the cases. A very small number of flies undergoing hemocyte-targeted IR^{mtm} expression managed to eclose but died shortly afterward. When the behaviors of the rare newly-eclosed flies were examined, they were unable to crawl up glass vial walls. When placed on a flat upright for prolonged periods of time. The legs of these flies appeared unable to support the weight of their bodies and they constantly fell onto their backs. Altogether, such phenotypes may be indicative of weakened or nonfunctional leg muscles. Fly mobility defects caused by hemocyte-specific *mtm* loss of function are suggestive

Table 3: Hemocyte-specific RNAi against *mtm* results in lethality at the pharate adult stage

GAL4 Driver	Expression Pattern	UAS-construct	Phenotype	Comments
Cg-GAL4	Hemocytes and fat body	UAS-IR^{mtm} (1x)	Lethal	Pharate adults and mid-eclosion.
	Hemocytes and fat body	UAS-IR^{mtm} (2x)	Lethal	Pharate adults and mid-eclosion.
	Hemocytes and fat body	UAS-lacZ	Viable	Adult flies are wild-type
	Hemocytes and fat body	UAS-IR^{mtm}, UAS-EGFP	Lethal	Pharate adults and mid-eclosion. Very few adults eclose.
	Hemocytes and fat body	UAS-IR^{mtm}, UAS-mtm:GFP	Viable	Adult flies are wild-type
Pxn-GAL4	Hemocytes	UAS-IR^{mtm} (1x)	Lethal	Pharate adults and mid-eclosion. Very few adults eclose.
	Hemocytes	UAS-IR^{mtm} (2x)	Lethal	Pharate adults and mid-eclosion. Very few adults eclose.
	Hemocytes	UAS-lacZ	Viable	Adult flies are wild-type
	Hemocytes	UAS-IR^{mtm}, UAS-EGFP	Lethal	Pharate adults and mid-eclosion. Very few adults eclose.
	Hemocytes	UAS-IR^{mtm}, UAS-mtm:GFP	Viable	Adult flies are wild-type

Lethal phase of animals overexpressing 1 or 2 copies of the UAS-IR^{mtm} transgene under control of the hemocyte-speicifc GAL4 drivers, Cg-GAL4 and Pxn-GAL4.

of a functional requirement for wild-type *mtm* in hemocyte processes important for muscle strength and stability, such as secretion of ECM components to promote development or the remodeling of adult tissues. Additionally, along with a suggested requirement in hemocytes, a survey of different tissue-specific RNAi

also identified an *in vivo* requirement for *mtm* in other tissues including the muscles (data not shown).

Mtm function affects hemocyte distribution in adult flies in a cell-autonomous manner

Loss of *mtm*-dependent hemocyte function could negatively affect fly viability through a number of avenues. For example, disruption of hemocyte functions could cause disruptions in development, tissue remodeling, or pathogen elimination. Impairments in hemocyte viability, migration, attachment to specific sites of activity, ECM secretion, or differentiation caused *mtm* loss of function could all result in a disruption in fly development, remodeling, or immunity. Given a proposed role for *mtm* in cell morphogenesis, hemocyte migration and/or attachment to their normal sites of activity within the animal could be disrupted with *mtm* knockdown. Failure of hemocytes to appear at normal sites of activity would then provide an explanation to the lethality caused by hemocyte-specific Mtm depletion. To test whether hemocyte distribution could be effected by *mtm* function (and if such impaired distribution then correlated with reduced animal viability), the distribution of *mtm*-deficient hemocytes in live wild-type and *mtm* mutant flies was observed. Pxn-GAL4 driven co-expression of GFP with IR^{mtm} allowed for the detection of hemocytes in live adults via fluorescence microscopy. Examination of the ventral side of control flies carrying Pxn-GAL4-

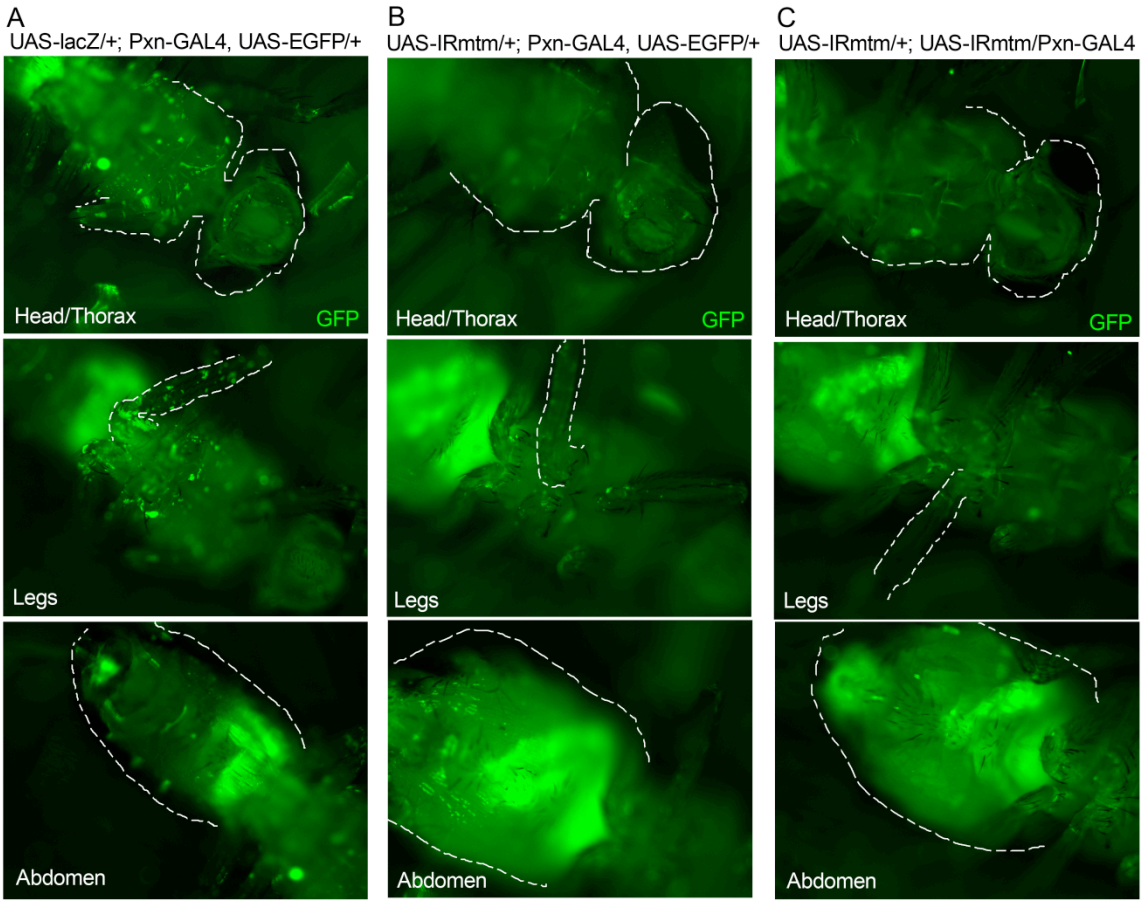

Figure 6: Hemocyte distribution in adult flies following hemocyte-specific Mtm depletion

Distribution of GFP-expressing hemocytes in the head, thorax, legs, and abdomen of adult flies overexpressing the (**A**) UAS-lacZ, (**B**) UAS-IR^{mtm}, and (**C**) UAS-IR^{mtm}; UAS-IR^{mtm} transgenes with the Pxn-GAL4 driver. Dotted lines outline the relevant body parts in each image. Bright central staining appears to be from ectopic GAL4 expression in the gut.

driven lacZ and GFP overexpression revealed the extensive population of hemocytes dispersed throughout the head and thorax (Fig. 6A). Analysis of *Drosophila* legs displayed an abundance of hemocytes throughout the leg segments and joints, as well as a high concentration of cells within and proximal to the coxae (Fig. 6A). Further examination also revealed a sparse distribution of hemocytes within the abdomen (Fig. 6A). Hemocyte distribution was vastly

different in IR^{mtm} and GFP co-expressing hemocytes. In animals expressing either one or two copies of the UAS-IR^{mtm} transgene with the Pxn-GAL4 driver, hemocytes rarely localized to the head or thorax (Fig. 6B-C). A few hemocytes localized to the leg joints and coxal-proximal regions, but the leg segments were almost entirely devoid of GFP-positive cells (Fig. 6B-C). Inspection of the abdomen revealed strong GFP fluorescence (Fig. 6B-C). However, these GFP-expressing structures could not be positively identified as hemocytes because the strong fluorescence signal prevented the morphology-based identification of individual cells. These results raise the possibility that hemocyte-targeted *mtm* RNAi disrupts hemocyte distribution, which then causes leg instability, and then subsequently causes lethality of the fly at eclosion. The question then arises of whether the *mtm* blood cell requirement reflects a complete lack of blood cell functions, or instead, is indicative of inappropriate blood cell behavior producing a unique phenotype. To test this possibility, we can compare the phenotypes of flies with RNAi-mediated knockdown of *mtm* with flies completely ablated of hemocytes through overexpression of the apoptotic gene *reaper*.

Mtm loss of function does not affect hemocyte viability

Mtm could potentially be important in a number of different processes important for hemocyte distribution (and subsequently leg stability and fly viability) including hemocyte survival, migration, ECM secretion, attachment, or differentiation. To address the affect of *mtm* on cell survival, a two-color

fluorescence assay was used to measure cell vability in *mtm* null mutant hemocytes compared to wild-type. The first component of this assay, calcein, relies on the enzymatic activity of live cells to convert the non-fluorescent calcein-acetoxymethyl (calcein-AM) to GFP-fluorescent calcein (which is also well-retained in live cells). The second component, ethidium homodimer-1, on the other hand can only enter damaged cells and produces a bright red fluorescence following its binding to nucleic acids. Using this assay, the percentage of live (calcein-positive) and dead (ethidium homodimer-1-positive) hemocytes spilled from early-wandering third instar larvae were measured in each condition. Both the *mtm* trans-heterozygous mutants and wild-type hemocytes exhibited similar levels of viability (between 85-90%) (Fig. 7). Therefore, the effects of *mtm* loss of function in hemocytes cannot be attributed to increased levels of cell death.

Hemocyte morphology and cytoskeletal organization is dependent on *mtm*

Earlier work done in Kc cells proposed that the Mtm phosphatase may regulate PIP-mediated localization and/or activity of cytoskeletal remodeling factors to mediate changes in cell shape. Given a functional requirement for *mtm* in primary hemocytes, we investigated the cell spreading and morphology of hemocytes bled from third instar larvae. Hemocytes were stained with phalloidin-546 to visualize the F-actin cytoskeleton and anti-tubulin antibody to visualize microtubules, and then imaged by immunofluorescence microscopy. Control hemocytes spread on glass coverslips and displayed a wild-type phenotype,

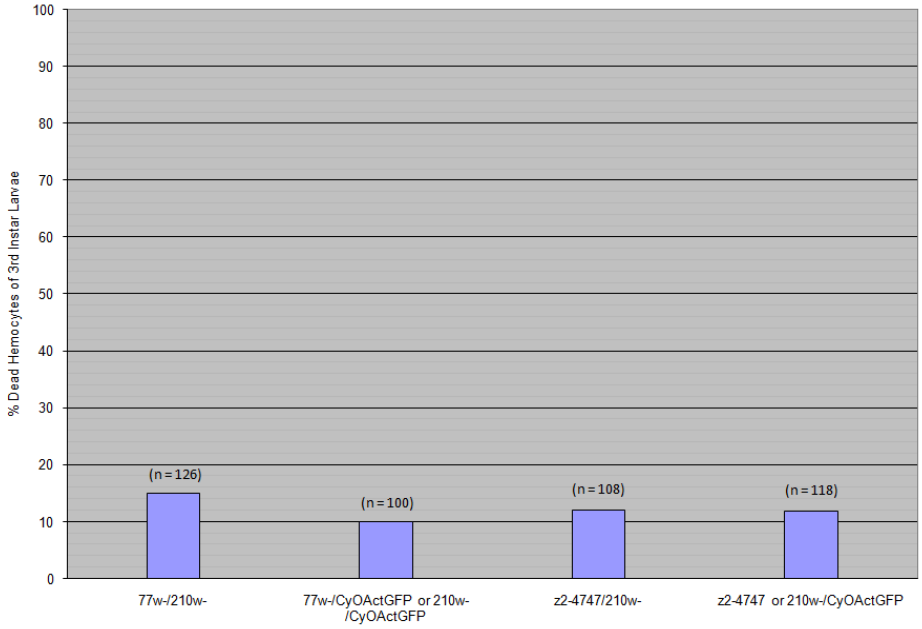

Figure 7: Mtm loss of function does not affect hemocyte viability

Percentage of ethidium homodimer-1-stained (dead) hemocytes in relation to the total stained hemocyte population spilled from *mtm* genomic mutants and wild-type siblings. Hemocytes were allowed to spread in PBS for 1 hour prior to staining with calceim-AM (stain for live cells) and ethidium homodimer-1 (stain for dead cells).

forming approximately a dozen F-actin-rich protrusions extending radially from the cell body (Fig. 8A). Conversely, the majority of the *mtm* mutant cells displayed a smooth edge and round cell morphology (67%). The mutant hemocytes also appeared generally 1.5-2 times larger in area and flatter than wild-type cells. Upon closer inspection, *mtm* mutant hemocytes exhibited altered filamentous actin organization compared to wild-type cells. The majority of the round mutant cells exhibited membrane ruffling and contained abnormally oriented actin bundles (71%), two features not often seen in wild-type cells. Rather than extend radially from the cell body, the actin bundles in the *mtm* mutants instead wrapped around the periphery of the cell and looked as if they

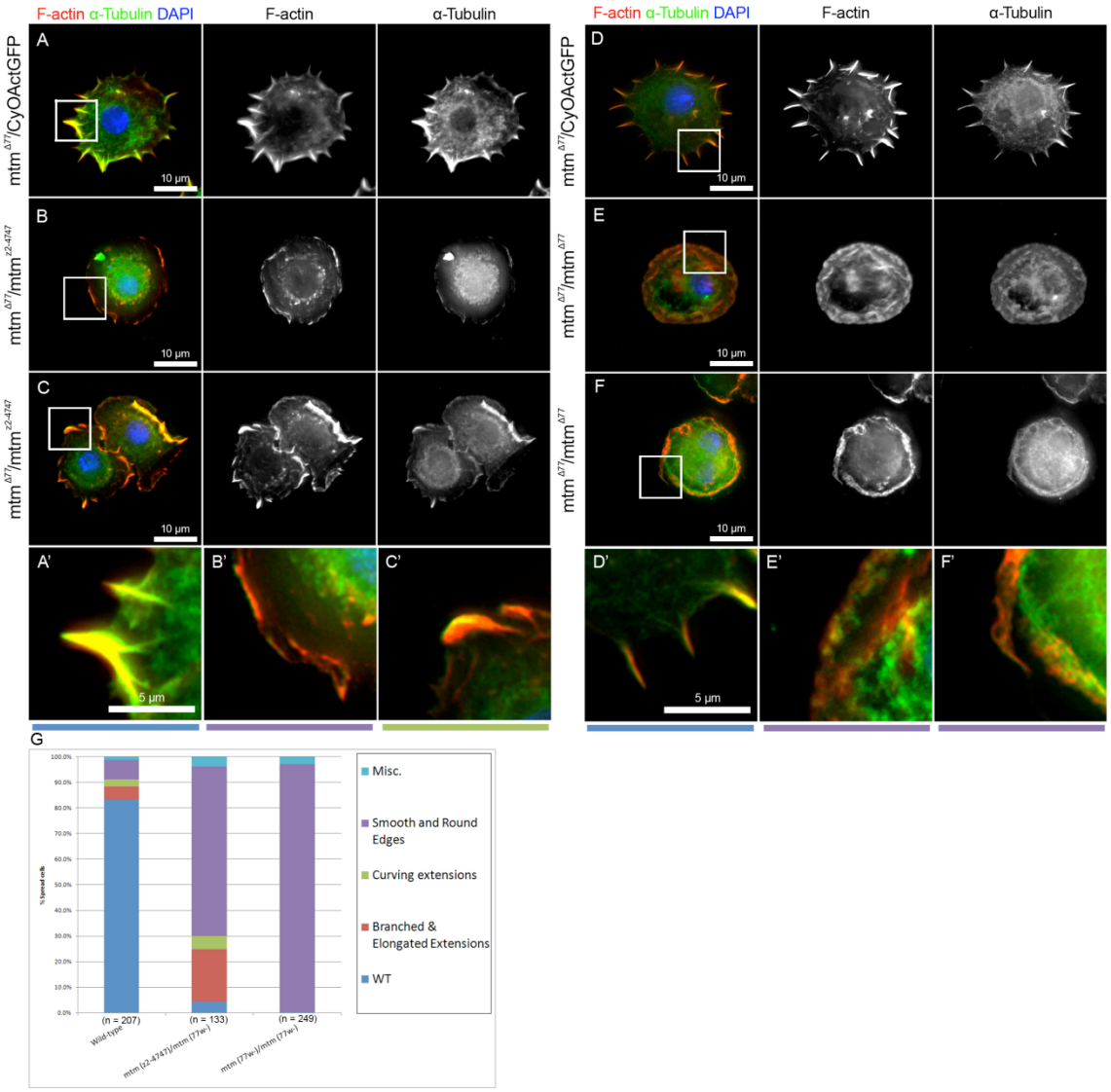

Figure 8: Hemocytes of *mtm* transheterozygous and homozygous mutants possess abnormally organized cytoskeletons

Morphology of F-actin and microtubule stained wild-type and *mtm* mutant hemocytes following attachment onto glass slides. Hemocytes were spilled from late third-instar larvae. (**A**) Control hemocytes and (**B-C**) *mtm* transheterozygous mutants were allowed to spread in PBS for one hour prior to visualization using fluorescence microscopy. These conditions were repeated for (**D**) Control hemocytes and (**E-F**) *mtm* homozygous mutants. (**G**) Distribution of phenotypes for the entire population of spread cells for each *mtm* mutant genotype. Images were taken using immunofluorescence microscopy and represent Z-projections of multiple focal planes. Enlarged images highlighting cell cytoskeleton phenotypes for (**A'**) Control hemocytes with normal F-actin rich protrusions and *mtm* transheterozygous mutants exhibiting (**B'**) curving actin protrusions and (**C'**) membrane ruffling. (**D'**) Control hemocytes with normal, radially extending extensions and (**E'-F'**) *mtm* homozygous mutants displaying membrane ruffling.

Figure 9: *Mtm* RNAi hairpin expression in hemocytes results in abnormal morphology and organization of the actin cytoskeleton

Morphology of F-actin and microtubule stained, UAS-IR^{mtm} expressing hemocytes under control of various hemocyte-specific drivers spread for one hour on glass slides. (**A**) UAS-lacZ and (**B-C**) UAS-IR^{mtm} expressing hemocytes under control of the Cg-GAL4 driver spilled from third-instar larvae and spread in PBS. (**D**) UAS-lacZ expressing hemocytes and (**E-F**) hemocytes expressing two copies of the UAS-IR^{mtm} transgene using the Cg-GAL4 driver. (**G**) UAS-lacZ and (**H-I**) UAS-IR^{mtm} expressing hemocytes under control of the Pxn-GAL4 driver. Hemocytes undergoing Pxn-GAL4-driven expression of (**J**) UAS-lacZ and (**K-L**) UAS-IR^{mtm}, UAS-IR^{mtm}. Enlarged images highlighting cytoskeleton phenotypes for (**A', G'**) wild-type with normal cellular protrusions, (**B', H'**) single *mtm* hairpin expressing hemocytes with branched actin networks, and (**C', I'**) *mtm* mutant hemocytes displaying membrane ruffles. (**M**) Distribution of phenotypes for the entire population of spread cells in each *mtm* mutant genotype. Images were taken using immunofluorescence microscopy and represent Z-projections of multiple focal planes.

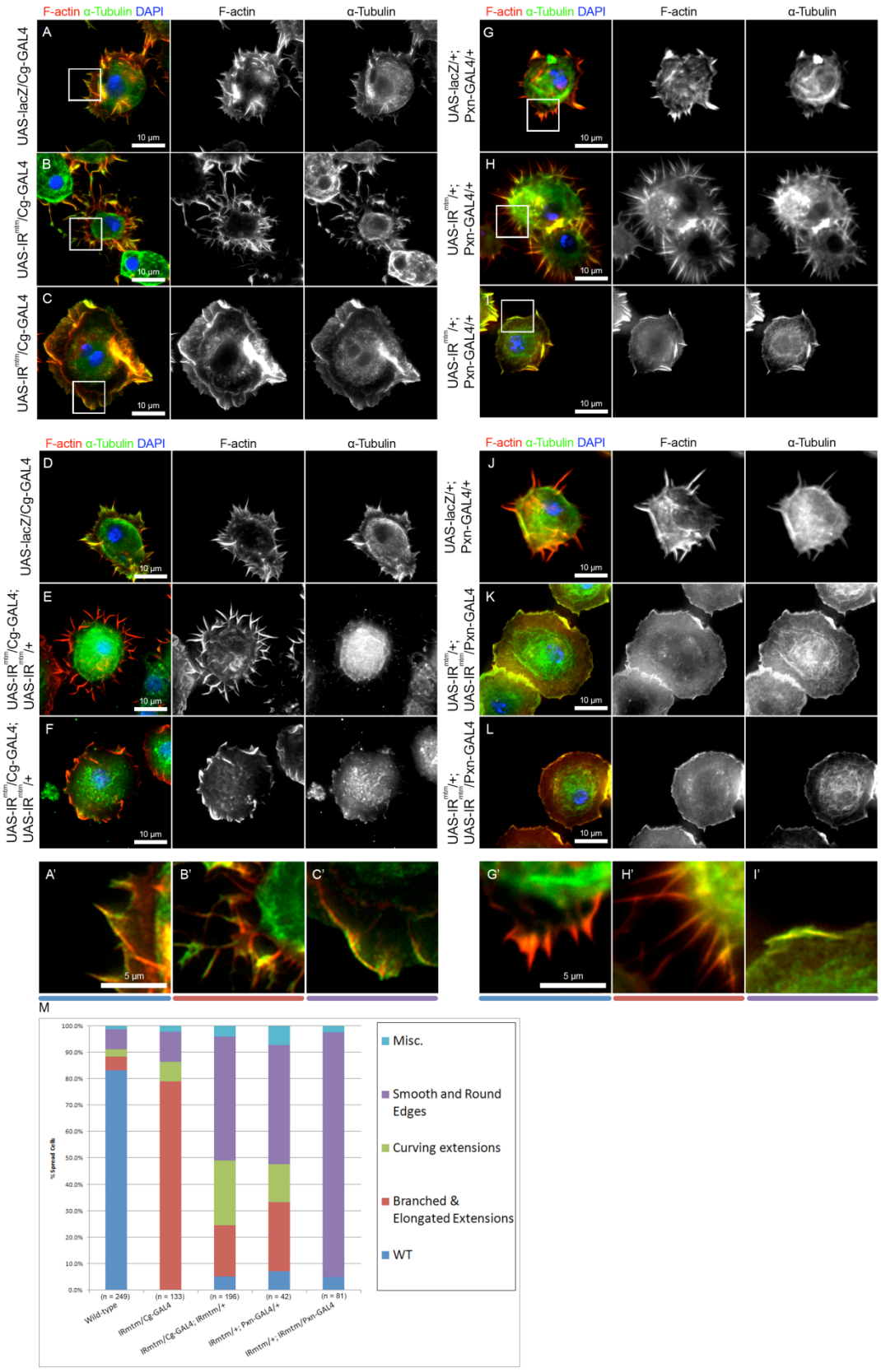
F-actin α-Tubulin DAPI
F-actin
α-Tubulin
UAS-lacZ/Cg-GAL4
UAS-IR^rtm/Cg-GAL4
UAS-IR^rtm/Cg-GAL4
UAS-lacZ/+; Pxn-GAL4/+
UAS-IR^rtm/+; Pxn-GAL4/+
UAS-IR^rtm/+; Pxn-GAL4/+
UAS-lacZ/Cg-GAL4
UAS-IR^rtm/Cg-GAL4; UAS-IR^rtm/+
UAS-IR^rtm/Cg-GAL4; UAS-IR^rtm/+
UAS-lacZ/+; Pxn-GAL4/+
UAS-IR^rtm/+; UAS-IR^rtm/Pxn-GAL4
UAS-IR^rtm/+; UAS-IR^rtm/Pxn-GAL4
10 µm
5 µm
M
% spread Cells
Misc.
Smooth and Round Edges
Curving extensions
Branched & Elongated Extensions
WT
(n = 249)
(n = 133)
(n = 196)
(n = 42)
(n = 81)
Wild-type
iRmtm/Cg-GAL4
iRmtm/Cg-GAL4; iRmtm/+
iRmtm/+; Pxn-GAL4/+
iRmtm/+; iRmtm/Pxn-GAL4

were severely curved filopodia-like protrusions (Fig. 8B-C, 8B'-C'). Though microtubule stainings in some conditions were too poor in quality to allow for a definitive assessment of microtubule organization, in instances where microtubule staining allowed for the visualization of a clear microtubule network, its organization looked similar in both wild-type and mutant hemocytes. This is consistent with Kc cell results in which the addition of actin-depolymerizing drugs in *mtm* depleted cells allowed for normal microtubule polymerization, suggesting normal microtubule behavior in *mtm* depleted cells at least at the level of assembly (M. Velichkova, A. Kiger, unpublished work). These results indicate a role for *mtm*-dependent mechanisms in regulating the formation of cell protrustions, perhaps at the level of F-actin cytoskeleton organization, in hemocytes.

To determine if the trans-heterozygous *mtm* mutant phenotype was caused by the point-mutation ($mtm^{z2\text{-}4747}$) resulting in a dominant-negative rather than a loss of function effect, the morphology of homozygous *mtm* excision allele mutant ($mtm^{\Delta 77}$) hemocytes were compared to trans-heterozygous mutant cells ($mtm^{\Delta 77}/mtm^{z2\text{-}4747}$). The hemocyte morphology from homozygous excision allele mutants resembled those of the trans-heterozygous mutants, with round, smooth edges and extensive membrane ruffling (96%). This suggests that the *mtm* point mutant acts as a loss of function allele rather than as a dominant-negative mutation (Fig. 8E-F, 8E'-F').

Mtm affects cell morphology and cytoskeletal organization in a cell-autonomous manner

To test whether *mtm* affects hemocyte morphology in a cell-autonomous manner, the effect of hemocyte specific, *mtm* RNAi on hemocyte shape and cytoskeletal organization was examined. Cg-GAL4 driven expression of a single copy of the IR^{mtm} transgene resulted in larval hemocytes with a round, smooth phenotype similar to *mtm* null mutants, suggesting that *mtm* RNAi reduced levels of *mtm* gene product to a degree with comparable effects as the null alleles (Fig. 9B, 9B'). However, the majority of Cg-GAL4/IR^{mtm} hemocytes exhibited a seemingly opposite phenotype, with these cells containing an estimated 2-3 times more filopodia-like, radial extensions than seen in wild-type cells, a phenotype found to a much lesser extent in *mtm* null mutants (79% vs. 20%). The abnormal extensions were usually at least twice the length of wild-type protrusions and significantly more branched (Fig. 9A, 9A'). Cg-GAL4 driven expression of two copies of the IR^{mtm} construct (predicted to result in higher expression levels of *mtm* RNAi hairpins, and thus greater level of mRNA knockdown) shifted the population of hemocytes to phenotypically resemble the genomic null alleles: 45.2% of hemocytes appeared "null" like (smooth edges, round morphology) with single IR^{mtm} construct expression, while 92.6% of hemocytes appeared "null" like with double *mtm* hairpin construct expression. Thus, as strength of *mtm* knockdown was increased through the introduction of additional IR^{mtm} constructs, a larger population of hemocytes with phenotypes

Figure 10: Expression of Mtm:GFP cDNA rescues the actin cytoskeleton organization defects of *mtm* RNAi hairpn expression

Hemocyte morphology of immunostained spread hemocytes expressing the (**A**) UAS-lacZ, (**B-C**) UAS-IR^{mtm}, and (**D**) UAS-IR^{mtm}, UAS-Mtm:GFP trangenes under control of the Cg-GAL4 driver. Enlarged images highlighting the wild-type cell morphologies of (**A'**) control and (**D'**) IRmtm, Mtm:GFP co-expressing hemocytes compared to the mutant morphologies of *mtm* mutant hemocytes exhibiting (**B'**) long protrusions and (**C'**) curving extensions. (**E**) Distribution of phenotypes for the entire population of spread cells in each *mtm* mutant genotype.

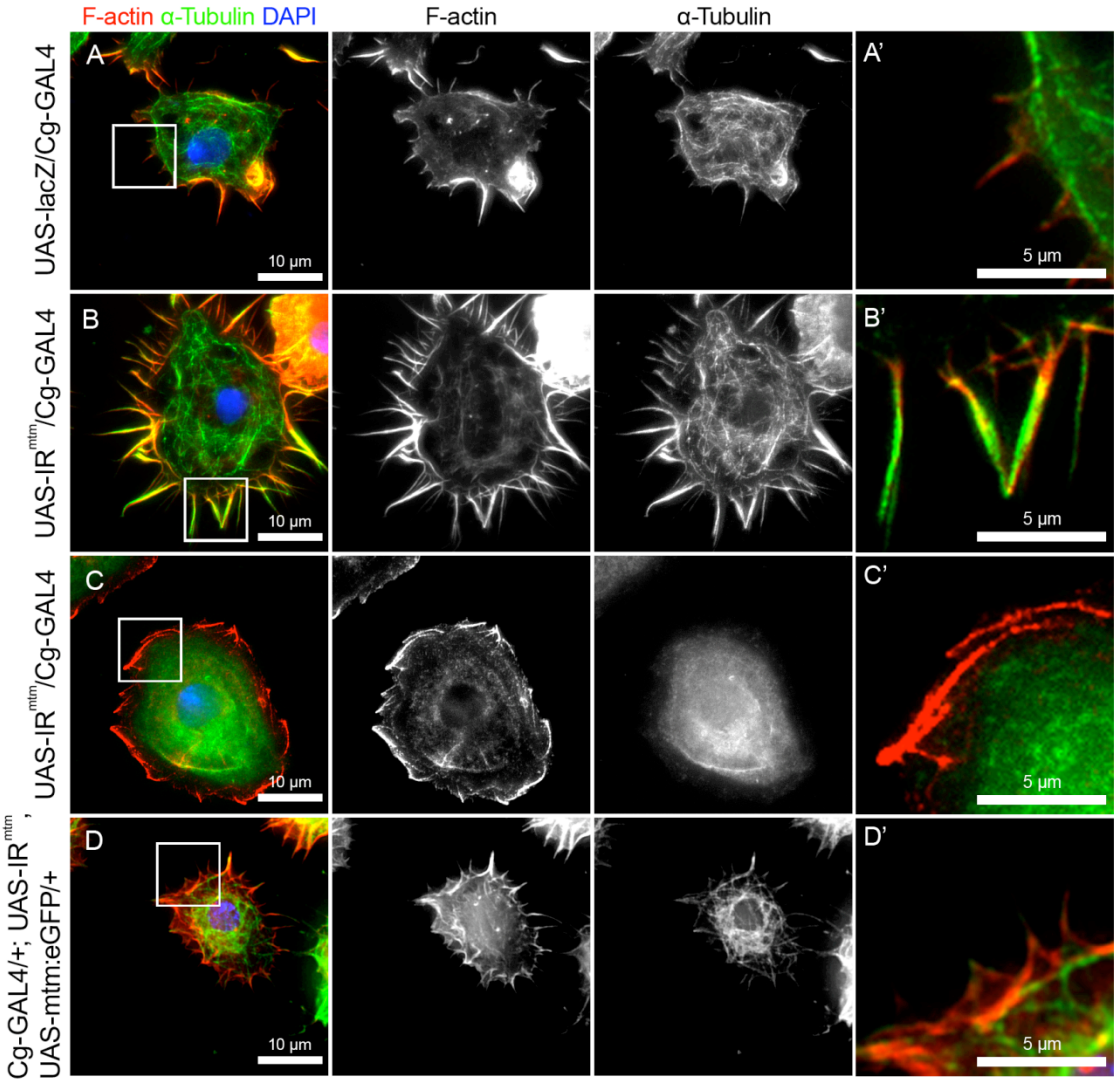
F-actin α-Tubulin DAPI
F-actin
α-Tubulin
A
A'
B
B'
C
C'
D
D'
10 µm
5 µm
UAS-lacZ/Cg-GAL4
UAS-IR mtm /Cg-GAL4
UAS-IR mtm /Cg-GAL4
Cg-GAL4/+; UAS-IR mtm , UAS-mtm:eGFP/+

E

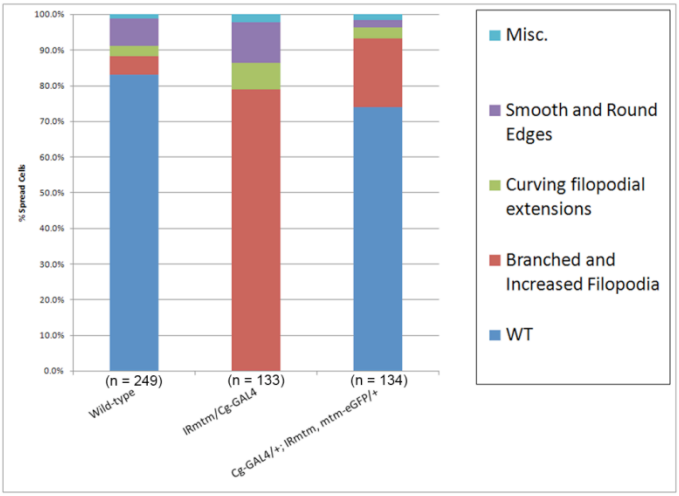
% Spread Cells
100.0%
90.0%
80.0%
70.0%
60.0%
50.0%
40.0%
30.0%
20.0%
10.0%
0.0%
(n = 249)
(n = 133)
(n = 134)
Wild-type
IRmtm/Cg-GAL4
Cg-GAL4/+; IRmtm, mtm-eGFP/+
Misc.
Smooth and Round Edges
Curving filopodial extensions
Branched and Increased Filopodia
WT

similar to those seen in trans-heterozygous and homozygous excision allele mutants were produced (Fig. 9M). Use of another hemocyte-specific driver (Pxn-GAL4) to induce expression of either one or two copies of the IR^{mtm} construct also resulted in a lack of cellular protrusions, a phenotype similar to that seen in the trans-heterozygous and homozygous *mtm* excision allele mutants (Fig. 9I, 9I', 9K, 9L). These results indicate that hemocyte-specific depletion of *mtm* can be attributed to cell morphology abnormalities in *mtm* mutant conditions.

To test that specific loss of *mtm* function was responsible for the abnormal morphology seen in IR^{mtm}-expressing hemocytes, the ability of wild-type *mtm* cDNA expression to rescue the hemocyte morphology phenotypes was examined. Cell morphology was insptected following co-expression of the UAS-controlled *mtm:GFP* and IR^{mtm} transgenes in hemocytes. While 97.7% of hemocytes expressing a single copy of the IR^{mtm} transgene exhibited mutant phenotypes, only 24.6% of hemocytes expressing both the UAS-Mtm:GFP and UAS-IR^{mtm} transgenes appeared morphologically abnormal, indicating that GFP:Mtm overexpression was sufficient to overcome the RNAi effects of *mtm* hairpin expression (Fig. 10). Rescue of the hemocyte morphology phenotypes was not simply the result of the dilution of UAS-driven RNAi hairpin expression as rescue was not observed for hemocytes co-expressing the UAS-IR^{mtm} and UAS-GFP constructs using the Pxn-GAL4 driver (Fig. 17D). These results further support the hypothesis that the cytoskeletal defects associated with *mtm* RNAi hairpin expression were due specifically to reduced levels of Mtm protein.

Effects of *mtm* on cell morphology and cytoskeletal organization is not due to impaired hemocyte development

Loss of *mtm* function in hemocytes could either directly affect the architecture of the actin cytoskeleton or instead indirectly affect cell morphology through the disruption of normal hemocyte differentiation earlier in development. To investigate this, levels of RNAi-mediated knockdown of *mtm* were temporally regulated to minimize RNAi-mediated knockdown of *mtm* until after hemocytes were fully differentiated. To take advantage of the temperature-sensitivtiy of the UAS/GAL4 system, larvae were shifted from GAL4 "restrictive" (18°C) to "permissive" temperatures (29°C), so that *mtm* RNAi would be prevented until after hemocytes were fully differentiated into plasmatocytes and released into circulation. Indeed, raising IR^{mtm}/Pxn-GAL4 larvae at 18°C was sufficient to prevent the fly lethality associated with this genotypic background, indicating reduced levels of UAS-IR^{mtm} expression and *mtm* knockdown (data not shown). Along with these results, hemocytes spilled from early-wandering third instar larvae raised at 18°C, both in control and *mtm* RNAi backgrounds, displayed a wild-type cell morphology, indicating that raising larvae at this temperature was sufficient to suppress the *mtm* RNAi cell defects (Fig. 11A-C). In contrast, larvae raised at 18°C and then shifted to 29°C 24 hours prior to reaching the early-wandering third instar larval stage displayed an abnormally arranged actin cytoskeleton in *mtm* RNAi hemocytes. These round cells with smooth edges

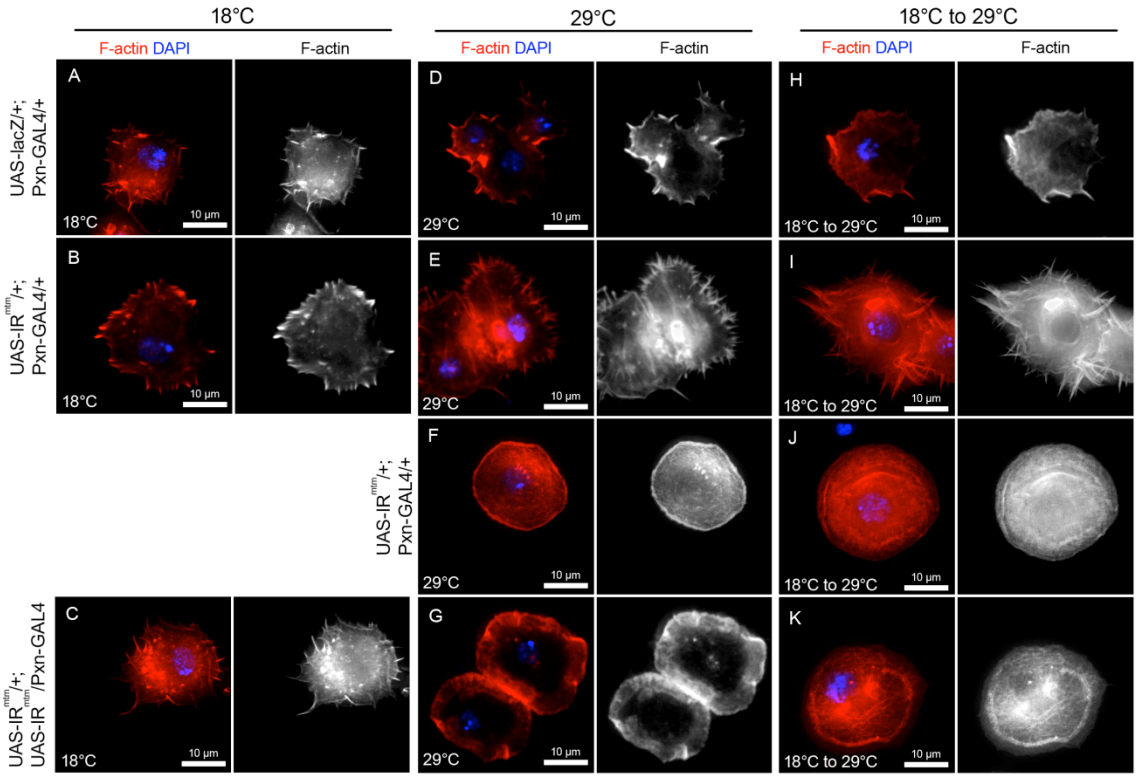

Figure 11: Hemocyte-targeted *mtm* RNAi hairpin expression for only 24 hours in early-third instar larvae is sufficient to disorganize hemocyte actin cytoskeleton organization.

Morphology of phalloidin-546 stained hemocytes spilled from UAS- transgene carrying third-instar larvae raised at various temperature conditions. UAS- constructs expression was induced with the Pxn-GAL4 driver. (**A**) LacZ, (**B**) single *mtm* RNAi hairpin, and (**C**) double *mtm* RNAi hairpin expressing hemocytes spilled from larvae raised continuously at 18°C spread in PBS for 1 hour. (**D**) LacZ, (**E-F**) single *mtm* RNAi hairpin, and (**G**) double *mtm* RNAi hairpin expressing hemocytes spilled from larvae raised continuously at 29°C. (**H**) LacZ, (**I-J**) single *mtm* RNAi hairpin, and (**K**) double *mtm* RNAi hairpin expressing hemocytes spilled from larvae initially raised 18°C and then shifted at the early third-instar stage to 29°C for 24 hours prior to spilling. Images are Z-stacks of multiple focal planes acquired via fluorescence microscopy.

lacking radial extensions were similar in morphology to IR^{mtm}-expressing hemocytes from larvae continuously raised at 29°C (Fig. 11D-K). Therefore, knockdown of *mtm* for a relatively brief time period in fully-differentiated plasmatocytes was sufficient to induce the same actin cytoskeletal defects previously seen in hemocytes continuously expressing the *mtm* RNAi hairpin,

suggesting that these defects are the direct effect of *mtm* loss of function rather than an indirect consequence of disrupted hemocyte development.

Mtm overepxression induces a gain-of-function phenotype in hemocytes

To test whether the *mtm* requirement for hemocyte protrusion formation was permissive or instructive, increased *mtm* expression was tested for the ability to induce a gain-of-function morphology phenotype. Hemocyte-specific overexpression of the UAS-Cherry:Mtm transgene was performed with the Cg-GAL4 driver, and dissected hemocytes were stained for F-actin using phalloidin-488. Interestingly, Cherry:Mtm overexpressing hemocytes had a phenotype that appeared opposite to that of *mtm* null mutants. While *mtm*-deficient hemocytes are characterized by round, smooth edges, the *mtm*-overexpressing cells displayed a dramatic increase in both the length and number of radially-extended filopodial protrusions (Fig. 12A-B). Nearly all *mtm* overexpressing cells contained at least 4-5 times more cellular protrusions which were often at least twice the length as those seen in wild-type hemocytes. Altogether, both the loss and gain of function results demonstrate the sensitivity of actin cytoskeletal organization and protrusion formation to both decreases as well as increases in *mtm* levels.

Mtm loss of function affects the morphological dynamics of hemocytes

The cytoskeletal defects seen in fixed and stained *mtm* mutant hemocytes suggest a role for *mtm* in regulating and maintaining normal F-actin and

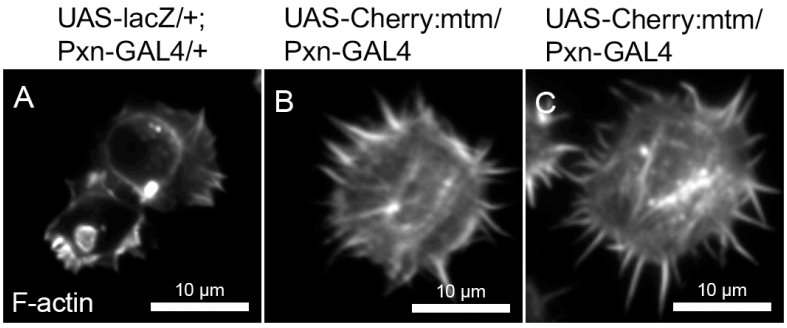

Figure 12: Cherry:Mtm overexpression affects hemocyte actin cytoskeleton organization

Morphology of Mtm overexpressing third-instar larval hemocytes stained for F-actin following attachment to and spreading on glass slides for 1 hour. UAS-lacZ and UAS-Cherry:Mtm expression was under the control of the Pxn-GAL4 driver. (**A**) LacZ overexpressing hemocytes spread in PBS. (**B-C**) Cherry:mtm overexpressing hemocytes.

microtubule cytoskeletal architecture necessary for protrusion formation. To determine whether the lack of cytoskeletal-rich protrusions caused by *mtm* loss of function was the result of reduced kinetics of remodeling, changes in the structures formed, or changes in the type of movements made, time lapse microscopy was utilized to study the dynamics of live hemocyte morphology. Using Pxn-GAL4 driven UAS-GFP expression to mark the cytoplasm of IR^{mtm} and lacZ-expressing hemocytes, live fluorescence microscopy was utilized to inspect the morphological dynamics of Mtm-deficient cells. Time-lapse imaging hemocytes revealed that wild-type hemocytes continuously extended and retracted radial extensions (Fig. 13A). In contrast, live IR^{mtm}-expressing hemocytes exhibited extensive membrane ruffling and smooth cell edges with a lack of protrusions, similar to what was seen in fixed and stained hemocytes (Fig. 13B). Rather than contain radially-projecting extensions, live cell imaging revealed that *mtm* RNAi cells possessed very short cellular protrusions that

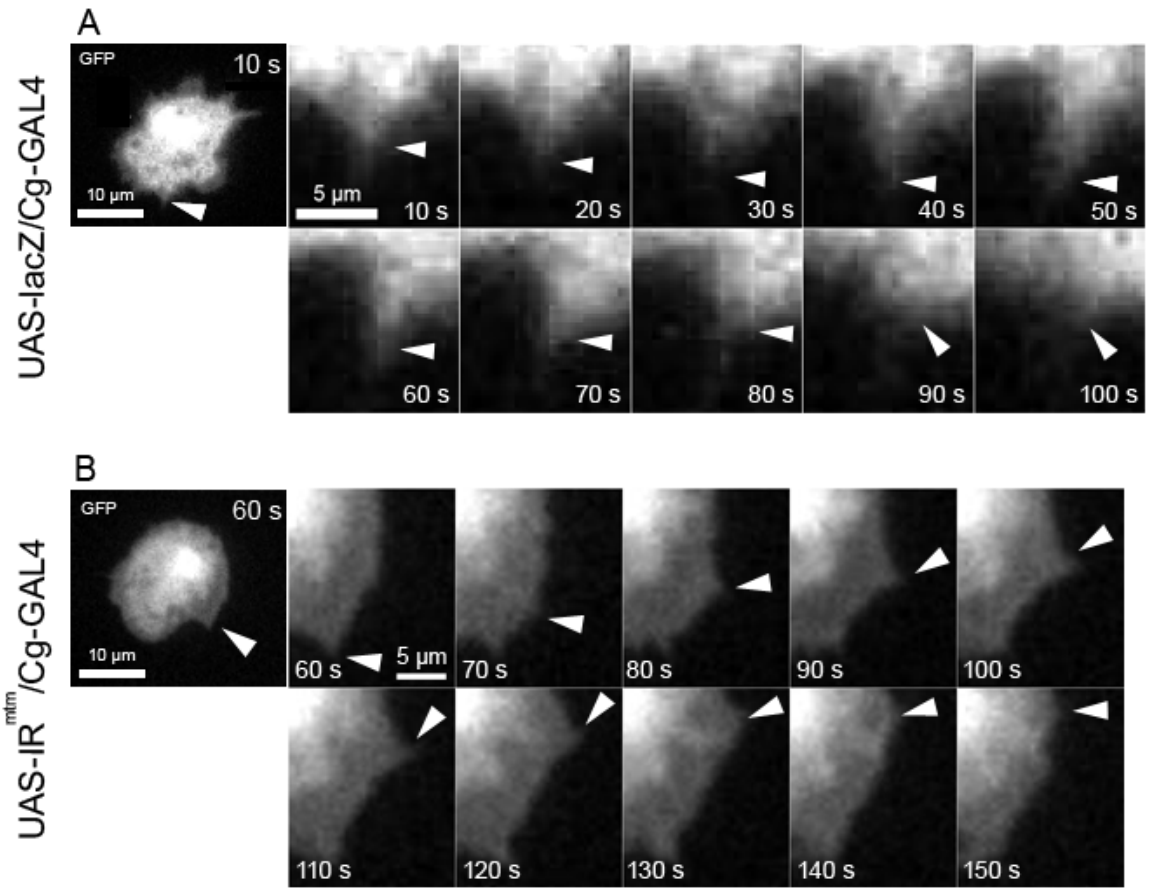

Figure 13: Morphological dynamics of Mtm-deficient hemocytes are abnormal compared to wild-type

Still images from time-lapse experiments examining the morphological dynamics of (**A**) lacZ and (**B**) UAS-IR^{mtm} overexpressing third-instar larval hemocytes. Arrowheads follow the trajectories of individual cellular protrusions. Images represent a single focal plane acquired with live fluorescence microscopy. Elapsed time in seconds is shown in the upper-right corner.

instead moved along the cell body (Fig. 13C). These results reveal that loss of *mtm* function in hemocytes did not disrupt the dynamics of hemocyte morphology, as both wild-type and mutant cells displayed morphological changes over the course of the time-lapse. Instead, *mtm* loss of function altered the type of movements and the type of structures made by hemocytes. This supports the involvement of wild-type *mtm* in regulating the specific remodeling events

required for the formation of cell protrusions rather than the ability of cells to remodel their cytoskeleton.

ENDOLYSOSOMAL MEMBRANES AND PHOSPHOINOSITIDE REGULATION

Phosphoinositides provide spatiotemporal regulation through which aspects of cellular morphogenetic programs occur. The predicted phosphoinositide phosphatase activity of *mtm* therefore suggests that the control of cellular morphogenesis by *mtm* occurs through phosphoregulation of specific phosphoinositide pools. To relate *mtm* biochemical and cellular functions, we wanted to explore the effects of *mtm* on its reported substrates PI(3)P and $PI(3,5)P_2$, the roles of *mtm* in maintaining endolysosomal membrane homeostasis through phosphoinositide regulation, and the contributions of these cellular events to morphogenesis in *Drosophila* hemocytes.

Mtm loss of function in hemocytes results in enlarged lysosomes

Endosomes play critical roles in maintaining membrane homeostasis throughout the cell by providing the intersection to various membrane trafficking routes. Due to the presence of known *mtm* substrates [PI(3)P and $PI(3,5)P_2$] at endolysosomal compartments and because of our previous work demonstrating a role for *mtm* in regulating endolysosomal membrane trafficking in cell cultures, *mtm* phosphatase activity at these sites could serve to regulate endolysosomal membrane and protein trafficking routes crucial for cellular morphogenic

processes. To explore the roles for *mtm* in endolysosomal membrane trafficking and homeostasis, the lysosome size of *mtm*-deficient hemocytes was analyzed through use of live fluorescence microscopy. Lysosomal homeostasis was examined because of the presence of an *mtm* substrate, $PI(3,5)P_2$, at these organelles. It would be predicted that lack of $PI(3,5)P_2$ turnover at the lysosomes may affect the dynamics of membrane influx and/or efflux from the lysosomal compartments. To visualize the lysosomes, Lysotracker was used to label acidic organelles (i.e., late endosomes and lysosomes) within live cells. Trans-heterozygous *mtm* mutant hemocytes exhibited enlarged endolysosomes when compared to wild-type (Fig. 14A-B). Hemocyte-specific knockdown of *mtm* also resulted in an increase in endolysosome size when compared to hemocyte controls (Fig. 14C). Though each condition exhibited a range of lysosome sizes, lysosomes in *mtm* mutant conditions were often several times larger than those in wild-type cells, similar to what was described with *mtm* RNAi in Kc cell cultures. Hemocytes containing normally sized lysosome upon co-expression of *mtm:GFP* indicate the specificity of *mtm* RNA and its function in lysosome homeostasis (Fig. 14A, 14D). Together, such results suggest a requirement for *mtm*-mediated phosphoinositide turnover in regulating the dynamics of lysosome size. However, other possibilities regarding the relationship between *mtm* activity and lysosome size exist. Subsequent studies done in our lab have also shown that Rab7-positive late endosomes are also significantly enlarged with *mtm*

Figure 14: Enlarged lysosomes of *mtm* mutants

Size of LysoTracker-stained compartments in third-instar larval hemocytes spilled into complete media from late third-instar larvae of various *mtm* mutants. Lysosomes in hemocytes spilled from (**A**) controls and (**B**) *mtm* homozygous mutants. Lysosomes in hemocytes undergoing Cg-GAL4 driven (**C**) GFP overexpression in *mtm* depleted cells did not rescue lysosome size phenotypes, (**D**) Mtm:GFP was able to rescue the effects of IR^{mtm} expression. (**E)** Mtm:GFP overexpression on its own did not noticeably affect lysosome size

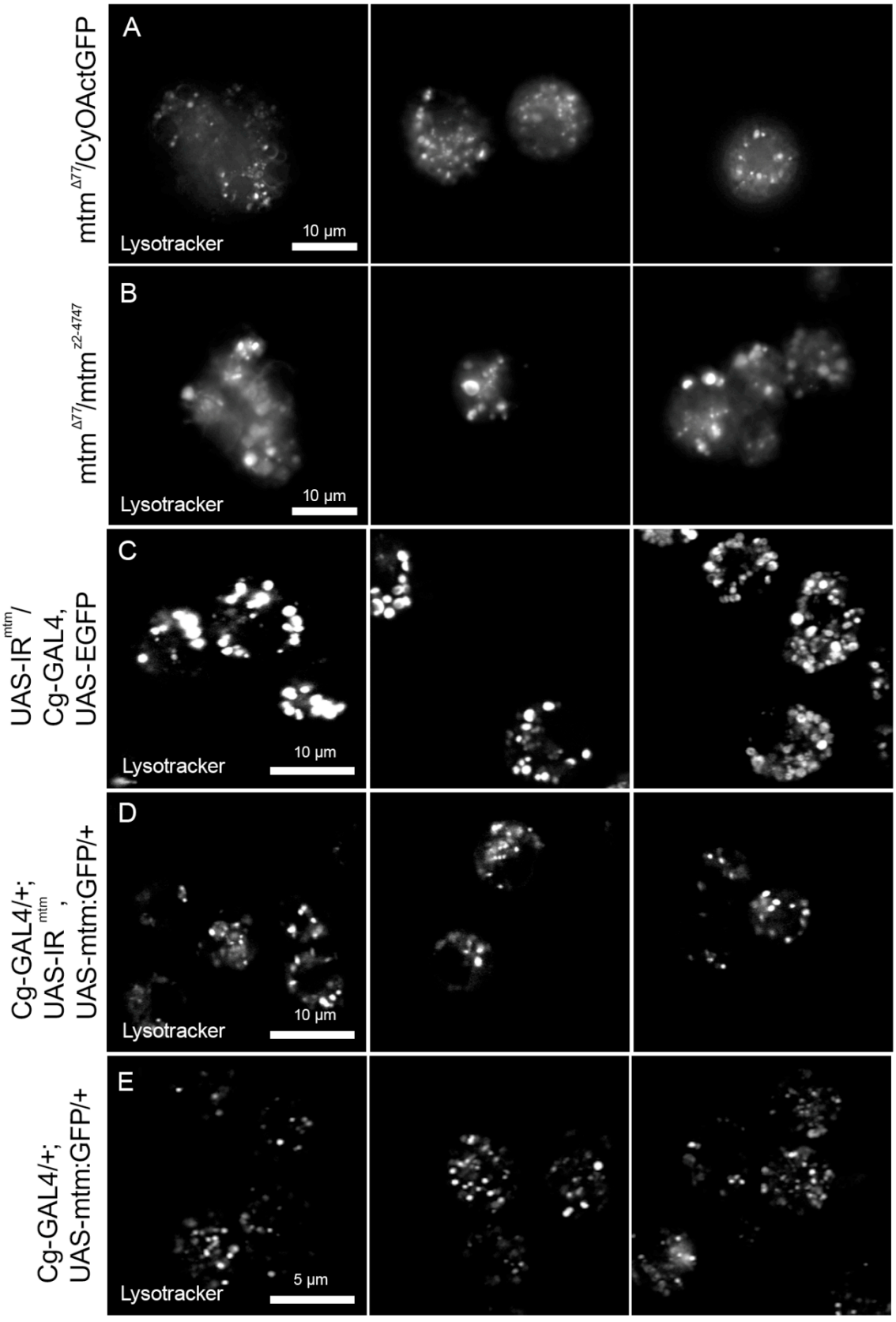
A
mtm Δ77/CyOActGFP
Lysotracker
10 µm
B
mtm Δ77/mtm z2-4747
Lysotracker
10 µm
C
UAS-IR mtm /
Cg-GAL4,
UAS-EGFP
Lysotracker
10 µm
D
Cg-GAL4/+;
UAS-IR mtm ,
UAS-mtm:GFP/+
Lysotracker
10 µm
E
Cg-GAL4/+;
UAS-mtm:GFP/+
Lysotracker
5 µm

knockdown, suggesting that this may actually be primary site affected by *mtm* loss of function (M. Velichkova, A. Kiger, unpublished work).

To determine whether endolysosomal membrane homeostasis is also sensitive to increases in *mtm* function, the effect of Mtm:GFP overexpression on hemocyte lysosome size was investigated. Despite the ability of the Mtm:GFP fusion protein to rescue the *mtm* RNAi lysosomal size defects, overexpression of Mtm:GFP did not noticeably reduce or affect lysosome size in hemocytes (Fig. 14E). Therefore, while the presence of *mtm* function is necessary to maintain normal lysosome size, an increase of *mtm* gene product above wild-type levels is not sufficient to induce an opposite effect on lysosomal membrane homeostasis. One possible interpretation to the *mtm* overexpression results is that *mtm* function at the lysosomes may require a limiting adaptor or cofactor. In this case, overexpression of *mtm* to levels above the saturation point for the endogenous cofactors would not result in additional increases to *mtm* activity (at least for functions requiring these adaptor proteins). Another interpretation is that *mtm* affects processes which are unable to produce a phenotype opposite of *mtm* loss of function. For example, Lysotracker-detected endolysosomes may have a minimum size below which these cellular compartments either cannot form or be detected.

Mtm-deficient hemocytes exhibit increases in 2xFYVE-detected PI(3)P

Because myotubularin is a predicted phosphatidylinositol 3-phosphate phosphatase (Laporte et al., 2002), we is hypothesize that the effects of *mtm* activity on cellular morphogenic processes occurs through changes in the localizations and concentrations of specific PIP species or subpools. Previous results indicated an accumulation of PI(3)P above wild-type levels upon *mtm* RNAi in Kc cell cultures. It was therefore important to establish the effects of *mtm* function on PI(3)P levels and distributions. To accomplish this, the effects of *mtm* loss of function or overexpression on PI(3)P concentration and localization, as detected by the Cherry:2xFYVE biosensor, was investigated in hemocytes using live fluorescence microscopy. Knockdown of *mtm* altered PI(3)P distribution. Whereas wild-type lacZ-expressing hemocytes exhibited a few moderately-sized Cherry:2xFYVE-positive dots and ring structures, IR^{mtm}-expressing hemocytes experienced an estimated four to five-fold increase in the number of Cherry:2xFYVE-positive compartments (Fig. 15A-B). Stronger knockdown of *mtm* through the introduction of additional copies of the IR^{mtm} construct increased the size of the individual Lysotracker-positive compartments (Fig. 15C). In contrast, overexpression of the UAS-Mtm:GFP transgene using the Cg-GAL4 driver had an opposite effect on PI(3)P levels. Although not sufficient to completely eliminate Cherry:2xFYVE puncta formation, overexpression of the Mtm fusion protein led to a significant decrease in Cherry:2xFYVE-positive compartments and converted the normally punctate Cherry:2xFYVE staining to a

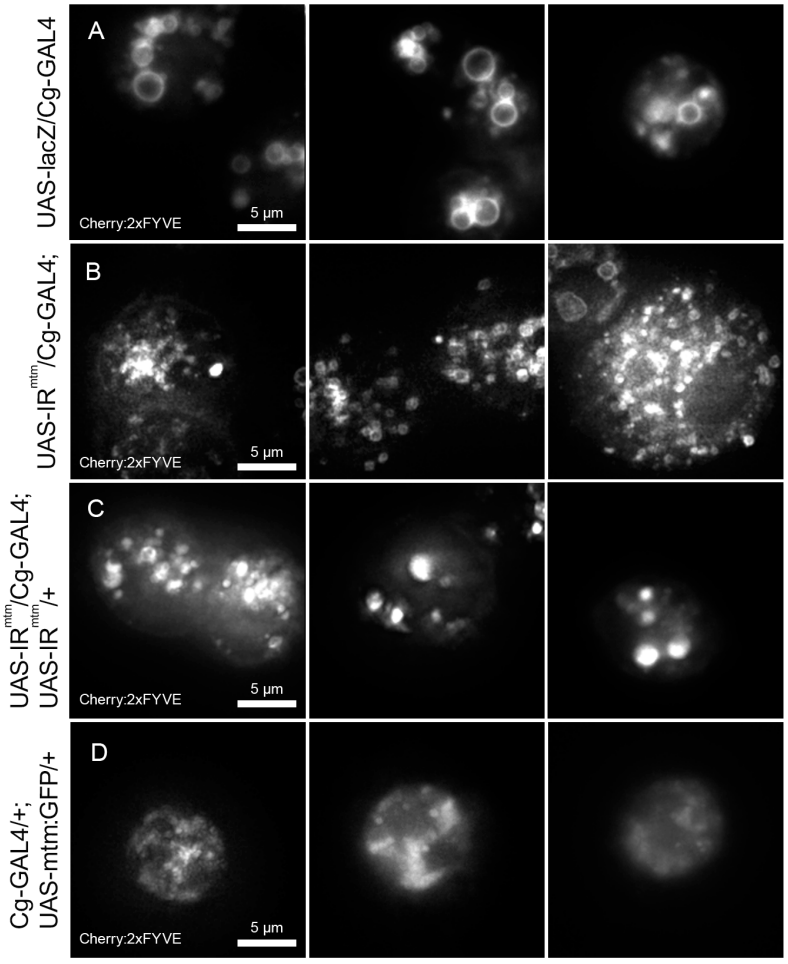

Figure 15: Mtm protein levels inversely affect cellular PI(3)P levels

2xFYVE-detectable levels of Cherry:2xFYVE-positive compartments following Cg-GAL4-driven overexpression of (**A**) UAS-lacZ, (**B**) UAS-IR^{mtm}. (**C**) UAS-IR^{mtm}, UAS-IR^{mtm}, and (**D**) UAS-Mtm:GFP in third-instar larval hemocytes. Images were acquired via fluorescence microscopy and represent Z-projections of multiple focal planes.

diffuse cytoplasmic distribution (15D). Consistent with its role as a PI(3)P phosphatase, these results indicate that *mtm* overexpression leads to an abolition of PI(3)P and dispersal of the PI(3)P-localized FYVE-domain-containing biosensor. Together, these findings suggest that PI(3)P levels are inversely

correlated to Mtm protein concentration and support the classification of *mtm* as a PI(3)P phosphatase.

Depletion of class II Pi3K68D completely rescues *mtm* RNAi defects in hemocytes

Previous results implicated an *mtm*-dependent PI(3)P subpool with roles in endolysosomal homeostasis and cellular elongation defects in cell culture. In Kc cells, reductions in the synthesis of specific PI(3)P pools via co-RNAi depletion of the class II lipid kinase, *Pi3K68D*, rescued all *mtm* RNAi phenotypes. To test whether animal viability, hemocyte morphology, and membrane homeostasis defects caused by *mtm* loss of function *in vivo* are also due to the misregulation of specific phosphoinositide concentrations and/or distributions, we tested the ability of Pi3K68D co-depletion to similarly rescue *mtm* RNAi in hemocytes.

To determine whether the endolysosomal membrane trafficking defects caused by *mtm* RNAi could be rescued by inihibiting the synthesis of specific PI(3)P pools, we tested whether co-disruption of class II *Pi3K68D* could rescue IR^{mtm} defects. Cg-GAL4-driven co-expression of *Pi3K68D* and *mtm* RNAi hairpins in hemocytes rescued enlarged lysosomes, while GFP co-expression did not (Fig. 16A-C). *Pi3K68D* knockdown alone did not appear to have a lysosome size phenotype opposite of *mtm* RNAi hairpin expression (Fig. 16D). This suggests that while accumulation of specific PI(3)P pools results in enlarged lysosomes, a predicted reduction in Pi3K68D-dependent PI(3)P pools is not sufficient to affect

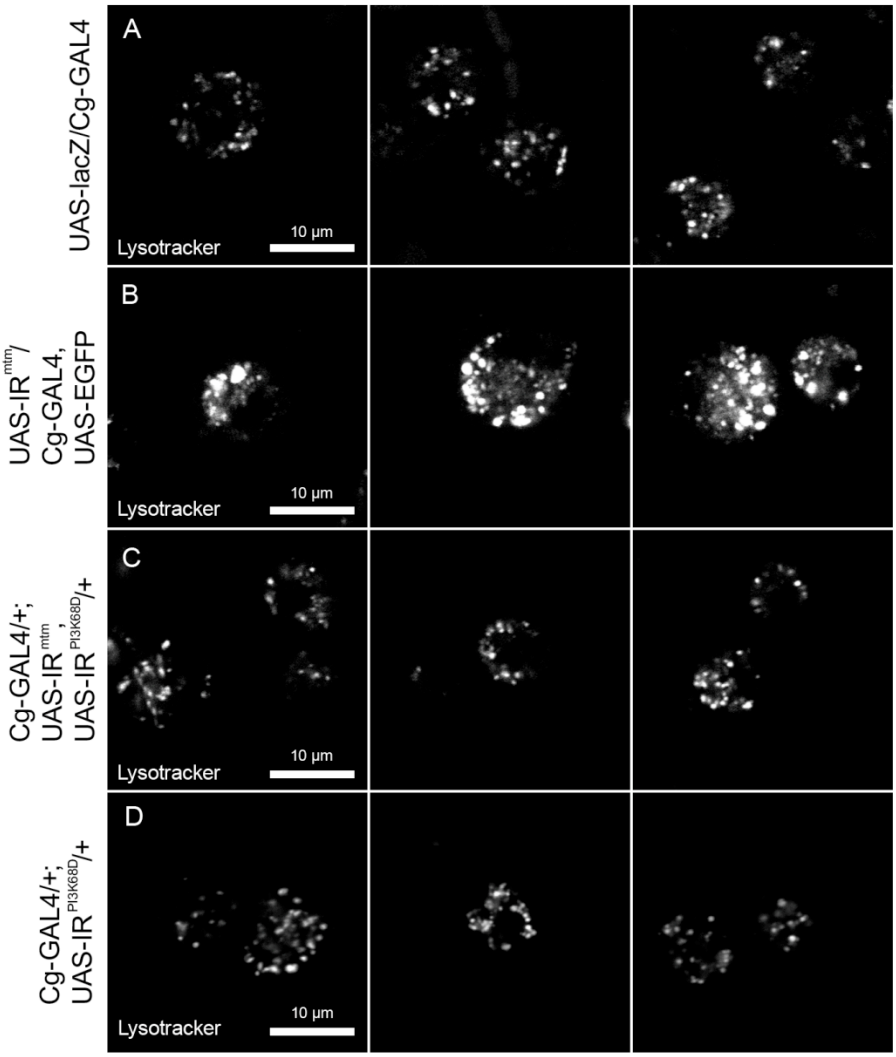

Figure 16: Depletion of class II Pi3K68D in Mtm-deficient hemocytes rescues the enlarged lysosome phenotype

Lysosome size in LysoTracker stained third-instar larval hemocytes expressing various UAS-IR^{mtm} and UAS-IR^{Pi3K68D} transgene combinations via the Cg-GAL4 driver. Lysosome size of (**A**) UAS-lacZ, (**B**) UAS-IRmtm, UAS-EGFP, and (**C**) UAS-IRmtm, UAS-IRPi3K68D expressing hemocytes spread in complete media. (**D**) LacZ and (**E**) IR^{Pi3K68D} overexpressing hemocytes. Images were taken via live fluorescence microscopy and represent a single focal plane.

lysosome size. The rescue of IR^{mtm}-related defects with *Pi3K68D* depletion suggests that the endolysosomal defects caused by *mtm* knockdown are mediated through abnormal accumulations and/or localizations of PI(3)P,

although there remains the possibility that these defects are due to the effects of *mtm* depletion on the concentrations and/or distributions of interrelated PIP subpools.

To determine whether *Pi3K68D* depletion could suppress *mtm* RNAi hemocyte morphology phenotypes, the F-actin cytoskeleton organization of phalloidin-546 stained *mtm* RNAi hemocytes were compared to wild-type cells. Co-expression of the *Pi3K68D* and *mtm* RNAi hairpins produced hemocytes exhibiting wild-type cell morphologies with normal F-actin-rich protrusions (Fig. 17A, 17B). Similar to lacZ-expressing control cells, hemocytes depleted of both *Pi3K68D* and *mtm* exhibited about a dozen, moderately-sized and radially extend F-actin-rich protrusions. In contrast, co-expression of the UAS-GFP construct with the UAS-IR^{mtm} construct did not (Fig. 17C). Therefore, similar to the ability of *Pi3K68D* depletion to rescue lysosome size, *Pi3K68D* depletion in *mtm* loss of function mutants was able to rescue the *mtm* mutant actin cytoskeleton phenotypes presumably due to the predicted reduction in PI(3)P levels.

As the above results demonstrate the ability of Pi3K68D knockdown in *mtm*-deficient cells to restore the normal operation of *mtm*-dependent processes, the functional relevance of restoring these processes was next investigated. In $IR^{Pi3K68D}$ and IR^{mtm} co-expressing animals, the lethality caused by hemocyte-specific Mtm-deficiency was rescued (Table 4), suggesting that *mtm* and *Pi3K68D*-dependent hemocyte functions, which we predict regulates phosphoinositide concentrations and distributions, are important for fly viability.

Figure 17: Depletion of class II Pi3K68D in Mtm-deficient hemocytes rescues the the actin cytoskeleton mutant phenotype

Morphology of phalloidin-546 stained third instar hemocytes expressing (**A**) lacZ, (**B**) IR^{mtm}, $IR^{Pi3K68D}$, (**C**) IR^{mtm}, GFP, and (**D**) $IR^{Pi3K68D}$. Co-expression of $IR^{Pi3K68D}$ with IR^{mtm} is sufficient to rescue the mutant F-actin cytoskeleton phenotypes while co-expression of GFP with IR^{mtm} does not rescue these morphological defects. Knockdown Pi3K68D alone does not produce a mutant phenotype.

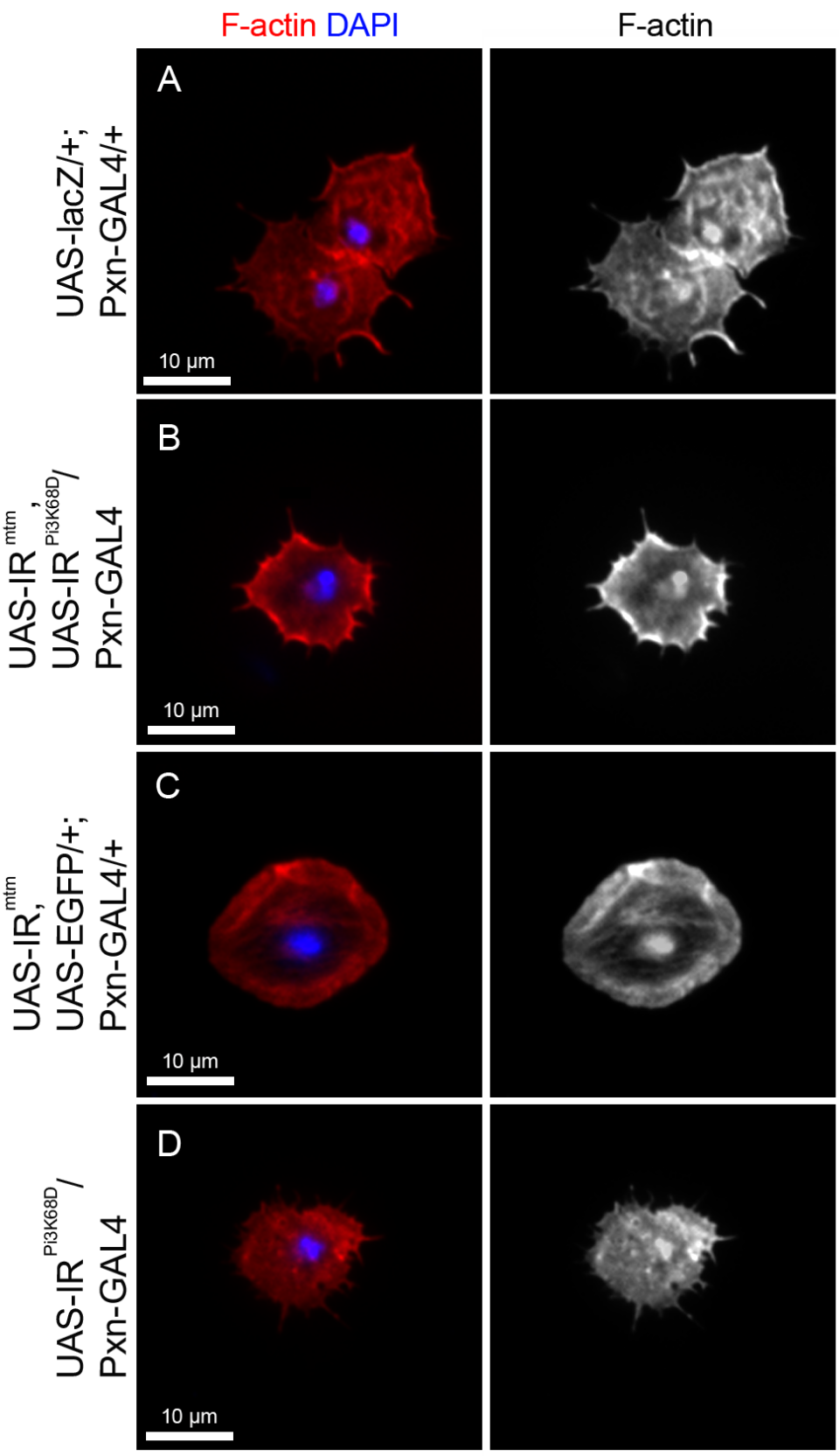
F-actin DAPI
F-actin
A
UAS-lacZ/+;
Pxn-GAL4/+
10 µm
B
UAS-IR mtm,
UAS-IR Pi3K68D/
Pxn-GAL4
10 µm
C
UAS-IR mtm,
UAS-EGFP/+;
Pxn-GAL4/+
10 µm
D
UAS-IR Pi3K68D/
Pxn-GAL4
10 µm

Table 4: RNAi-mediated depletion of Pi3K68D in *mtm* depleted hemocytes rescues lethality, while *Pi3K68D* depletion alone does not affect fly viability

GAL4 Driver	Expression Pattern	UAS-construct	Phenotype	Comments
Cg-GAL4	Hemocytes and fat body	UAS-lacZ	Viable	Adult flies are wild-type
		UAS-IR^{mtm}	Lethal	Pharate adults and mid-eclosion.
		UAS-IR^{mtm}, UAS-GFP	Lethal	Pharate adults and mid-eclosion.
Pxn-GAL4	Hemocytes	UAS-IR^{mtm}, UAS-IR^{Pi3K68D}	Viable	Adult flies are wild-type
		UAS-IR^{Pi3K68D}	Viable	Adult flies are wild-type

Lethal phase of animals carrying various combinations of the UAS-IR^{mtm} and UAS-IR^{Pi3K68D} transgenes under the control of hemocyte-specific GAL4 drivers.

RNAi against *Pi3K68D* alone was not lethal. The inability of *Pi3K68D* depletion in hemocytes to produce mutant phenotypes may be due to compensatory kinase activities triggered from the class I or class III PI 3-kinases when cellular PI(3)P levels are reduced below certain thresholds.

Creation and localization of functional fluorescently tagged Mtm

It is postulated that the strict spatiotemporal control of phosphoinositides requires the restriction of phosphoinositide kinase and phosphatase activity to specific subcellular domains. Therefore, identification of the sites of Mtm phosphatase activity within the cell will help elucidate which cellular mechanisms important in cellular morphogenesis are dependent on *mtm* function. To identify Mtm protein localization via fluorescence microscopy, UAS-controlled protein

fusion constructs for fluorescent, N-terminally tagged Mtm proteins were first created (UAS-GFP:Mtm and UAS-Cherry:Mtm; simultaneously, UAS-3xFLAG:Mtm and UAS-Mtm:6xMyc constructs were also created for use in other projects). Although a UAS-Mtm:GFP construct was already available, it could not be used for colocalization studies utilizing available GFP-tagged cellular markers. Also, due to the possibility that fluorescent tags fused to the C-terminus of Mtm might affect its localization by disrupting possible protein-protein interactions occurring at the coiled-coil domain, the creation of additional N-terminally tagged constructs for *in vivo* localization studies was necessary.

To create UAS-controlled *mtm* constructs, the wild-type *mtm* cDNA was introduced into the appropriate pUAST destination vectors. PCR sequencing was used to verify the in-frame insertion of the *mtm* cDNA into each destination vector (data not shown) and the expression of full-length protein was confirmed via Western blot for the GFP, myc, and FLAG tagged constructs (Fig. 18). Expression of full-length Mtm protein from the GFP:Mtm and Cherry:Mtm constructs was also confirmed by comparing the localization pattern of the transgenic protein products to the products of the C-terminally tagged UAS-Mtm:GFP construct (previously determined to be a full-length protein which can rescue Mtm loss of function phenotypes), and to GFP alone.

Creation of transformed flies allowed for the examination of Mtm protein localization patterns in hemocytes expressing the UAS-Mtm:GFP, UAS-

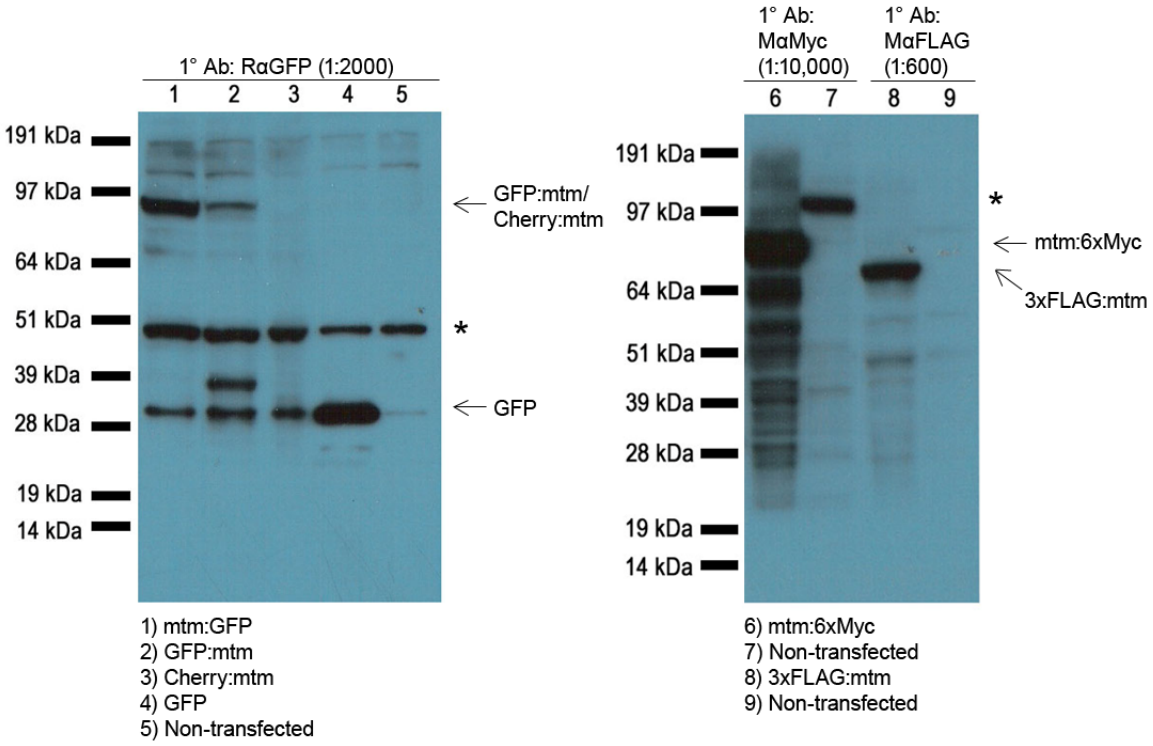

Figure 18: UAS-controlled Mtm fusion protein constructs produce full-length Mtm proteins

Size of tagged proteins expressed from UAS-Mtm:GFP, UAS-GFP:Mtm, UAS-Cherry:Mtm, UAS-Mtm:6xMyc, and UAS-3xFLAG:Mtm constructs. Arrows indicate the expected size of each Mtm fusion protein. Asterisk marks non-specific bands.

Cherry:Mtm, UAS-GFP:Mtm, and UAS-GFP transgenes under control of the Cg-GAL4 driver. Both C- and N-terminally tagged proteins exhibited a cytoplasmic localization pattern distinct from that of GFP alone, with enriched accumulation in discrete regions and exclusion from the nucleus as well as some unidentified compartments. Interestingly, the N-terminally tagged Mtm fusion proteins were less cytoplasmic and more punctate in localization than the C-terminally tagged proteins (Fig. 19A-D). In addition, the N-terminally tagged proteins also exhibited a perinuclear localization not found with the C-terminally tagged protein. Similar

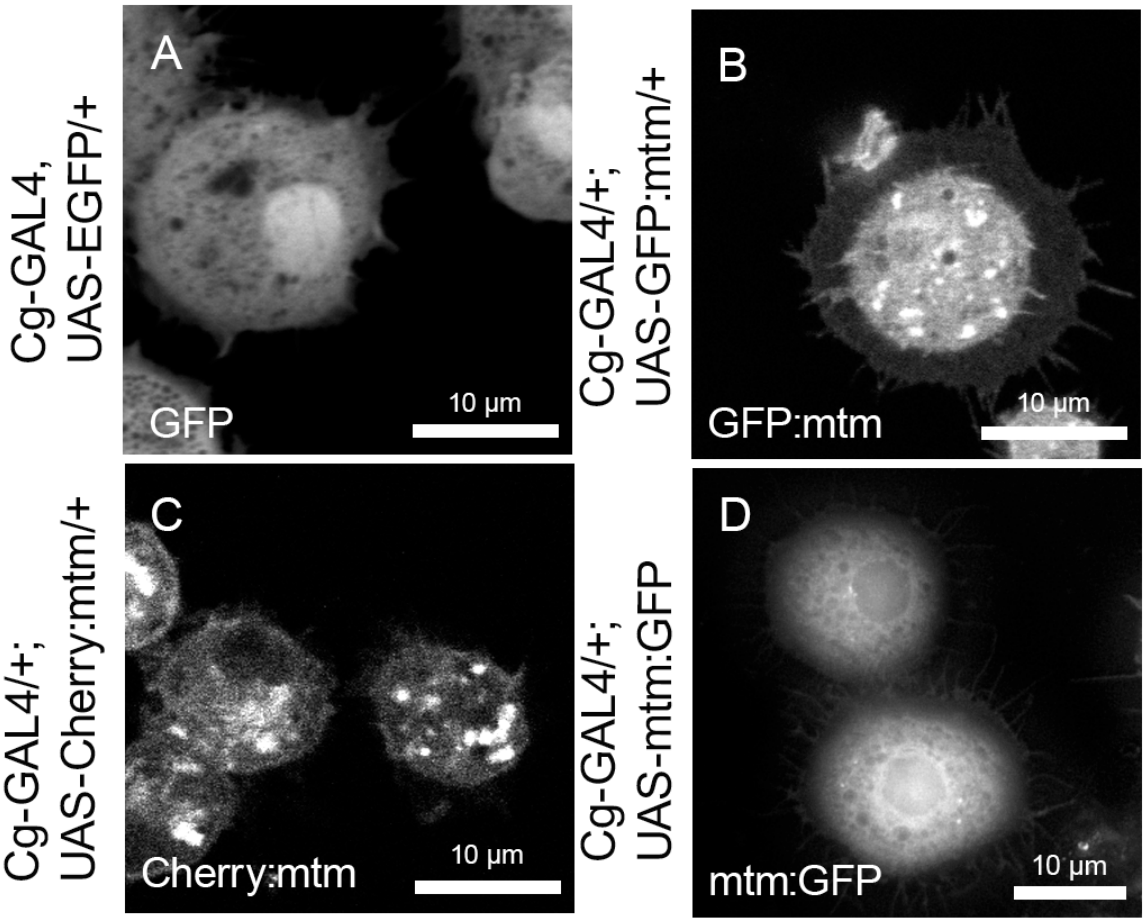

Figure 19: N-terminally tagged Mtm fusion proteins exhibit punctate localization patterns while C-terminally tagged Mtm fusion proteins display a more cytoplasmic distribution

Distribution pattern of (**A**) GFP, (**B**) GFP:Mtm, (**C**) Cherry:Mtm, and (**D**) Mtm:GFP in spread third-instar larval hemocytes spilled into full media. Images were taken via live fluorescence microscopy and represent a single focal plane.

localization patterns were also observed in transfected Kc cells (data now shown).

Given the slight differences in localization between the C- and N-terminally tagged proteins and the previously established functionality of the Mtm:GFP protein (through its ability to reduce PI(3)P levels and complement *mtm* RNAi phenotypes), the possibility arose that the N-terminally tagged proteins

were mislocalized and/or inactive. It was therefore necessary to test function of these N-terminally tagged proteins for their ability to affect PI(3)P concentrations and distributions. Using either Cherry:2xFYVE or GFP:2xFYVE to mark PI(3)P, transfection and subsequent overexpression of either UAS-Cherry:Mtm or UAS-GFP:Mtm in Kc cells resulted in a dispersal of GFP:2xFYVE or Cherry:2xFYVE from its normal punctate localization to a mostly diffuse cytoplasmic distribution (Fig. 20). These results confirm the ability of the N-terminally tagged Mtm proteins to perform their normal functions involving PI(3)P turnover.

Mtm protein localizes to puncta and motile particles

To better understand the nature of Mtm localization throughout the cell, the dynamics of these accumulations were determined via time-lapse microscopy. The goal was to determine whether Mtm remained docked to defined sites or instead were highly dynamic and existed on motile particles that were possibly vesicles trafficking to or from organelles. Overexpression of GFP:Mtm, Cherry:Mtm, or Mtm:GFP was induced in hemocytes, and the localization of each fusion protein was imaged by timelapse microscopy. Similar to what was seen previously in static images, the N-terminally tagged proteins exhibited punctate and perinuclear localizations. Time-lapse imaging also revealed that Mtm accumulations on smaller puncta displayed dynamic behavior typical of vesicles. While larger Mtm puncta remained for the most part static, smaller Mtm particles exhibited directed motility. There also appeared to be the

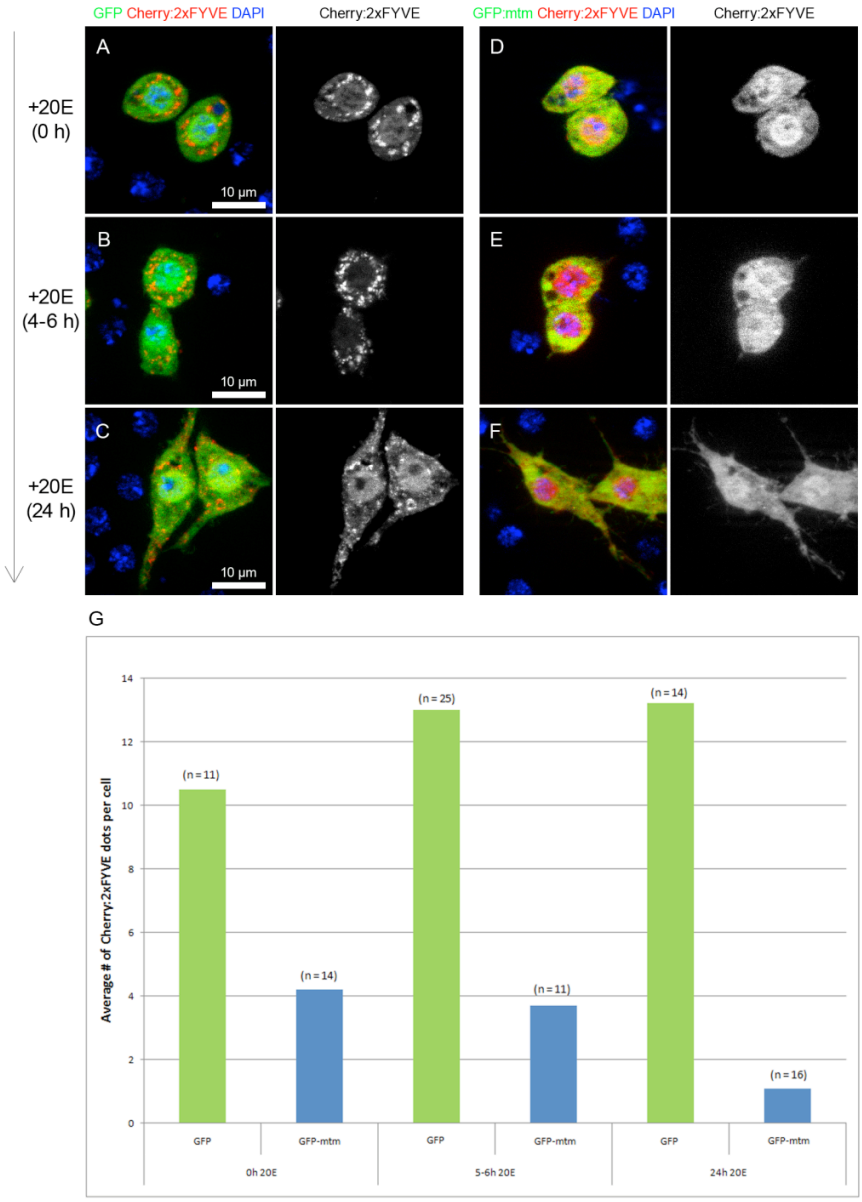

Figure 20: Overexpression of N-terminally tagged Mtm proteins mediates increased PI(3)P turnover

Kc cells transfected with and overexpressing the UAS-GFP:Mtm or UAS-GFP expression vectors in conjunction with the UAS-Cherry2x:FYVE construct. Kc cells were kept in complete media and elongation was induced via addition of the ecdysone hormone to this media at various time-points. Cherry:2xFYVE distribution in GFP overexpressing Kc cells (**A**) 0 hours, (**B**), 4-6 hours, and (**C**) 24 hours following addition of ecdysone. Cherry:2xFYVE distribution in GFP:Mtm overexpressing Kc cells (**D**) 0 hours, (**E**), 4-6 hours, and (**F**) 24 hours following addition of ecdysone. Images were acquired using live fluorescence microscopy and represent Z-projections of multiple focal planes. (**G**) Automated quantification (using CellProfiler) of the number of Cherry:2xFYVE puncta in each GFP or GFP:Mtm overexpressing condition.

fusion and fission of these smaller Mtm-containing structures with one another (Fig. 21A-B). The movement of the smaller Mtm particles seemed to be within a defined, larger structure, whose relative location remained fairly static. The C-terminally tagged Mtm:GFP protein was more cytoplasmic in its localization than the N-terminally tagged proteins. Despite increased cytoplasmic localization, Mtm:GFP also localized to discrete sites that exhibited a dynamic nature as they frequently formed and disappeared over the course of the time-lapse videos (Fig. 21C). Thus, these results suggest that puncta formed by the Mtm fusion proteins may represent their localization to motile particles, which are likely membrane compartments.

Mtm protein localizes at or near PI(3)P and PI(3,5)P_2 in both hemocytes and Kc cells

To elucidate the possible identity of Mtm sites of activity, I next explored Mtm sub-cellular colocalization. With the hypothesis that morphogenic *mtm* roles are mediated through phosphoinositide regulation, and that PI(3)P and PI(3,5)P_2 are both substrates for Mtm phosphatase activity, one possible site of Mtm localization could be at or adjacent to PI(3)P and PI(3,5)P_2-rich compartments. To test this proposal, the distributions of fluorescently tagged Mtm proteins in relation to markers for PI(3)P and PI(3,5)P_2 were analyzed in both Kc cells and hemocytes. Localization of Mtm in relation to PI(3)P was examined in elongating Kc cells co-transfected with the UAS-Cherry:2xFYVE and UAS-GFP:Mtm

Figure 21: Mtm fusion proteins exhibit dynamic, vesicle-like behavior

Still images from time-lapse experiments examining the dynamics of (**A**) Cherry:Mtm, (**B**) GFP:Mtm and (**C**) Mtm:GFP puncta in spread hemocytes undergoing Cg-GAL4-driven expression of the fluorescently tagged Mtm constructs. Images represent a single focal plane acquired with live fluorescence microscopy. Elapsed time in seconds is shown in the upper-right corner. Arrowheads indicate sites of potential *mtm* puncta formation, fusion, or fission.

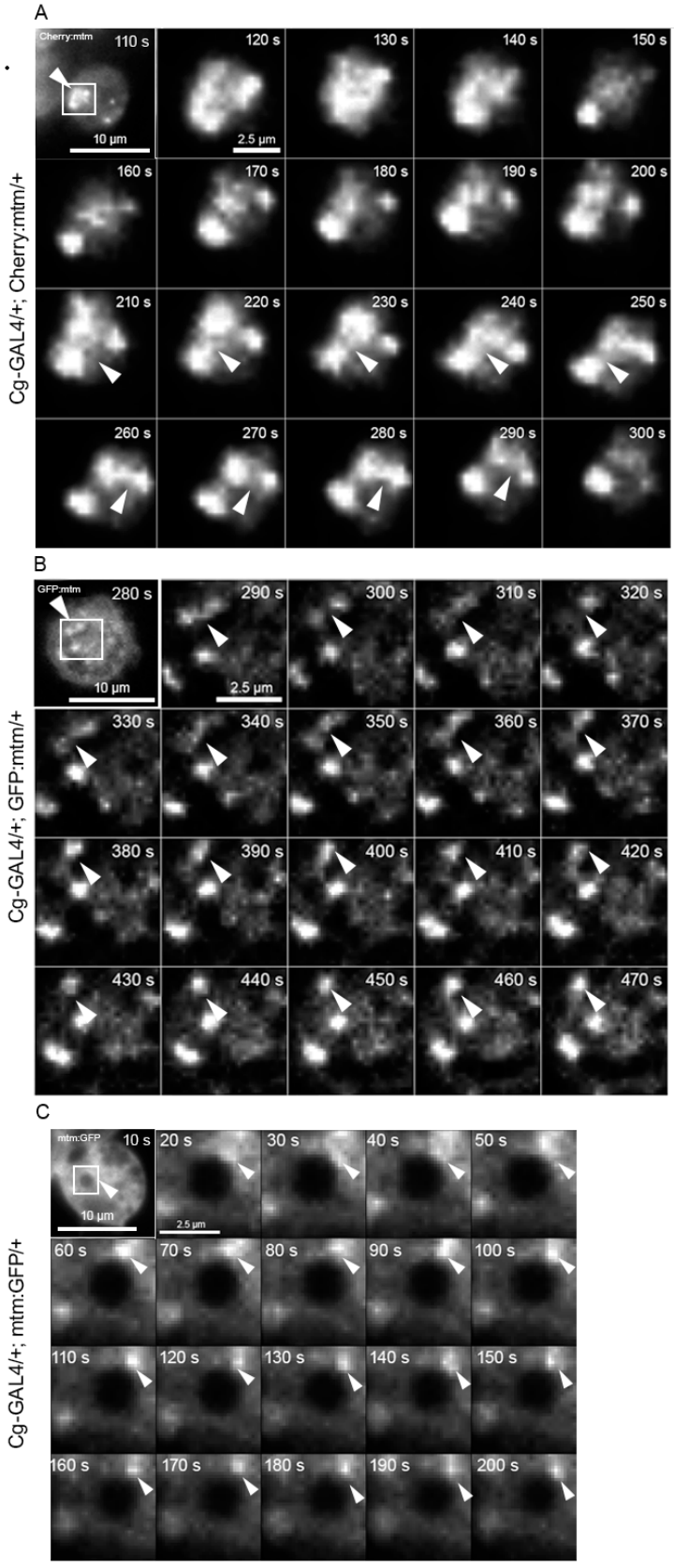
A
Cherry:mtm
110 s
120 s
130 s
140 s
150 s
10 µm
2.5 µm
160 s
170 s
180 s
190 s
200 s
210 s
220 s
230 s
240 s
250 s
260 s
270 s
280 s
290 s
300 s
Cg-GAL4/+; Cherry:mtm/+
B
GFP:mtm
280 s
290 s
300 s
310 s
320 s
10 µm
2.5 µm
330 s
340 s
350 s
360 s
370 s
380 s
390 s
400 s
410 s
420 s
430 s
440 s
450 s
460 s
470 s
Cg-GAL4/+; GFP:mtm/+
C
mtm:GFP
10 s
20 s
30 s
40 s
50 s
10 µm
2.5 µm
60 s
70 s
80 s
90 s
100 s
110 s
120 s
130 s
140 s
150 s
160 s
170 s
180 s
190 s
200 s
Cg-GAL4/+; mtm:GFP/+

constructs using live fluorescence microscopy. To determine the dynamics of Mtm localization in relation to PI(3)P-positive compartments during cellular remodeling, ecdysone hormone was added to these transfected cells to induce cellular elongation. However, GFP:Mtm localization in relation to PI(3)P could not be observed because the Mtm overexpression led to the almost complete dispersal of Cherry:2xFYVE localization (Fig. 20D-F). However, unlike in Kc cells, Mtm overexpression in hemocytes did not completely abolish localized PI(3)P domains. It was therefore possible to study Mtm localization in relation to remaining PI(3)P in hemocytes. Though little to no colocalization was observed, GFP:Mtm-enriched regions were often localized adjacent to Cherry:2xFYVE-positive structures (Fig. 22). Time-lapse imaging was performed on live GFP:Mtm and Cherry:2xFYVE-expressing cells to determine whether a dynamic relationship could be observed between Mtm and PI(3)P compartments. While relatively small GFP:Mtm and Cherry:2xFYVE-positive vesicles were motile and seemed to behave independent of one another, large accumulations of GFP:Mtm and Cherry:2xFYVE were often found stably localized adjacent to one another (Fig. 23), indicating that overexpressed Mtm protein localized near the remaining sites of PI(3)P accumulation *in vivo*.

One caveat in the interpretation of the co-localization data is that overexpression of *mtm* in hemocytes may cause complete elimination of the PI(3)P pools *mtm* normally acts on *in vivo*, and therefore remaining FYVE-detected PI(3)P pools may represent subpools not normally regulated by *mtm*.

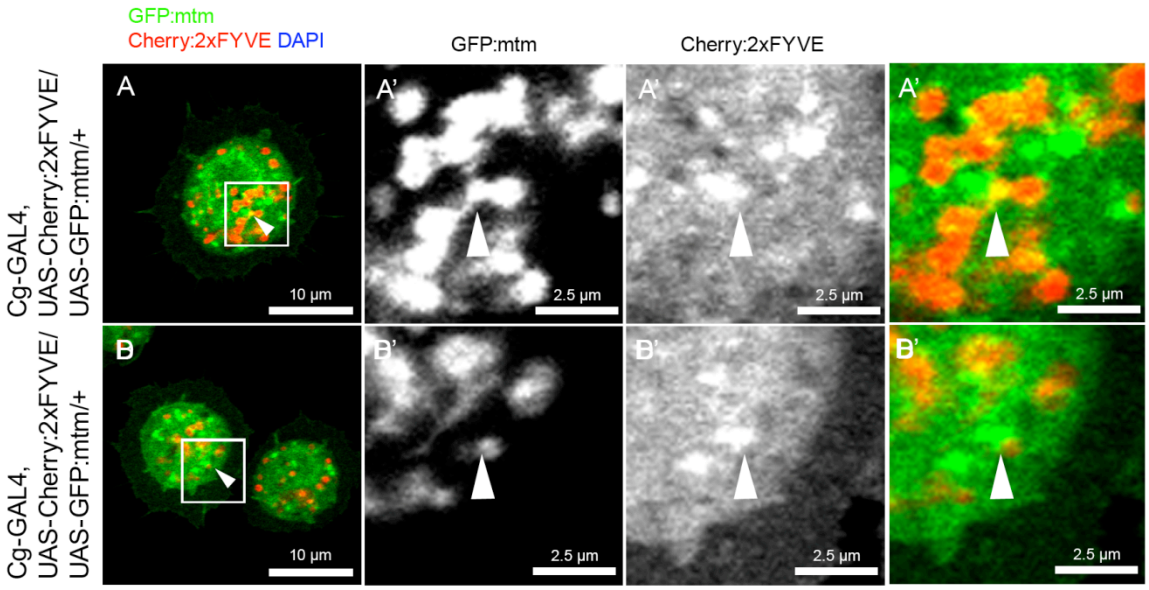

Figure 22: GFP:Mtm partially localizes to sites adjacent to Cherry:2xFYVE-positive structures in spread hemocytes

Spatial relationship of GFP:Mtm to Cherry:2xFYVE-positive structures in third-instar larval hemocytes spread in complete media(**A-F)**. UAS- transgene expression was induced with Cg-GaL4. Arrowheads indicate sites of colocalization. Images were acquired using live fluorescence microscopy and represent single focal planes. (**A', D'**) Enlarged images highlighy regions of partial colocalization.

The localization of GFP:Mtm near FYVE-positive membrane domains may not reveal its normal distribution with respect to its normal substrate. To get around the complications caused by overexpression of an active phosphatase, the localization of *mtm* in relation to PI(3)P can be investigated through use of antibody staining for Mtm upon generation of specific anti-Mtm antibodies with the PI(3)P 2xFYVE biosensor. We could also look at the localization of a phosphatase-dead form of *mtm* to prevent the inappropriate elimination of its *in vivo* substrates following overexpression.

To study Mtm localization in relation to $PI(3,5)P_2$, a GFP:Atg18 biosensor was used (though this protein is also reported to bind PI(3)P subpools). Kc cells

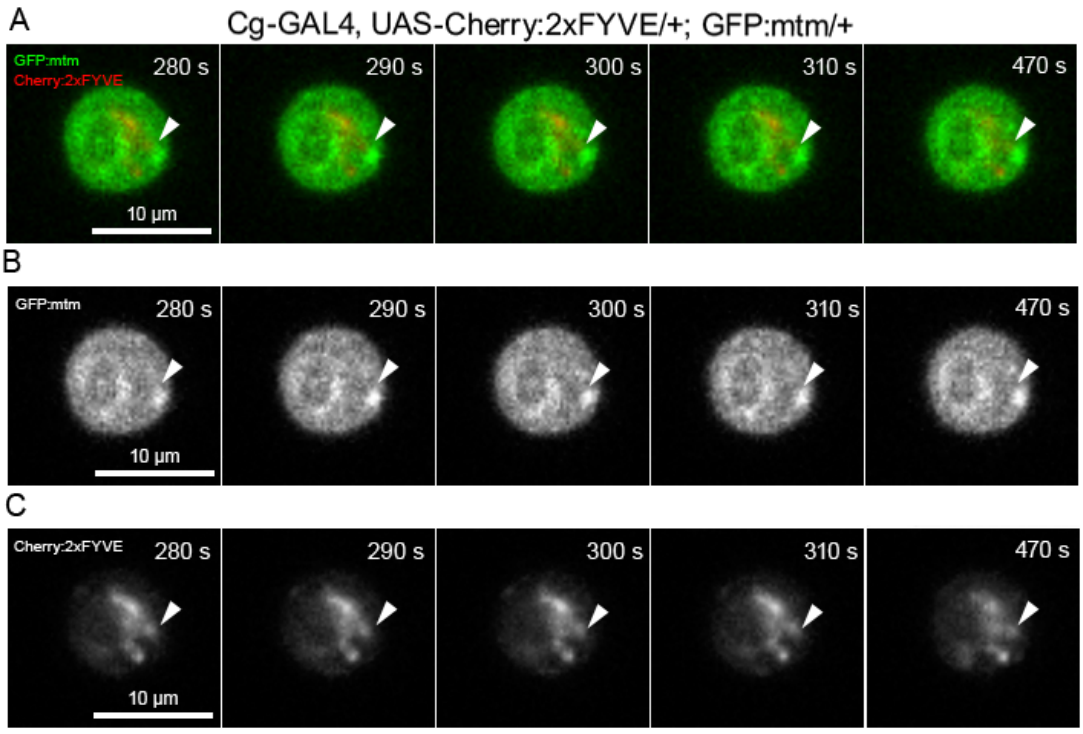

Figure 23: Mtm:GFP puncta are stably anchored to Cherry:2xFYVE-positive organelles

Still images from time lapse experiments examining the dynamics of Mtm:GFP localization in relation to Cherry:2xFYVE in hemocytes. Hemocytes were spilled from UAS-Cherry:2xFYVE, UAS-Mtm:GFP transgene carrying third-instar larvae. Expression of the UAS- transgenes was mediated through the Cg-GaL4 driver. Arrowheads indicate sites where GFP:Mtm puncta directly touch Cherry:2xFYVE-marked compartments in the (**A**) merged, (**B**) green, and (**C**) red channels. Images were acquired using live fluorescence microscopy and represent single focal planes. Elapsed time in seconds is shown in the upper-right corner.

were co-transfected with the UAS-Cherry:Mtm and UAS-GFP:Atg18 constructs, and elongation of these cells was induced with ecdysone. Unlike the Cherry protein alone, up to approximately one-half of all Cherry:Mtm puncta in each Kc cell co-localized with GFP:Atg18-positive compartments during all stages of elongation (Fig. 24). Due to the putative detection of both $PI(3,5)P_2$ and PI(3)P by the GFP:Atg18 protein, definitive conclusions regarding Mtm localization in relation to $PI(3,5)P_2$ specifically cannot be made. However, given previous

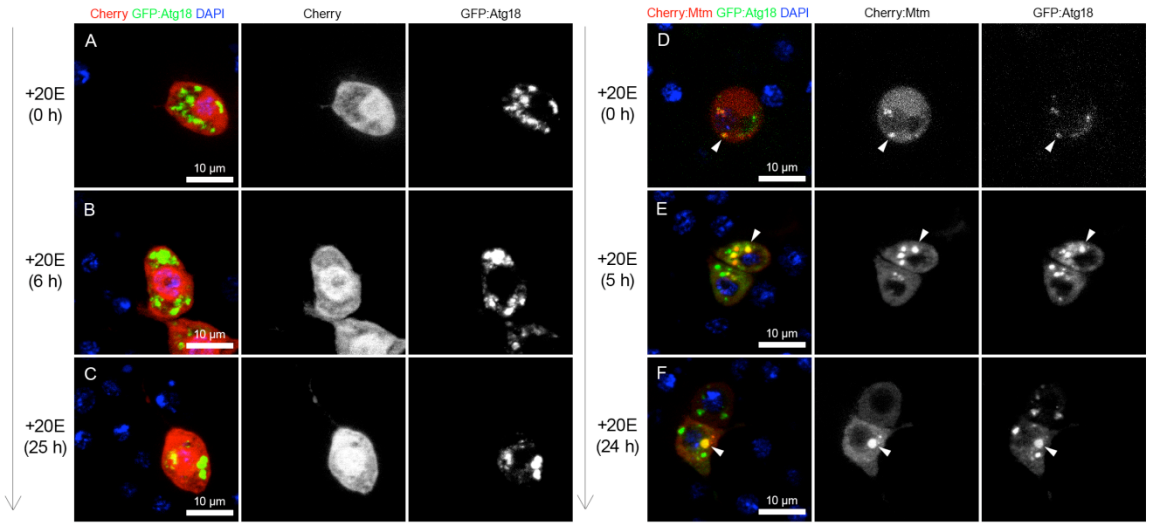

Figure 24: Cherry:Mtm partially colocalizes with GFP:Atg18 puncta

Kc cells transfected with and overexpressing UAS-Cherry or UAS-Cherry:Mtm constructs in conjunction with the UAS-GFP:Atg18 expression vector. Kc cells were kept in complete media and elongation was induced via addition of the ecdysone hormone at various time-points. Cherry distribution in relation to GFP:Atg18 in Kc cells (**A**) 0 hours, (**B**), 6 hours, and (**C**) 25 hours following addition of ecdysone. Cherry:Mtm localization in relation to GFP:Atg18 in Kc cells (**D**) 0 hours, (**E**), 5 hours, and (**F**) 24 hours following addition of ecdysone. Arrowheads indicate sites of colocalization between Cherry:Mtm and GFP:Atg18. Images were acquired using live fluorescence microscopy and represent Z-projections of multiple focal planes.

results demonstrating non-colocalization between Mtm and PI(3)P in hemocytes and the nearly total elimination of GFP:2xFYVE-detected PI(3)P with Mtm overexpression in Kc cells, it is possible that these sites of Cherry:Mtm and GFP:Atg18 colocalization may represent areas of Mtm and PI(3,5)P_2 colocalization. These sites could also be sites of PI(3)P not detected by 2xFYVE and not sensitive to Mtm activity.

Mtm localizes at or near endolysosomal compartments

One idea is that in order to regulate the cellular functions of specific compartments, Mtm is recruited to or resides in distinct membranes to alter or regulate their resident phosphoinositide levels. Therefore, knowing the exact subcellular localization of Mtm may allow for the identification of *mtm*-dependent cellular processes important for cell morphogenesis. With the functional residence of the *mtm* substrate, $PI(3,5)P_2$, at various endolysosomal organelles (i.e., the late endosomes and lysosomes), and due to the defects on late endolysosomal homeostasis upon *mtm* disruption, Mtm localization in relation to the early and late endosomes and lysosomes was examined using live fluorescence microscopy. Because Mtm may be differentially localized at various stages of the cellular morphogenetic program, Mtm distribution was also examined at various stages of ecdysone-induced Kc cell elongation.

To determine the subcellular localization of Mtm in relation to endosomes, Kc cells were co-transfected with the UAS-Cherry:Mtm expression vector and either the UAS-Rab5:GFP construct (as a marker for early endosomes) or the UAS-GFP:Rab7 construct (as a marker for late endosomes). Live fluorescence microscopy in these cells revealed, as before, a cytoplasmic and punctate distribution pattern for Cherry:Mtm. Similarly, Rab5:GFP completely localized to discrete cellular compartments. At all stages of elongation, while there was no co-localization between tagged Mtm and Rab5:GFP, about one-third of all Cherry:Mtm puncta were localized adjacent to and directly touching Rab5:GFP-

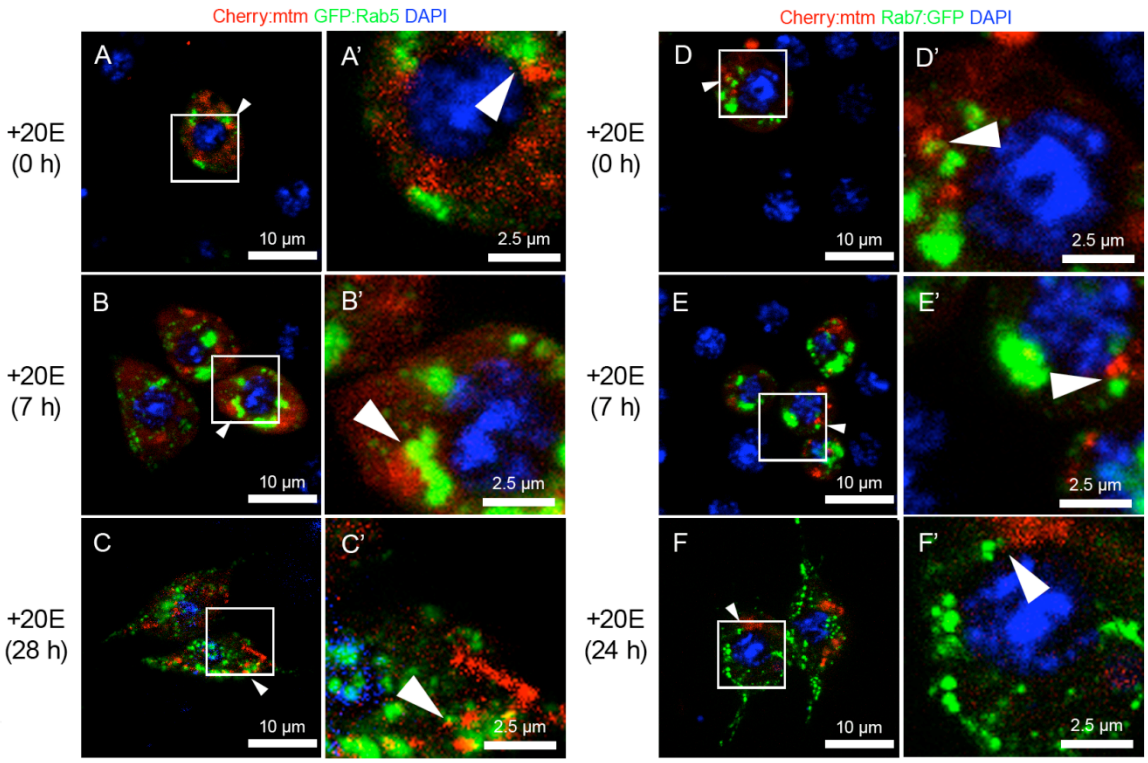

Figure 25: Mtm partially localizes to sites adjacent to the early and late endosomes

Kc cells transfected with and overexpressing UAS-Cherry:Mtm expression vector in conjunction with the UAS-GFP:Rab5 or UAS-GFP:Rab7 expression vectors. Kc cells were kept in complete media and elongation was induced via addition of the ecdysone hormone to this media at various time-points. Cherry:Mtm distribution in relation to the early endosomal marker GFP:Rab5 in Kc cells (**A**) 0 hours, (**B**), 7 hours, and (**C**) 28 hours following addition of ecdysone. Cherry:Mtm localization in relation to the late endosomal marker Rab7:GFP in Kc cells (**D**) 0 hours, (**E**), 7 hours, and (**F**) 24 hours following addition of ecdysone. Arrowheads indicate sites where the endosomal markers and Mtm localize adjacent to one another. Images were acquired using live fluorescence microscopy and represent Z-projections of multiple focal planes. Enlarged images highlight regions of adjacent localization for (**A'-C'**) Cherry:Mtm and GFP:Rab5 and (**D'-F'**) Cherry:Mtm and Rab7:GFP.

positive domains (Fig. 25A-C). Similar to Rab5:GFP, the late endosomal marker GFP:Rab7 also displayed a discrete punctate distribution. At various time points following ecdysone-treatment of transfected Kc cells, showed no co-localization between tagged Mtm and GFP:Rab7 (Fig. 25D-F). These results indicate that in Kc cells, while no co-localization is seen between Mtm and the early and late

endosomes, Mtm partially localizes to sites directly touching the early endosomes in a morphogenesis-independent manner.

Given the enlarged lysosomes in *mtm* mutant cells, it is possible that *mtm* localizes to lysosomes to dephosphorylate specific phosphoinositides on their membrane surfaces, for example, to regulate membrane efflux. To assess Mtm localization in relation to the lysosomes, UAS-GFP:Mtm transfected Kc cells using were marked with either Lysotracker stain or LAMP:GFP. Lysotracker is an indicator of acidic compartments that detects the late endosomes and lysosomes. GFP:Mtm puncta overlapped with both Lysotracker and LAMP:GFP during pre- and early hormone-induced Kc cellular elongation stages (0 hours and 4-7 hours following ecdysone hormone addition respectively) (Fig. 26G-H, 26J-K). In later elongation stages (25-26 hours post-ecdysone addition), while Cherry:Mtm partially colocalized with LAMP:GFP it failed to colocalize with Lysotracker-positive structures (Fig. 26I, 26L). While seemingly contradictory, these results are reasonable given the previously mentioned incomplete overlap of Lysotracker localization with LAMP:GFP. Thus, one interpretation is that in non- and early-elongating cells Mtm partially colocalized with the lysosomes, while at later stages of elongation, Mtm localized to what could be non-acidified, non-Rab7-positive late endosomal compartments. The change in Mtm localization patterns during different stages of cellular morphogenesis may be indicative of a differential requirement for Mtm activity and localization (at least with respect to the lysosomes) during varying stages of cell shape change. When Mtm

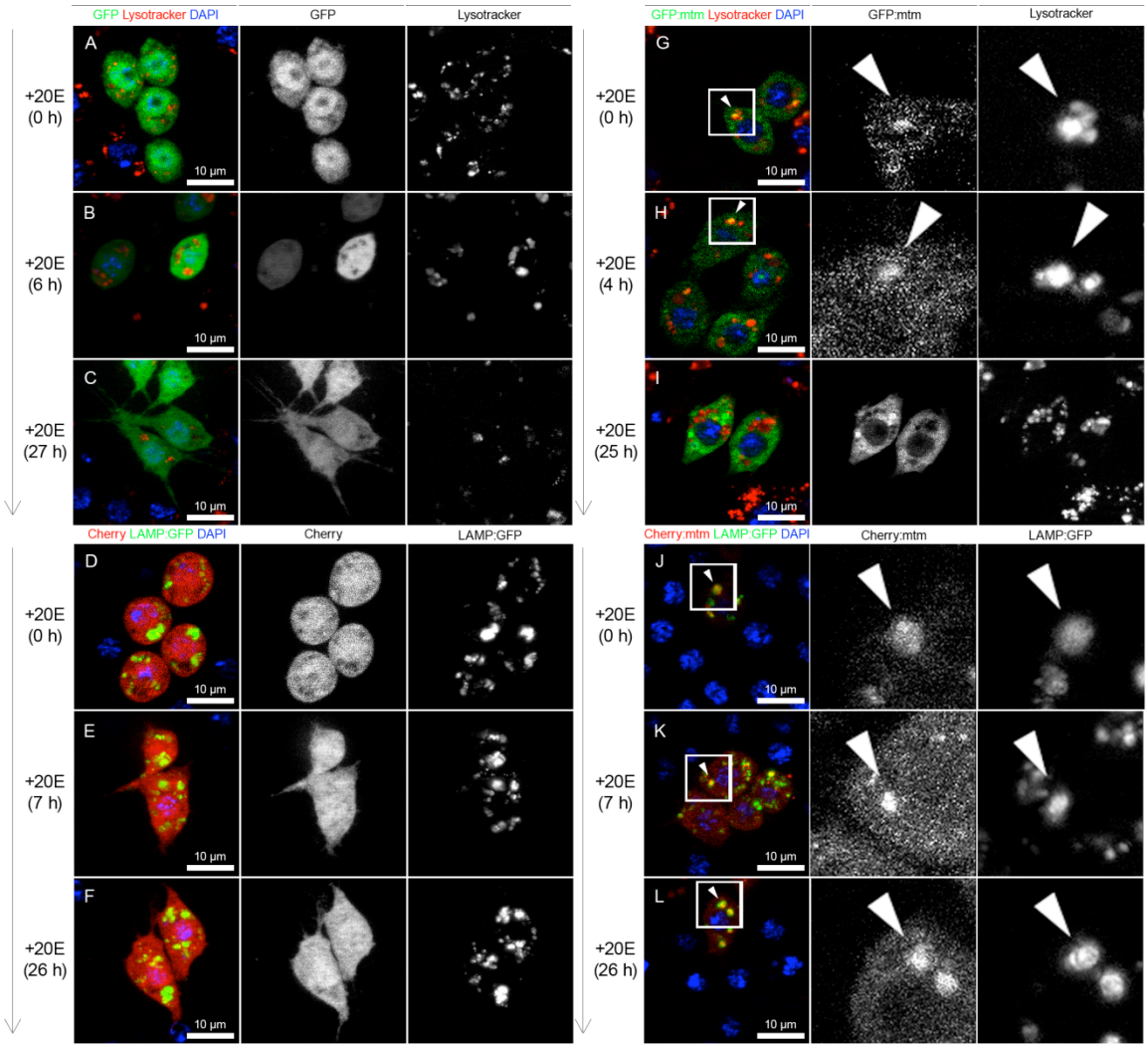

Figure 26: Mtm partially localizes to lysosomal markers at particular stages of cellular elongation

Kc cells transfected with and overexpressing the UAS-GFP or UAS-GFP:Mtm expression vector in conjunction with LysoTracker staining, or the UAS-Cherry or UAS-Cherry:Mtm expression vector in conjunction with the UAS-LAMP:GFP construct. Kc cells were kept in complete media and elongation was induced via addition of the ecdysone hormone to this media at various time-points. GFP distribution in relation to LysoTracker staining in Kc cells (**A**) 0 hours, (**B**), 6 hours, and (**C**) 27 hours following addition of ecdysone. Cherry localization in relation to LAMP:GFP in Kc cells (**D**) 0 hours, (**E**), 7 hours, and (**F**) 26 hours following addition of ecdysone. GFP:Mtm distribution in relation to LysoTracker staining in Kc cells (**G**) 0 hours, (**H**), 4 hours, and (**I**) 25 hours following addition of ecdysone. Cherry:Mtm localization in relation to LAMP:GFP in Kc cells (**J**) 0 hours, (**K**), 7 hours, and (**L**) 26 hours following addition of ecdysone. Arrows indicate sites of colocalization for Mtm and the lysosomal markers. Images were acquired using live fluorescence microscopy and represent Z-projections of multiple focal planes.

localization in relation to lysosomes was further studied in spread hemocytes, GFP:Mtm did not colocalize with Lysotracker-positive compartments similar to its localization pattern in elongated Kc cells (Fig. 27).

Despite this lack of colocalization between Mtm and Lysotracker in spread hemocytes, there still remained the possibility that Mtm-containing vesicles quickly transport to and from the lysosomes in these cells. Live time-lapse microscopy was therefore performed to determine whether Mtm and lysosome interactions were transient in nature and therefore not easily captured with static imaging techniques. In Lysotracker stained UAS-GFP:Mtm expressing hemocytes, GFP:Mtm puncta transiently localized to regions directly adjacent to Lysotracker-positive organelles, as they often appeared and disappeared next to these acidic structures throughout the duration of the time-lapse movies (Fig. 28). Hence, while Mtm does not colocalize with lysosomes in spread hemocytes, time-lapse microscopy demonstrated that Mtm transiently associated with these compartments.

MTM INTERACTORS: *SBF* AND *SPIR*

The mediation of cellular morphogenesis by *mtm* likely requires the integration of different signaling pathways by *mtm* important for both Mtm localization and activity. *Mtm* then influences multiple downstream PIP-mediated effectors. To better understand the mechanisms through which *mtm* controls cellular

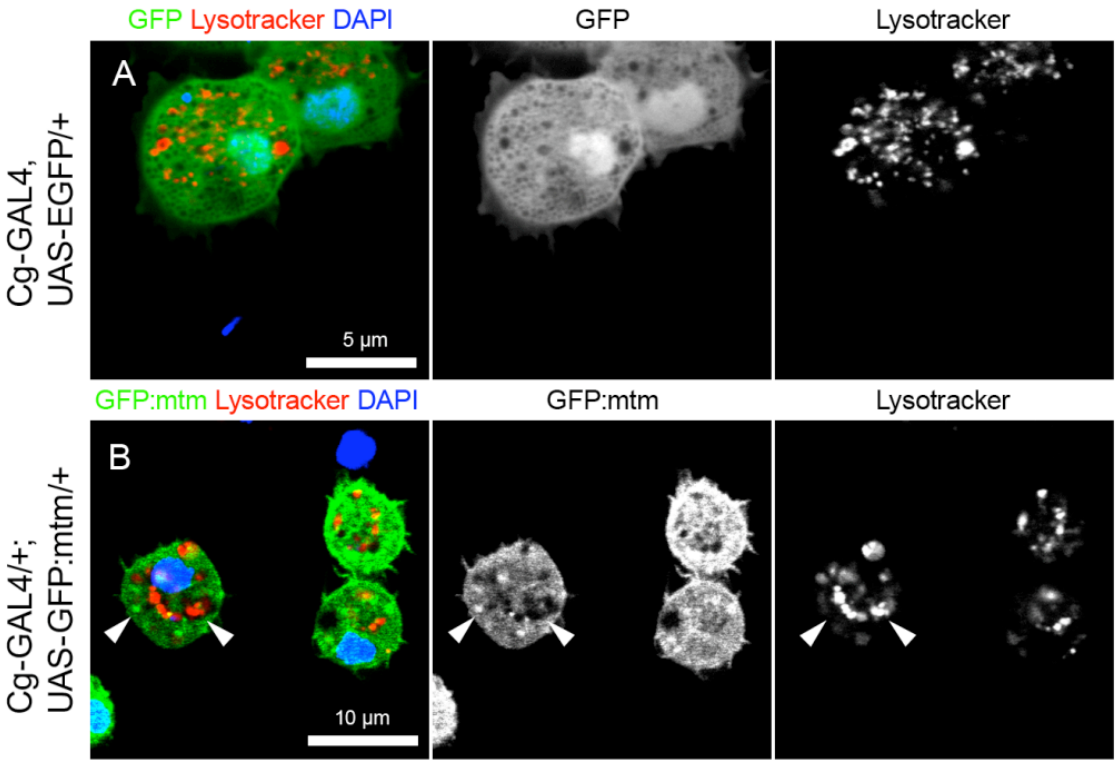

Figure 27: GFP:Mtm and LysoTracker do not colocalize in spread hemocytes

(**A-B**) GFP:Mtm distribution in relation to LysoTracker-positive compartments in hemocytes spilled from third-instar larvae and spread in complete media. Arrowheads indicate regions that are Mtm:GFP-positive but LysoTracker-negative, and LysoTracker-positive but Mtm:GFP-negative, respectively. Images were acquired via live fluorescence microscopy and represent a single focal plane.

remodeling, we looked to identify the pathways both upstream and downstream of *mtm*-dependent functions.

Sbf loss of function and overexpression mimic *mtm* phenotypes

Despite the multiple co-expression studies describing multiple interactions between the active and inactive myotubularins, the functional significance of these interactions remain largely unknown. One thought is that the active myotubularins are regulated by their associations with the inactive myotubularins.

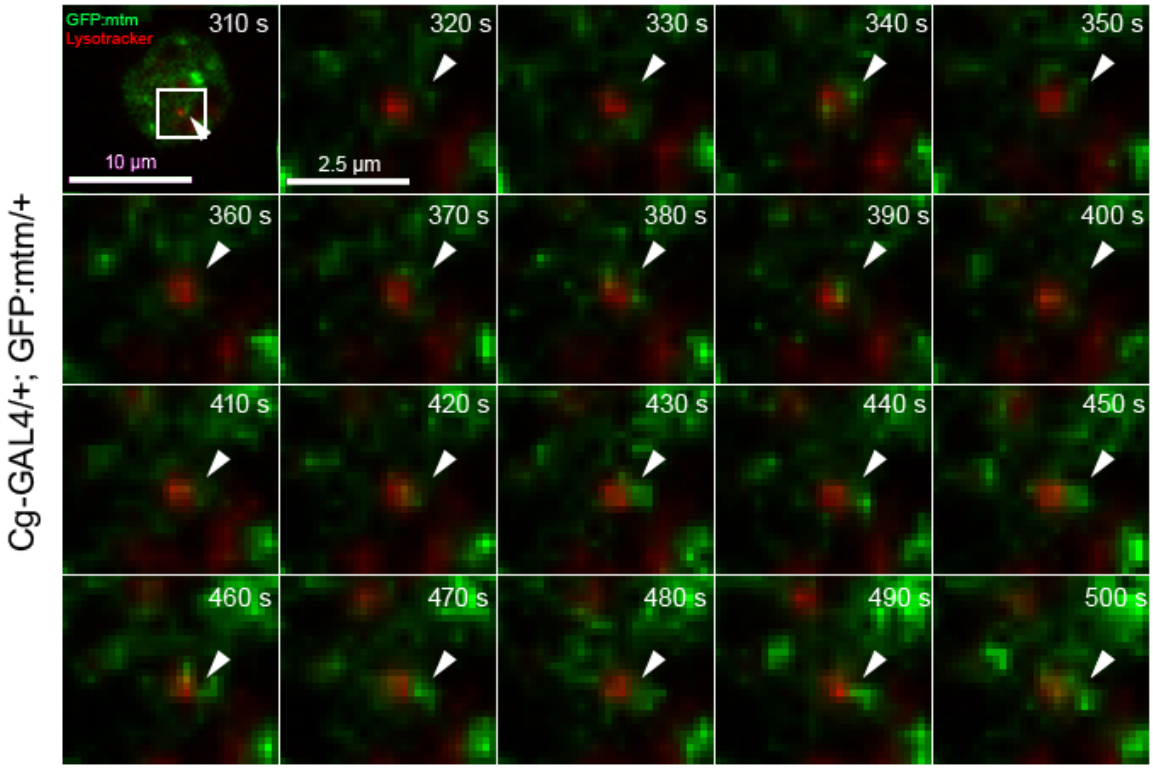

Figure 28: GFP:Mtm exhibits a dynamic spatial relationship with LysoTracker-positive compartments

Still images from a time-lapse experiment studying the dynamic spatial relationship between Mtm and the lysosomes in spread third-instar larval hemocytes. (**A**)The dynamics of the Mtm:GFP puncta and LysoTracker-positive structures can be seen throughout the time lapse. Arrowheads indicate a site adjacent to a LysoTracker-positive compartment where GFP:Mtm puncta transiently localize. Images were taken using live fluorescence microscopy and represent a single focal plane. Elapsed time in seconds is shown in the upper-right corner.

Therefore, one potential regulator of Mtm activity is Sbf, the *Drosophila* homolog of the human gene for the catalytically inactive myotubularin MTMR13. Mutations in MTMR13 result in a similar human disease to that caused by mutations in MTMR2 (CMT4B2 and CMT4B1 respectively). In addition, studies in the mammalian system show that association of MTMR13 with MTMR2 dramatically enhances the phosphatase activity of MTMR2 (Berger et al., 2006; Kim et al.,

Table 5: *Sbf* RNAi hairpin expression in hemocytes results in lethality at the pharate adult stage

GAL4 Driver	Expression Pattern	UAS-construct	Phenotype	Comments
Pxn-GAL4	Hemocytes	UAS-IR^{Sbf}	Lethal	Pharate adults and mid-eclosion. Very few adults eclose
		UAS-IR^{mtm}, UAS-IR^{Sbf}	Lethal	Pharate adults and mid-eclosion.
		UAS-lacZ	Viable	Adult flies are wild-type
Cg-GAL4	Hemocytes and fat body	UAS-IR^{Sbf}	Lethal	Pharate adults and mid-eclosion.
		UAS-lacZ	Viable	Adult flies are wild-type

Lethal phase of animals overexpressing the UAS-IR^{sbf} transgene under control of the hemocyte-speicifc GAL4 drivers Cg-GAL4 and Pxn-GAL4.

2003). To determine if a functional relationship exists in *Drosophila* between *mtm* and *Sbf*, the genetic interactions between *mtm* and *Sbf* were studied by observing the ability of Sbf overexpression (UAS-Cherry:Sbf) and depletion (UAS-IR^{Sbf}) to modify, mimic, or enhance *mtm* phenotypes. With its proposed role as a positive regulator of *mtm* activity, we predicted that *Sbf* loss of function and overexpression would mimic the phenotypes observed with corresponding changes in *mtm* activity.

Hemocyte-specific knockdown of *Sbf* via targeted RNAi hairpin expression resulted in lethality at the same developmental stages as hemocyte-specific *mtm* depletion (Table 5). *Sbf* depletion in hemocytes resulted in animall lethality at the pharate and eclosion stages, with very few flies managing to eclose from their pupal cases. To assess the basis for the hemocyte-dependent role for viability, blood cell distribution following hemocyte-targeted Sbf knockdown was examined via live fluorescence microscopy. Animals containing Sbf-depleted hemocytes exhibited the same altered distribution patterns as animals experiencing hemocyte-specific *mtm* RNAi. While wild-type animals had GFP-positive hemocytes spread throughout, *Sbf* RNAi animals had an almost total lack of hemocytes in the head, thorax, and leg segments (Fig. 29A, 29C). Similar to what was seen with Pxn-GAL4 driven IR^{mtm} expression, the abdomen of these animals also possessed very strong GFP fluorescence, though the source of this GFP expression was not determined (Fig. 29B, 29C). The shared lethal phase and disrupted hemocyte distribution phenotypes between *mtm* and *Sbf* depletion is consistent with the possibility that *Sbf* regulates *mtm* phosphatase activity. These results point toward a functionally relevant role for *Sbf* in hemocyte biology.

To test possible regulatory roles of Sbf on Mtm activity, the effects of Sbf overexpression on PI(3)P and $PI(3,5)P_2$ levels were explored. As a suspected positive-regulator of Mtm, *Sbf* overexpression may inappropriately stimulate Mtm phosphatase activity to mimic *mtm* overexpression. To test whether the effects on PI(3)P and/or $PI(3,5)P_2$ levels were differentially regulated in a cellular

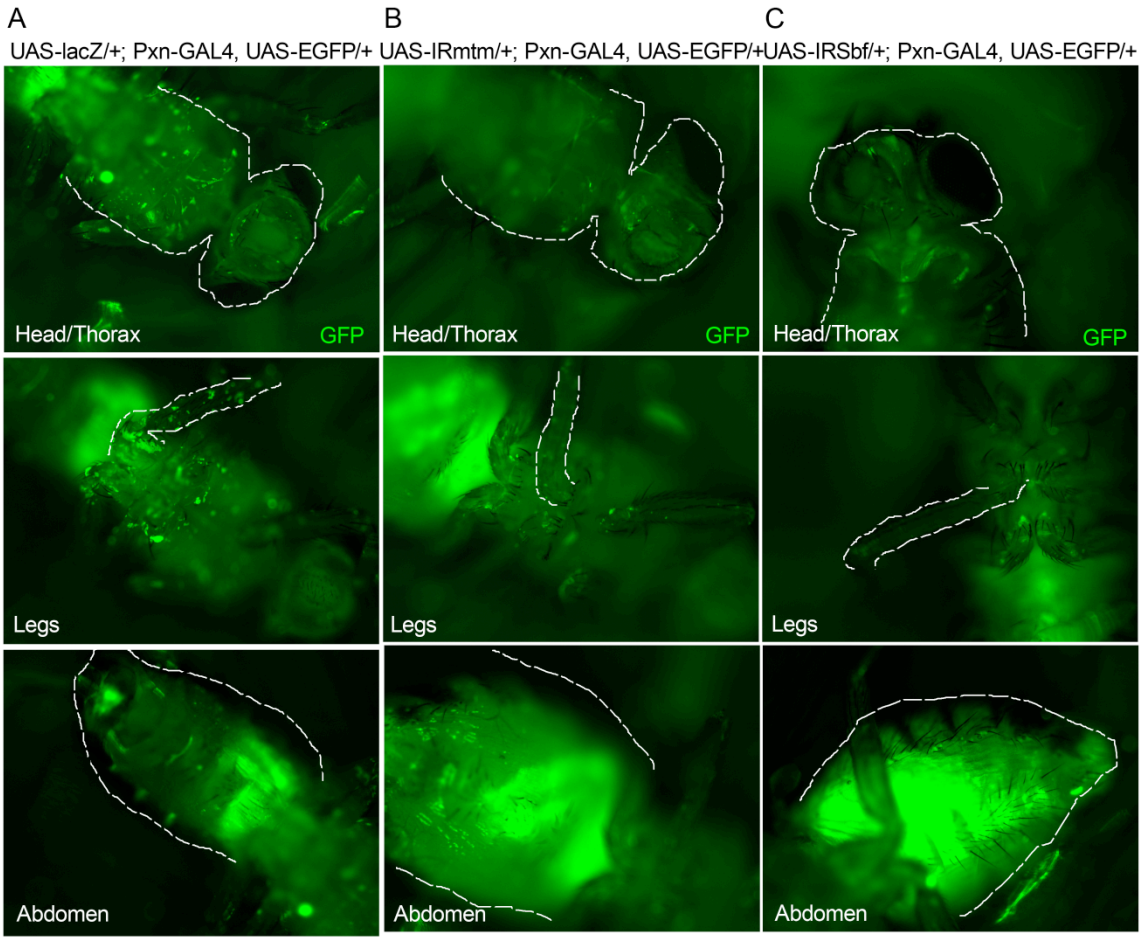

Figure 29: Hemocyte distribution in adult flies following hemocyte-specific Sbf depletion

Distribution of GFP-expressing hemocytes in the head, thorax, legs, and abdomen of adult flies overexpressing the (**A**) UAS-lacZ, (**B**) UAS-IR^{mtm}, and (**C**) UAS-IR^{Sbf} transgenes with the Pxn-GAL4 driver.

morphogenesis-dependent manner, ecdysone hormone was added to these cells to induce elongation. The effects of *Sbf* overexpression on the localizations of the PI(3)P and PI(3,5)P_2-binding reporters, 2xFYVE and Atg18, were the same as the effects of *mtm* overexpression. While a few Cherry:2xFYVE-positive structures remained in some positively transfected Kc cells, the majority of the PI(3)P biosensor was dispersed by GFP:Sbf overexpression (Fig. 30A-C, 30G-I),

suggesting that *Sbf* overexpression mediates the nearly complete elimination of cellular PI(3)P from Kc cells. Cherry:Sbf expression in Kc cells also caused significant dispersal of GFP:Atg18 localization (Fig. 30D-F, 30J-L). The effects of *Sbf* overexpression on GFP:Atg18 distribution present the possibility that Sbf is also able to mediate the downregulation of cellular $PI(3,5)P_2$ levels. However, a definitive conclusion cannot be made on the effects of Sbf overexpression on this phosphoinositide species since the GFP:Atg18 detection of PI(3)P versus $PI(3,5)P_2$ are indistinguishable.

If *Sbf* and *mtm* operate within the same pathway to regulate cell morphology, we would expect *Sbf* hemocyte spreading phenotypes to mimic *mtm* mutant phenotypes. Fluorescence microscopy of phalloidin-546-stained hemocytes revealed that individually, IR^{mtm} and IR^{Sbf} expressing hemocytes exhibited similar cytoskeletal phenotypes to those seen in *mtm* null mutants. Specifically *mtm* and *Sbf* RNAi resulted in round cell morphologies that lacked obvious protrusions and increased membrane ruffling (Fig. 31B-C). *Mtm* and *Sbf* co-RNAi phenocopied the single loss of function morphology phenortpes, with abnormally organized F-actin cytoskeletons and a lack of cell protrusions (Fig. 31D). As with *mtm* overexpression, Cherry:Sbf overexpression in hemocytes exhibited a gain-of-function morphology phenotype, with an estimated three to four-fold increase in radial F-actin-rich protrusions (Fig. 31E-G). Taken altogether, the similarities between the *mtm* and *Sbf* mutant phenotypes suggest a positive regulatory relationship between *Sbf* and *mtm* in actin remodeling.

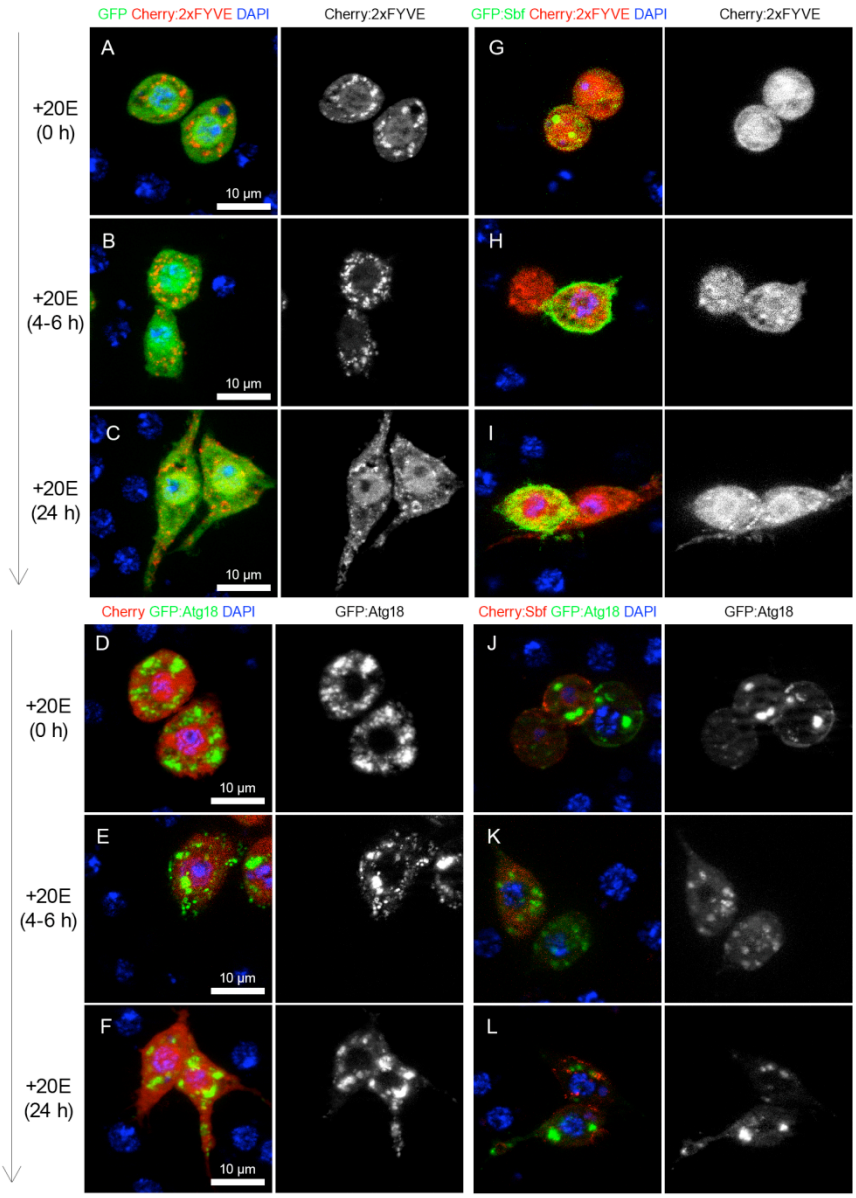

Figure 30: Overexpression of Cherry:Sbf mediates the dispersal of the Cherry:2xFYVE and GFP:Atg18 reporter PIP binding proteins

Kc cells transfected with and overexpressing Cherry:2xFYVE with GFP (**A-C**) and GFP:Sbf cells (**G-I**). GFP:Atg18 with Cherry (**D-F**) and Cherry:Sbf (**J-L**). Kc cells at 0 hours (**A, D, G, J**); 4-6 hours (**B, E, H, K**), and 24 hours (**C, F, I, L**) after treatment with ecdysone.

Sbf colocalization patterns are similar to that of Mtm

If Sbf indeed regulates Mtm activity directly, one would expect to see evidence of physical interactions and colocalization between their gene products. The spatial relationship of Sbf to Mtm as well as to markers for phosphoinositides and endolysosomal compartments was analyzed in transfected Kc cells at different stages of elongation via live fluorescence microscopy.

The UAS-GFP:Mtm and UAS-Cherry:Sbf expression vectors were co-transfected into ecdysone-treated Kc cells. As demonstrated previously on its own, GFP:Mtm displayed a punctate localization pattern, while Cherry:Sbf localized to both discrete puncta as well as to the plasma membrane. The puncta formed by Cherry:Sbf exhibited nearly total colocalization with GFP:Mtm-enriched sites (Fig. 31A-C). Similar to what was seen with Mtm, Sbf partially colocalized with LAMP:GFP accumulations at all stages of KC cell elongation (Fig. 31D-F). These findings point toward possible physical interactions between the two proteins *in vivo* and also demonstrate a shared spatial distribution between Mtm and Sbf.

The extensive colocalization and shared distribution patterns of Sbf and Mtm, along with previous data confirming shared genetic phenotypes between the two genes, support a model in which Mtm and Sbf make functionally relevant physical interactions with one another *in vivo*, possibly in order for *Sbf* to regulate *mtm* phosphatase activity and/or localization.

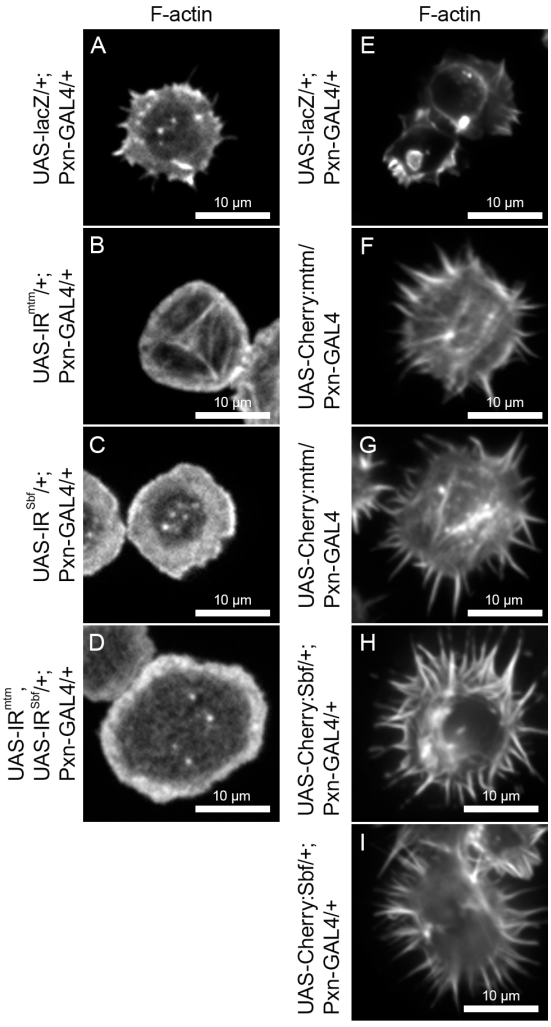

Figure 31: *Sbf* depletion and overexpression results in the same cell morphology phenotypes as *mtm* depletion and overexpression

Morphology of phalloidin-546-stained hemocytes spilled from third-instar larvae into PBS and allowed to spread for 1 hour. Actin cytoskeleton organization of (**A**) lacZ, (**B**) IR^{mtm}, (**C**) IR^{Sbf}, (**D**) IR^{mtm}, IR^{Sbf}, (**E**) lacZ, (**F-G**), Cherry:Mtm, and (**H-I**) Cherry:Sbf overexpressing hemocytes. Images were taken via fluorescence microscopy and represent Z-projections of multiple focal planes.

$Spir^{RC}$, but not $Spir^{RD}$, partially colocalizes with Cherry:2xFYVE-positive structures

It is hypothesized that downstream factors respond to *mtm*-mediated changes in phosphoinositide levels and distributions to initiate or regulate cellular morphogenetic machinery. Proteins with predicted PI(3)P-binding domains are

candidate effectors that could be misregulated with *mtm* loss of function. *Spire* is one such candidate with a modified FYVE PI(3)P-binding domain at the C-terminal region and roles in actin nucleation and actin-microtubule crosslinking (Otto et al., 2000; Quinlan et al., 2005; Rosales-Nieves et al., 2006). Due to the presence of a modified FYVE domain, we hypothesized that Spir could exhibit an affinity for PI(3)P-rich membranes. In mammalian cells, *Spir* proteins were shown to localize outside the endosomes, while its localization in relation to PI(3)P-containing organelles such as the endosomes was untested in *Drosophila*. To determine the spatial relationship between Spir and PI(3)P in hemocytes, the localization of fluorescently tagged $Spir^{RC}$ and $Spir^{RD}$ isoforms with the Cherry:2xFYVE membrane-binding reporter protein were examined. Hemocytes expressing $Spir^{RD}$:GFP, which contains the N-terminal end and the G-actin-binding domain, showed no direct relationship to Cherry:2xFYVE-positive structures (Fig. 33A-B). In contrast, $Spir^{RC}$:GFP, which contains the C-terminal end and the FYVE/actin-microtubule crosslinking domains, displayed a punctate distribution pattern that was restricted to the cell body and rarely seen within the cell skirt (Fig. 33C). As predicted, the $Spir^{RC}$ isoform localized to Cherry:2xFYVE-positive structures, indicating a likely recruitment of $Spir^{RC}$ to PI(3)P. The majority of the Cherry:2xFYVE-positive cellular compartments in each cell were either co-localized with or flanked by $Spir^{RC}$:GFP, with puncta of $Spir^{RC}$:GFP often docked to the outer membranes of Cherry:2xFYVE ring structures. When PI(3)P domains

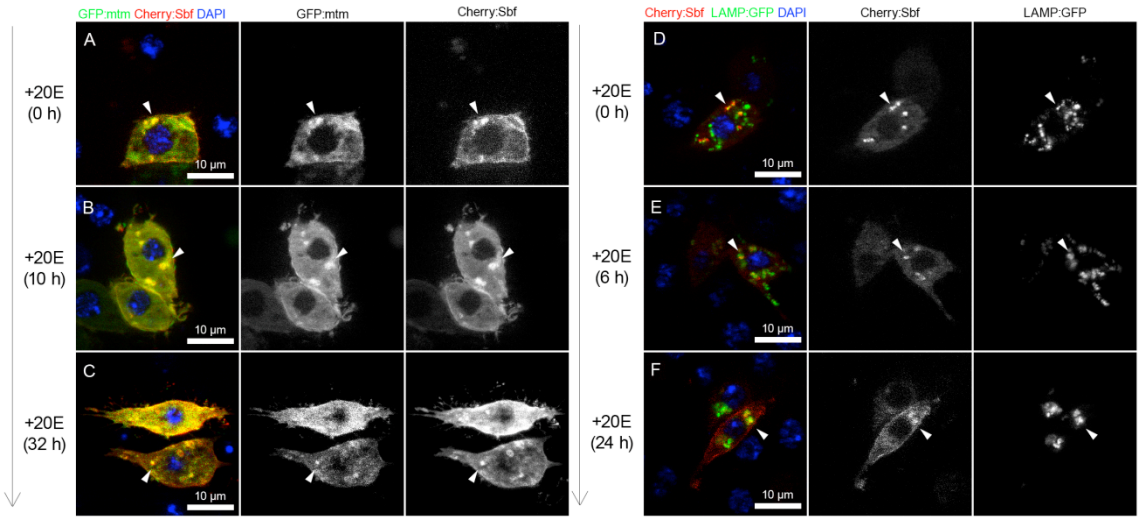

Figure 32: Sbf and Mtm colocalize extensively and share similar distribution patterns

Kc cells transfected with and overexpressing the UAS-Cherry:Sbf expression vector in conjunction with either the UAS-GFP:Mtm, UAS-GFP:Atg18, or UAS-LAMP:GFP vectors. Kc cells were kept in complete media and elongation was induced via addition of the ecdysone hormone to this media at various time-points. Cherry:Sbf distribution in relation to GFP:Mtm at (**A**) 0 hours, (**B**) 10 hours, and (**C**) 32 hours following addition of ecdysone. Cherry:Sbf distribution in relation to LAMP:GFP at (**D**) 0 hours, (**E**) 6 hours, and (**F**) 24 hours following addition of ecdysone. Arrows indicate sites of colocalization. Images were acquired using live fluorescence microscopy and represent Z-projections of multiple focal planes.

were expanded with RNAi-mediated *mtm* depletion, Spir^{RC}:GFP continued its strong association with Cherry:2xFYVE-positive compartments, often forming Spir^{RC}:GFP-positive rings around enlarged Cherry:2xFYVE structures (Fig. 33D). To further characterize the spatial relationship between Spir^{RC} and PI(3)P-containing membranes, time lapse microscopy was utilized to determine the dynamics of Spir^{RC}:GFP localization in relation to Cherry:2xFYVE. Movies revealed that Spir^{RC}:GFP puncta were mostly immobile, though on some occasions, a small number of Spir^{RC}:GFP puncta localized near one another could be seen slowly arranging themselves into a linear array (Fig. 34B). Spir^{RC}:GFP puncta localized to Cherry:2xFYVE-positive structures in an almost

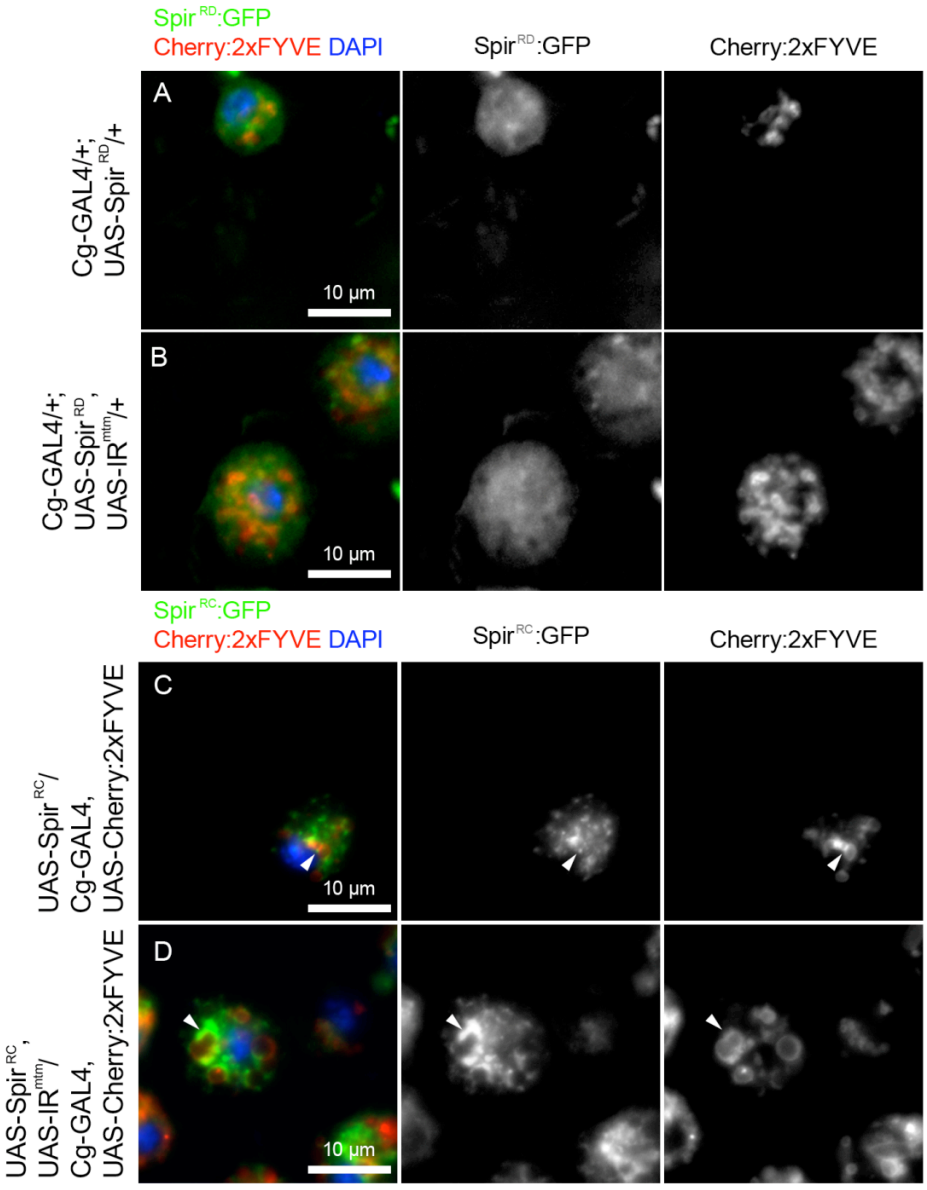

Figure 33: Spir^{RC}:GFP, but not SpirRD:GFP partially localizes to Cherry:2xFYVE-positive structures

Hemocytes spilled from third-instar larvae carrying UAS-controlled transgenes. Transgene expression was induced with the Cg-GAL4 driver. SpirRD:GFP localization in relation to Cherry:2xFYVE both (**A**) with *mtm* RNAi hairpin expression and (**B**) without hairpin expression. Spir^{RC}:GFP localization in relation to Cherry:2xFYVE both (**C**) with *mtm* RNAi hairpin expression and (**D**) without hairpin expression. Arrowheads indicate sites of Spir and Cherry:2xFYVE co-localization. Images were taken using live fluorescence microscopy and represent Z-projections of multiple focal planes.

strictly static manner, rarely deviating in its spatial position relative to these compartments (Fig. 34A-C). Such findings indicate that the Spir^{RC} isoform is stably anchored to PI(3)P-rich membranes. We speculate that this stable localization of Spir^{RC}:GFP to FYVE-positive membrane domains may be reflective of a possible *mtm* role in F-actin organization and/or focal adhesion localization.

Spir^{RC}, but not SpirRD localization is affected by Mtm loss of function

The effects of Mtm activity on cellular PI(3)P, along with Spir^{RC} colocalization with PI(3)P-rich domains, revealed Spir localization as potentially responsive to Mtm activity. To determine if Spir localization changes with *mtm* loss of function, Spir^{RC}:GFP and SpirRD:GFP localization in wild-type and IR^{mtm} expressing hemocytes were compared to each other via live fluorescence microscopy. In wild-type cells, Spir^{RC}:GFP formed numerous small puncta localized almost exclusively within the cell body (Fig. 35A). In contrast, SpirRD:GFP exhibited diffuse nonuniform cytoplasmic staining, with the majority of the protein localized to the cell body and aggregating to a few SpirRD:GFP-enriched sites (Fig. 35C). While SpirRD:GFP localization seemed largely unaffected by *mtm* RNAi hairpin expression, SpirRD:GFP was also seen localized to the long filopodia-like extensions formed with expression of a single copy of the IR^{mtm} transgene under the control of the Cg-GAL4 driver (Fig. 35D), a structure which does not form in wild-type cells. In contrast, following depletion of

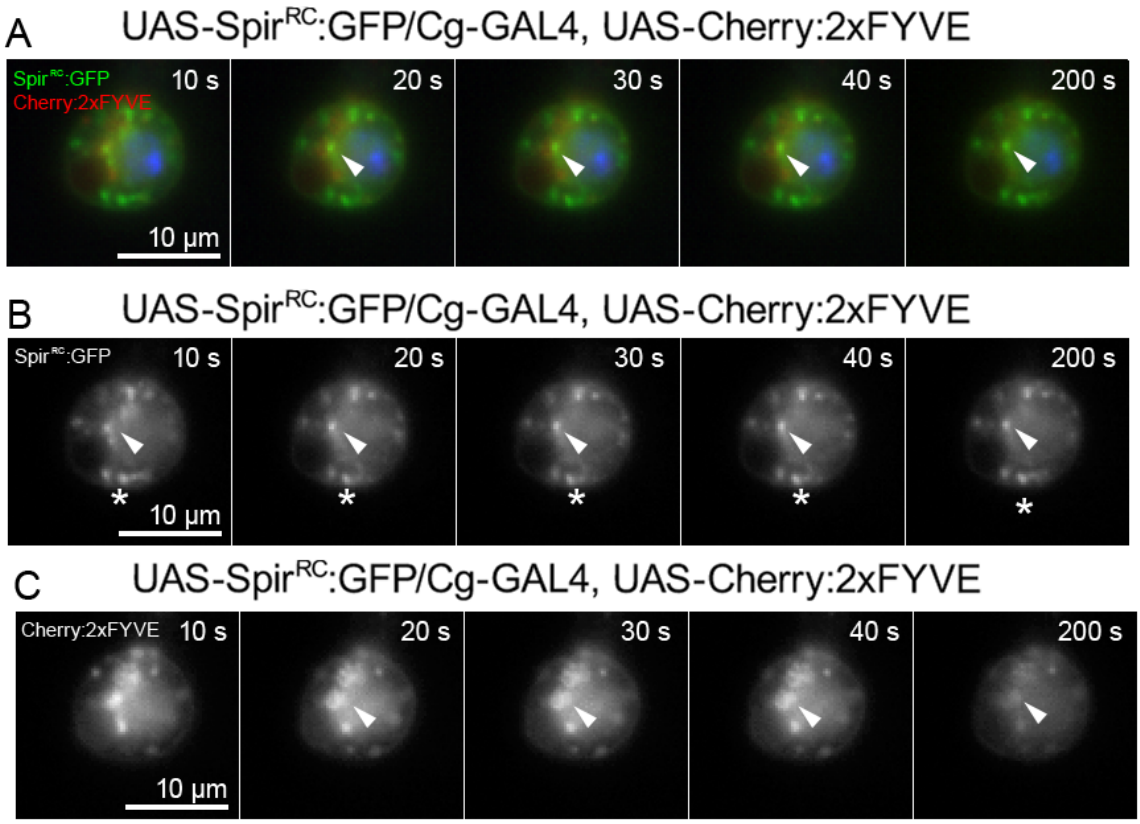

Figure 34: Spir^{RC}:GFP puncta are relatively static and remain localized to Cherry:2xFYVE-positive compartments

Still images from a time-lapse experiment studying the dynamics of Spir^{RC}:GFP localization in relation to Cherry:2xFYVE. The dynamics of the Spir^{RC}:GFP puncta in relation to Cherry:2xFYVE-positive structures can be seen in the (**A**) merged, (**B**) green, and (**C**) red channels. Arrowheads indicate a site of Spir^{RC}:GFP and Cherry:2xFYVE colocalization. Images were taken using live fluorescence microscopy and represent a single focal plane. Elapsed time in seconds is shown in the upper-right corner. Asterisk indicates area where Spir^{RC}:GFP form a linear array.

Mtm, Spir^{RC}:GFP exhibited a modified distribution. Spir^{RC}:GFP distribution was altered from discrete puncta to a slightly more diffuse localization (Fig. 33B). Though more dispersed, Spir^{RC}:GFP still did not spread ubiquitously throughout the cytoplasm and instead localized to poorly defined regions. Spir^{RC}:GFP puncta could still be detected, but now had less defined edges and often merged with one another into cloud-like masses. These observations reveal the sensitivity of

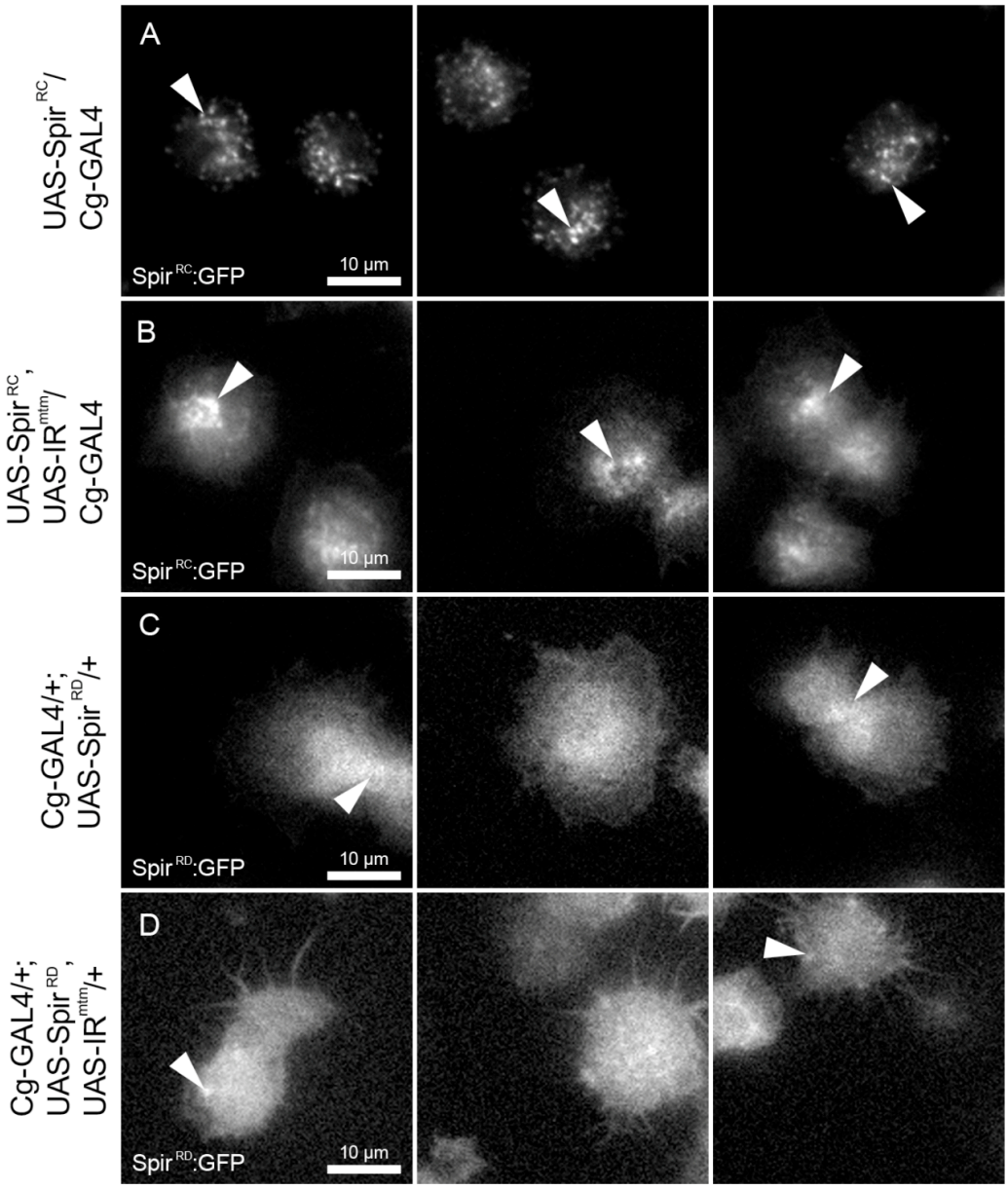

Figure 35: Localization of Spir^{RC}:GFP, but not SpirRD:GFP, is affected by *mtm* RNAi hairpin expression

Third instar-larval hemocytes overexpressing the Spir^{RC}:GFP or SpirRD:GFP transgenes spilled into complete media. Localization of Spir^{RC}:GFP in (**A**) wild-type and (**B**) IR^{mtm} expressing conditions and localization of SpirRD:GFP in (**C**) wild-type and (**D**) IR^{mtm} expressing conditions. Arrowheads indicate sites of Spir accumulation. Transgene expression was under the control of the Cg-GAL4 driver. Images were acquired using live fluorescence microscopy and represent Z-projections of multiple focal planes.

Spir distribution patterns to *mtm*-dependent changes in the phosphoinositides, possibly due to the Spir^{RC}-specific presence of the FYVE domain. The sensitivity to *mtm*-regulated phosphoinositide levels also implicates Spir as a potential conduit for Mtm regulation of cellular remodeling.

Spir^{RC}, but not SpirRD overexpression enhances the *mtm* loss of function hemocyte morphology phenotype

We hypothesized that Spir^{RC} could be a downstream effector of Mtm activity through possible localization to PI(3)P-rich membranes. To determine whether *Spir* and *mtm* act through a common cellular pathway, the genetic interactions between these two genes were studied by looking at the ability of Spir overexpression to phenocopy and enhance the *mtm* hemocyte spreading phenotypes.

Overexpression of Spir^{RC}:GFP altered the morphology of both wild-type and single *mtm* RNAi hairpin expressing hemocytes. When Spir^{RC}:GFP was overexpressed in a wild-type background, the hemocytes displayed an estimated three to four-fold increase in the number of elongated filopodia-like extensions, similar to the hypomorphic *mtm* RNAi phenotype of hemocytes undergoing Cg-GAL4 driven IR^{mtm} expression (Fig. 36A-B). RNAi depletion of *mtm* combined with Spir^{RC}:GFP overexpression shifted the hypomorphic phenotype to one resembling a null phenotype. While cells expressing only a single copy of IR^{mtm} hairpin exhibited long, thin, and more branched protrusions than their wild-type

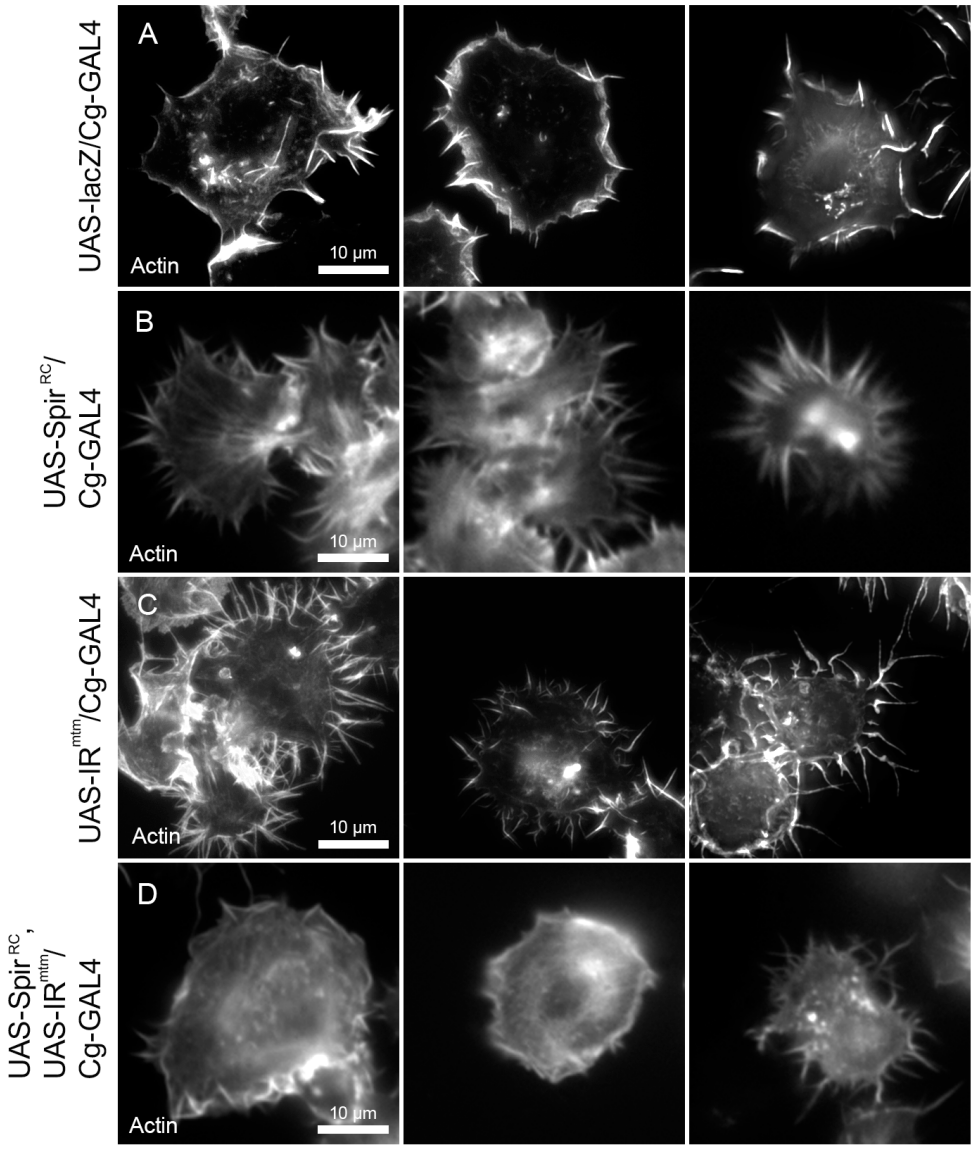

Figure 36: Spir^{RC}:GFP overexpression enhances the *mtm* RNAi actin cytoskeleton phenotypes

Larval hemocytes spilled from various UAS-transgene-containing third-instar larvae and allowed to spread in PBS for 1 hour prior to fixing and staining. The effects of (**A**) UAS-lacZ, (**B**), UAS-Spir^{RC}:GFP, (**C**) UAS-IR^{mtm}, and (**D**) UAS-Spir^{RC}:GFP, UAS-IR^{mtm} overexpression on hemocyte F-actin cytoskeleton organization were visualized using phalloidin-546 staining. Images were taken using live fluorescence microscopy and represent Z-projections of multiple focal planes.

counterparts, Spir^{RC}:GFP overexpression in conjunction with *mtm* RNAi resulted in a round cell morphology which matched that of cells expressing two copies of the IR^{mtm} hairpin, or of hemocytes from *mtm* null alleles (Fig. 36C-D). The majority of Spir^{RC}:GFP IR^{mtm} co-expressing cells also lacked protrusions and exhibited membrane ruffling. Therefore, overexpression of Spir^{RC} in hemocytes mimicked the effects of increased *mtm* depletion on cell morphology. These findings reveal the possibility that Mtm loss of function results in the overactivation and/or mislocalization of Spir activity.

Spir^{RC} localizes to areas of high actin accumulation while SpirRD partially localizes to the ends of actin filaments

Understanding how Spir^{RC} overexpression enhances the *mtm* RNAi hemocyte spreading phenotype may reveal mechanisms through which Spir could mediate *mtm*-dependent changes in cell morphology. One hypothesis is that because Spir^{RC} contains a domain capable of performing microtubule and actin filament crosslinking, mislocalization of this activity may contribute to abnormal F-actin cytoskeleton organization and cell morphology in *mtm* mutants. To investigate this hypothesis, the associations of the fluorescently-tagged and functionally diverse Spir isoforms with the F-actin cytoskeleton were examined via fluorescence microscopy. Spread hemocytes expressing either the UAS-Spir^{RC}:GFP construct or the UAS-SpirRD:GFP construct under the control of the Cg-GAL4 driver were stained for F-actin using phalloidin-546. Spir^{RC}:GFP co-

localized with regions within the cell body containing a high concentration of F-actin strands (Fig. 37E-F), indicating a close association between $Spir^{RC}$:GFP and the organization of filamentous actin structures. The $Spir^{RC}$/F-actin spatial relationship is consistent with a proposed role for $Spir^{RC}$ as an actin-microtubule crosslinker in oocytes. Study of $Spir^{RD}$ localization in relation to F-actin also revealed close associations between this Spir isoform and the actin cytoskeleton. However, the exact spatial relationship between $Spir^{RD}$ and F-actin differed from that of $Spir^{RC}$ and F-actin. While $Spir^{RC}$:GFP puncta localized to sites of F-actin accumulation, $Spir^{RD}$:GFP-enrichment was localized to what appeared to be the points of origin of F-actin strands (Fig. 37A-F). These results are in agreement with the presence of G-actin-binding sites in this $Spir^{RD}$ isoform and its proposed role as a formin-like actin-nucleation factor. When the experiment was repeated in IR^{mtm} expressing hemocytes, while the actin cytoskeleton organization and localization of $Spir^{RC}$ were significantly altered in these cells, the overall spatial relationship between $Spir^{RC}$:GFP and F-actin remained mostly unchanged (Fig. 37F). In the *mtm* RNAi hairpin expressing background, $Spir^{RC}$:GFP still remained localized to areas of high F-actin concentration despite its slight diffusion throughout regions of the cytoplasm. Such results support a hypothesis in which Spir responds to and mediates the effects of Mtm activity on cellular remodeling through the strictly regulated localization and unique domain-dependent interactions of Spir with the actin cytoskeleton. In contrast, no effect was seen with $Spir^{RD}$, which does not encode a modified FYVE domain. In contrast to

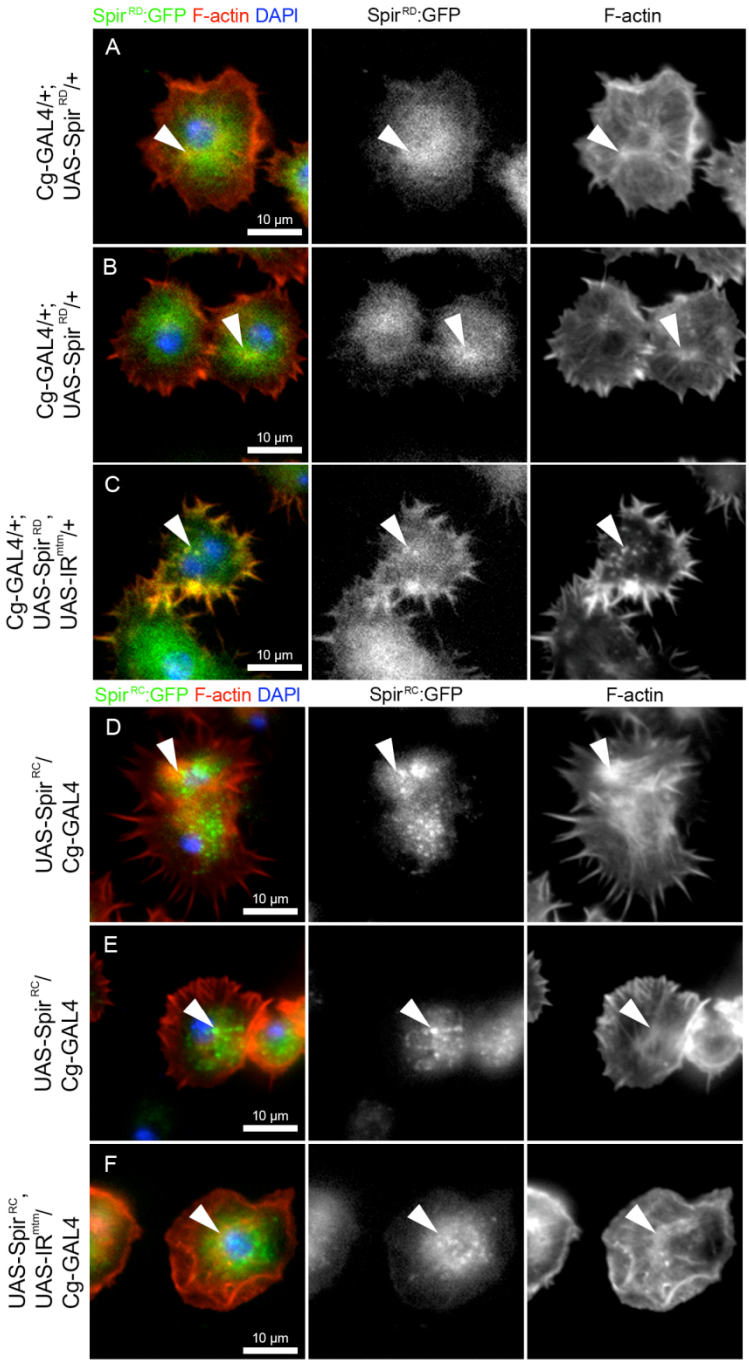

Figure 37: Spir^{RC}:GFP and SpirRD:GFP exhibit unique associations with F-actin

Hemocytes overexpressing the UAS-Spir^{RC}:GFP and UAS-SpirRD:GFP transgenes under control of the Cg-GAL4 driver spilled from third-instar larvae and allowed to spread in PBS for 1 hour prior to staining with phalloidin-546. The localization of SpirRD:GFP in relation to actin in (**A-B**) wild-type or (**C**) IR^{mtm} expressing conditions and localization of Spir^{RC}:GFP in (**D-E**) wild-type or (**F**) IR^{mtm} expressing conditions. Arrowheads indicate sites of actin and Spir co-localization. Images were taken using fluorescence microscopy and represent Z-projections of multiple focal planes.

Spir^{RC}:GFP, the morphology of SpirRD:GFP overexpressing hemocytes matched the phenotype of control hemocytes, as both exhibited moderately-sized and radially extending filopodial protrusions (Fig. 37A-B). Overexpression of SpirRD isoform in Mtm deficient conditions also failed to modify the morphology phenotypes of *mtm* RNAi (Fig. 37C). IR^{mtm} expressing hemocytes both with and without SpirRD:GFP overexpression exhibited highly branched and abnormally elongated actin protrusions. These results suggest that due to inappropriately regulated interactions with F-actin, mislocalized Spir protein caused by *mtm* loss of function may be the reason for these cells' inability to properly remodel their cytoskeletons into stable radial protrusions.

DISCUSSION

Cellular morphogenesis requires the concerted action of multiple processes to produce a functionally relevant response. While cell shape change is crucial for the function of most (if not all) cells, the mechanisms through which cells coordinate multiple operations to mediate cellular remodeling are not fully understood. Our data not only confirms an *in vivo* role for *mtm* in *Drosophila* cell morphogenesis, but also supports a model in which at least two major aspects of the cellular morphogenetic program (specifically cytoskeletal remodeling and membrane trafficking and homeostasis) are coordinated through the *mtm*-dependent spatiotemporal regulation of phosphoinositide concentrations and distributions. Both these processes play critical roles in cell morphogenesis: cytoskeletal remodeling provides the underlying mechanism driving changes in cell shape, while membrane homeostasis and trafficking not only maintains the necessary plasma membrane volume required to achieve and maintain specific cell morphologies, but also regulates the dynamics of protein composition at localized membrane domains (such as receptors, adhesion proteins, etc.). Therefore, the coordination of these two processes through *mtm*'s regulation of phosphinositide signaling is absolutely essential for cells to modify their morphologies.

Spatiotemporal regulation and integration of cellular morphogenesis-related processes by *mtm* occurs through regulation of PI(3)P

Our data suggest that effects of *mtm* on cellular morphogenesis occur through its influence on PI(3)P homeostasis. In my work, PI(3)P levels were shown to be sensitive to *mtm* function. Other work displaying the ability of MTM1, MTMR1, MTMR2, and MTMR3 to hydrolyze PI(3)P both in vitro and in mammalian cells also supports these findings (Tronchere et al., 2004). The overexpression of tagged *mtm* proteins in both hemocytes and Kc cells caused the dispersal of the PI(3)P-binding 2xFYVE reporter. Conversely, *mtm* depletion in hemocytes caused an expansion of PI(3)P domains. Finally, all *mtm* loss of function defects could be suppressed by depletion of class II PI 3-kinase. Therefore, we hypothesized that the defects caused by *mtm* loss of function are likely the result of the abnormal accumulation and mislocalization of a specific subpool of PI(3)P (possibly synthesized by the class II Pi3K).

However, alternative, more complex and indirect explanations are also possible. While our data suggests that PI(3)P is a direct functional substrate for Mtm, this interpretation is not without its caveats. Our work does not exclude the possibility that *mtm*-dependent effects on PI(3)P may instead be the indirect result of its regulation of other phosphoinositide species. Given the interconnections between the different phosphoinositides, it would be logical to predict that alterations in one species might affect the levels of others. It therefore becomes necessary to measure the levels of the other phosphoinositides in both

wildtype and *mtm* mutant conditions to determine the relationship between *mtm* activity and the distribution and concentration of the other lipid second messengers. If other phosphoinositides are found to be misregulated with *mtm* loss of function, we must determine whether this is a primary result of *mtm activity* or a secondary consequence of abnormal PI(3)P accumulation, and more importantly, determine the functional significance of any misregulated levels. We must identify which misregulated phosphoinositide pools contribute to which specific *mtm* mutant phenotypes. For example, the dispersal of the PI(3)P/PI(3,5)P_2-binding Atg18 reporter also provides the possibility that Mtm's affects on cell morphology are mediated through the dephosphorylation of PI(3,5)P_2. Given the perinuclear localization of tagged-Mtm in hemocytes, along with earlier work demonstrating an increase in nuclear PI(5)P levels with myotubularin overexpression in mammalian cells, it is possible that *mtm* roles are mediated through the active synthesis of PI(5)P upon dephosphorylation of PI(3,5)P_2 (Schaletzky et al., 2003). In order to investigate such mechanisms, methods for specific detection and quantification of PI(3,5)P_2 first need to be established and validated. For example, if a reporter specific for PI(3,5)P_2 could be created, by using this reporter, the responsiveness of PI(3,5)P_2 levels to Mtm activity and the effects of increased PI(5)P levels in regulating cell morphology could then be investigated. A direct relationship between *mtm* function and PI(3)P still remains the simplest and most likely model given the inverse relationship between *mtm* activity and cellular PI(3)P levels in *Drosophila*

hemocytes and cell lines. However, as mentioned earlier, further work must be done to confirm PI(3)P as a direct *in vivo* substrate for *mtm* in *Drosophila*.

Our data suggests that *mtm* regulates specific subpools of PI(3)P. Depletion of just the class II PI 3-kinase (*Pi3K68D*) in Mtm-deficient hemocytes is sufficient to completely rescue the mutant cellular remodeling phenotypes caused by *mtm* RNAi hairpin expression. In cells depleted of both *mtm* and *Pi3K68D*, lysosome size appears wild-type, indicating a restoration of lysosomal membrane homeostasis in these cells. These findings establish a genetic link between *mtm* and *Pi3K68D*. The findings also suggest that balancing specific PI(3)P pools in hemocytes by counteracting loss of PI(3)P phosphatase activity with a corresponding inhibition of PI(3)P synthesis is sufficient for the execution of normal cellular functions. Thus, *mtm* control over cellular operations is likely performed through its ability to balance the levels and distributions of Pi3K68D-synthesized PI(3)P pools. Given the importance of *mtm*-dependent PI(3)P homeostasis in cellular morphogenesis, we propose that the spatiotemporal coordination of the diverse cellular processes involved in cell shape change occurs through the distinct responses of different cellular components to the same phosphoinositide signaling events. For example, the converging and diverging trafficking routes at the late endosomes may be coordinated through strictly controlled PI(3)P signaling localized to these sites. Similarly, PI(3)P signaling at specific sites may serve dual functions in simultaneously activating and/or regulating actin nucleation as well as vesicular trafficking.

The importance of PI(3)P-mediated integration and regulation of cellular processes is demonstrated in our results as inihibition of *Pi3K68D*-mediated PI(3)P synthesis also rescues the fly lethality caused by loss of *mtm* function. This suggests that the *mtm*-dependent hemocyte functions important for fly viability are controlled by the strict regulation of PI(3)P levels. Due to the abnormal hemocyte distribution seen in flies with *mtm* depleted blood cells and the role of *mtm* and PI(3)P in cellular morphology, these PI(3)P-dependent hemocyte functions may include the morphology-based processes of migration and/or adhesion to crucial sites in the developing fly. Due to the lethal phase at eclosion caused by *mtm* depletion and the muscle-related phenotypes in *mtm* depleted flies, *mtm* loss of function could be affecting fly muscle development. One possible effect of *mtm* function in hemocytes could be the mediation of their migration to and subsequent phagocytosis of doomed larval tissues during tissue remodeling. However, with *mtm* RNAi in hemocytes, the abdominal muscles of pharate adults are intact and morphologically normal, indicative of normal abdominal tissue remodeling (I. Ribeiro, A. Kiger, unpublished work). Nonetheless, these results do not completely rule out the possibility that hemocytes are still involved in tissue remodeling as other, yet to be examined muscles and tissues dependent on hemocytes for remodeling may still be affected in *mtm* mutant conditions. Alternatively, due to the presence of extracellular matrix (ECM) proteins at sites where hemocytes normally localize (including the leg muscles), one current hypothesis is that hemocyte localization

to specific positions may allow for the secretion of critical ECM components involved in the stabilization and strengthening of fly components (including the limbs and leg muscles) and/or fly development (Luo and Dearolf, 2001). Lack of ECM components at their required sites (such as Tiggrin at the muscles) may be caused by the mislocalization of hemocytes due to their inability to migrate to these sites. This mislocalization and lack of ECM could also be caused by the inability of hemocytes to deposit ECM components due to disrupted secretory activity. If hemocytes use ECM components as a substrate to migrate upon, loss of secretory activity could help explain the *in vivo* mislocalization of these cells. This loss of localized ECM deposition could also explain the unsuccessful eclosion and weakened limbs of adults with mislocalized hemocytes following hemocyte-specific *mtm* RNAi hairpin expression. Such a hypothesis could be tested by comparing the distributions of specific ECM components in flies with wild-type hemocytes to their distributions in flies with Mtm-deficient hemocytes. We could also test the ability of wild-type and *mtm* depleted hemocytes to secrete ECM components.

Regulation of membrane trafficking and homeostasis by Mtm through PI(3)P and its contributions to cell morphology

Our data suggests the involvement of *mtm* in membrane trafficking and homeostasis of the endolysosomal pathway. In Kc cells, I identified that tagged-Mtm partially localized with the endolysosomes, suggestive of a cellular role for

mtm phosphatase activity at these organelles. Over the course of Kc cellular elongation, Mtm appeared to undergo a shift in localization. Mtm partially colocalized with Lysotracker staining in non-elongating and elongating cells, but displayed little to no colocalization in elongated cells. This same lack of colocalization is observed in spread primary hemocytes. Despite this lack of colocalization, live time lapse imaging revealed a transient association of tagged-Mtm with acidified Lysotracker compartments in spread hemocytes. Taken together, these results suggest that Mtm association with the lysosomal compartments may be modified under certain cellular conditions. The diverse localization of Mtm with the lysosomes may be important for the differential regulation of lysosome membrane homeostasis at various stages of the cellular morphogenetic program to support cellular remodeling. This hypothesis linking Mtm activity to lysosomal membrane trafficking is strengthened by the observation that *mtm* loss of function – either in *mtm* genomic mutants or through *mtm* RNAi hairpin expression – leads to noticeable alterations in lysosome size. The lysosomes are significantly enlarged in mutant conditions, and this may be indicative of defective *mtm*-dependent functions at these compartments. While the enlarged lysosome phenotype may be a later consequence of defects further upstream of the endolysosomal pathway (for example, at the late endosomes) it is equally possible that efflux from the lysosomes to the plasma membrane or other cellular compartments causes the enlarged lysosome phenotype. Previous work in fibroblasts has established lysosomal exocytosis as the major source of

membranes during plasma membrane repair as well as cell migration and is therefore a candidate effect of normal *mtm* function during cellular morphogenesis (Huynh et al., 2004; Proux-Gillardeaux et al., 2007). In this situation, impaired exocytosis could hinder cell morphogenesis due to an inadequate supply of membrane at the cell surface to support specific cell morphologies. To test whether defective lysosomal exocytosis is at least partly responsible for the *mtm* cell morphology phenotype, we can assay the level of lysosomal exocytosis in wild-type and *mtm* deficient Kc cells undergoing induced cellular morphogenesis by measuring the presence of the lysosomal marker LAMP:GFP (or Synaptotagmin VII:GFP) at the surface of these cells at various times following ecdysone treatment.

Along with association with the lysosomes, despite the non-colocalization of Mtm with Rab5 and Rab7, our studies also indicate that Mtm partially localizes to regions directly adjacent to early endosomal compartments. Mtm puncta display a non-overlapping but close association alongside markers for the early endosomes (Rab5:GFP) in elongated, elongating, and non-elongating cells. This provides the possibility that *mtm* plays a constitutive role at these compartments to then influence cellular remodeling. But how could *mtm* subcellular localization at the endolysosomal compartments mediate functional effects on morphology evident at the cell cortex? One possible explanation is that the endolysosomal pathway is an important route in attenuating receptor signaling involved in cell growth and motility (Rusten et al., 2006). Components of this pathway are

sensitive to deviations from normal PI(3)P levels. In mammalian cells, inhibition of PI(3)P synthesis at the endosomes prevented internal vesicle formation within multivesicular bodies, while depletion of either MTM1 or MTMR2 blocked the egress of epidermal growth factor receptors (Cao et al., 2008; Futter et al., 2001). Therefore, in *Drosophila*, *mtm* regulation of PI(3)P-dependent endolysosomal degradation and/or recycling of receptors could possibly contribute to the regulation of the cellular morphogenetic program. However, *mtm* mutants do not display phenotypes associated with any canonical receptor pathways and *mtm* is likely important in regulating other functions of the endolysosomal pathway involved in cellular morphogenesis. Endolysosomal trafficking may be important in controlling the localization and turnover of specific proteins (i.e., adhesion proteins) at the plasma membrane. There is also the possibility that *mtm* may play a role in specific retrograde or recycling routes that emanate from endocytic compartments. Monitoring the morphologies and dynamics of early and late endosomes in hemocytes after *mtm* depletion or overexpression along with the kinetics of integral plasma membrane protein sorting, trafficking, recycling, and degradation will give us a better idea of how endolysosomal trafficking contributes to cellular morphogenesis.

Mtm-mediated regulation of cytoskeletal remodeling and its effects on cell morphology

As indicated previously, the role of *mtm* in endolysosomal membrane homeostasis and trafficking has been well studied. In contrast, while work in Kc cells has implicated *mtm* as important for F-actin remodeling during cellular elongation, the relationship of *mtm* to cytoskeleton organization is much less well-characterized. In agreement with Kc cell studies, our results provide evidence of a regulatory role for *mtm* in actin cytoskeleton organization and remodeling in *Drosophila* hemocytes. Gene disruption or RNAi-mediated depletion of *mtm* in hemocytes resulted in membrane ruffling, a phenotype not normally seen in wild-type cells. The majority of *mtm* deficient hemocytes also had a round morphology and displayed an inability to form stable cytoskeletal-rich protrusions. In addition to the round morphological phenotype, a small subset of *mtm* mutant conditions displayed long, thin, and highly branched filopodia-like extensions. This phenotype likely represents a weaker *mtm* mutant phenotype, as this is only observed in conditions where only partial *mtm* depletion was expected (e.g., when fewer copies of the *mtm* RNAi hairpin was expressed). In contrast to the morphological phenotypes caused by *mtm* loss of function, nearly all hemocytes undergoing *mtm* overexpression possessed a seemingly opposite gain-of-function phenotype. *Mtm* overexpressing hemocytes possessed an estimated three to four-fold increase in the number of actin-rich protrusions extending radially from their cell bodies when compared to wild-type cells. Thus,

the combination of the loss of function and gain of function phenotypes point toward an active role for *mtm* phosphatase activity in actin cytoskeleton remodeling in hemocytes.

At least two possible explanations exist regarding a role for *mtm* influence in cytoskeletal remodeling. As mentioned previously, one explanation could be that *mtm* regulated PI(3)P-mediated endolysosomal trafficking effects protein composition and/or activity (e.g., activated receptor signaling) at certain membrane domains to influence effectors of F-actin remodeling. In this case, the role of *mtm*-regulated PI(3)P signaling in cytoskeletal remodeling is likely an indirect one. Because phosphoinositides (especially PIP_2) are also able to directly signal to cytoskeleton remodeling proteins, another possibility exists that the PI(3)P pools regulated by *mtm*/*Pi3K68D* signal directly to effectors of F-actin to spatially and temporally regulate their activities. *Mtm*'s restriction of PI(3)P to specific cellular domains would provide the spatial component to the regulation of these actin effectors. The abolishment of binding sites through the metabolism of cellular PI(3)P pools at specific stages of the cellular morphogenetic program would provide the temporal restriction of actin effector activity. In addition to the effects of *mtm* activity on the spatiotemporal localization of actin effectors, the *mtm* regulated recruitment of these effectors to specific PI(3)P pools could also serve to modulate effector protein activities (Yin, 2003). We would therefore expect to see proteins directly regulated PI(3)P to exhibit altered localizations and activity levels with changes in *mtm*/*Pi3K68D*-dependent PI(3)P subpool

concentrations. According to this model, if increases in cellular PI(3)P levels results in the misregulated activation of these actin effector proteins, we would also expect overexpression of these effectors to phenocopy and/or modify the effects of *mtm* depletion. These predicted results were exactly what we observed with the actin nucleator, *Spir*. The localization of the FYVE domain-containing Spir^{RC} isoform was sensitive to changes in *mtm*/*Pi3K68D*-dependent PI(3)P regulation, as RNAi-mediated knockdown of *mtm* resulted in alterations to its normally punctate distribution pattern. In addition, *Spir* also contributed to the *mtm* cell morphology phenotype, as overexpression of the Spir^{RC} protein phenocopied the *mtm* cell spreading phenotype in wild-type backgrounds, and exacerbated the *mtm* RNAi phenotype in mutant conditions. These findings provide the possibility that the overaccumulation of specific PI(3)P pools following *mtm* depletion result in the improper activation and/or localization of Spir^{RC} protein. Misregulated Spir activity could directly impact different aspects of cellular remodeling. Due to the unique characteristics of different interacting isoforms of *Spir* (i.e., as an actin nucleator and PI(3)P-binding protein), *Spir* is in an ideal position to link actin cytoskeleton reorganization and intracellular transport. In support of this hypothesis, work in a murine fibroblast line showed that the modified FYVE domain of Spir mediates its colocalization with the Rab11 GTPase (which is involved in recycling endosome/trans-golgi network to plasma membrane transport) (Kerkhoff et al., 2001). It was speculated that recruitment of Spir to specific domains by Rab11 stimulated Spir actin polymerization-driven

transport of vesicles to the plasma membrane. In such a model, Spir mediates the simultaneous reorganization of the actin cytoskeleton and the necessary transport of additional membranes to the plasma membrane in order to support specific changes in cell shape. With the presence of Rab11 at the recycling endosomes, this model connecting *mtm*, Rab11, and Spir activity would also provide an explanation to the enlarged endolysosomal compartments and impaired membrane trafficking caused by *mtm* loss of function. Hence, spatiotemporal regulation of Spir activity by *mtm* through its turnover of specific PI(3)P pools could serve as one method for integrating cytoskeletal remodeling events with plasma membrane remodeling, trafficking, and homeostasis during cellular morphogenesis. To test this, we must first determine whether *Spir* is normally expressed and required in hemocytes. Then we must examine the effects of *Spir* function on cytoskeletal and membrane dynamics, specifically the relationship between *Spir*-dependent actin nucleation and the trafficking of Rab11 compartments.

Another set of actin regulators possibly responsive to *mtm*-mediated changes in phosphoinositide levels are the Rho family of small GTPases. This family of proteins regulates actin organization either directly or through the activation of downstream targets (Johndrow et al., 2004). For example, Rac is a key regulator of membrane ruffling, a structural change observed during the cell's early responses to extracellular signaling and believed to be required for directed cell migration (Ridley, 1994). Hemocytes overexpressing either Rac1 alone or a

combination of dominant negative Rok (Rok^{catkg}) with constitutive active Rho1 ($Rho1^{V14}$) exhibit actin cytoskeleton phenotypes resembling those seen in *mtm* mutant hemocytes, with the majority of these cells possessing ruffled membranes (Williams et al., 2007). With the persistence of membrane ruffling following *mtm* depletion, one possibility is that *mtm* loss of function results in constitutive Rac activity. Interestingly, substrate trap forms of human MTM1 were recruited to plasma membrane ruffles induced by a dominant active form of Rac1 ($Rac1^{V12}$), suggesting an inverse functional relationship between Mtm activity and Rac1 in regulating membrane ruffling (Laporte et al., 2002). It is possible that subsequent to the induction of membrane ruffle formation, Mtm is recruited to these sites of actin remodeling to inhibit Rac1-mediated actin cytoskeleton reorganization. Previous work has demonstrated that clathrin/Rab5-mediated endocytic trafficking and recycling are necessary to activate and localize Rac during cell migration (Palamidessi et al., 2008). Mtm localization to sites of membrane ruffling may serve to control Rac activity through its influence on endocytosis via PI(3)P dephosphorylation. Thus, the activation and spatial restriction of Rac through endocytosis and recycling may serve as an additional node through which *mtm* is able to integrate actin cytoskeletal rearrangements with membrane remodeling. Similar to the interactions between *mtm* and Rac1 activity, the long, highly branched filopodial extensions observed during partial *mtm* knockdown may be due to prolonged PI(3)P effects on signaling to other Rho GTPases that control F-actin cytoskeleton organization. In this situation, insufficient *mtm* may

be available to terminate Rho GTPase-mediated F-actin nucleation/remodeling events in a timely manner, resulting in abnormally prolonged actin polymerization and the formation of aberrant F-actin structures. Given the diversity of effects mediated by the Rho GTPases (including adhesion, endocytosis, and actin cytoskeleton remodeling), these GTPase molecular switches may be one of the mechanisms through which Mtm phosphatase activity integrates multiple processes to influence cellular morphogenesis. To confirm this hypothesis, the biochemical and genetic relationships between the Rho family of GTPases and *mtm* in *Drosophila* can be explored by measuring Rho1/Rac1 activation (e.g., through the quantification of GTP vs. GDP-bound forms) in *mtm* mutant conditions, as well as the ability of constitutive active and/or dominant negative Rho1/Rac1 to modify the *mtm* mutant hemocyte morphology phenotypes.

Along with the previously mentioned Spir and Rho GTPase proteins, a search for proteins with predicted PI(3)P binding domains with known roles in F-actin organization may aid in the identification of additional *mtm*-regulated effectors of F-actin. Specific pools of PI(3)P may provide the interface mediating the localization and or activity of these proteins, making these predicted PI(3)P-binding proteins sensitive to *mtm* phosphatase activity. Identification of additional potential PI(3)P binding proteins will allow us to further explore the exact mechanisms through which *mtm* phosphatase activity impacts and influences cytoskeletal remodeling, and ultimately cellular morphogenesis.

Regulation of *mtm* activity

Evidence suggests that *mtm* acts at specific sub-cellular sites rather than ubiquitously throughout the cell. The simplest interpretation of the rescue of *mtm* mutant phenotypes with *Pi3K68D* depletion is that *mtm* dephosphorylates PI(3)P pools specifically synthesized by this class II PI 3-kinase. Additionally, overexpression of *mtm* in hemocytes did not completely eliminate cellular PI(3)P, suggesting that certain PI(3)P pools could be inaccessible to *mtm* activity. Despite this evidence, revealing the specific nature of *mtm* function, the mechanisms through which Mtm distinguishes between different PIP and PI(3)P pools remains unclear. One hypothesis is that the specificity of Mtm activity is regulated by its restricted localization to certain membrane domains. Indeed, our work provides evidence for Mtm recruitment to specific sub-cellular membranes, as suggested by both Mtm association into particles with vesicle-like behavior, as well as association with endolysosomal compartments. However, while the PH-GRAM domain of Mtm likely mediates associations with PI(3)P and PI(3,5)P_2-containing membrane domains, due to the conservation of this membrane-binding component within all active myotubularins and the differential targeting of human Mtm-related proteins to distinct pools of PI(3)P, the PH-GRAM domain alone fails to explain the specific targeting of Mtm (Begley and Dixon, 2005). Hence, recruitment of Mtm to cellular membranes may require the cooperative binding of Mtm to both its substrate as well as appropriate resident membrane proteins. The specific targeting of clathrin adaptor AP-1 to the Golgi makes use of

this dual-binding requirement and it is reasonable to expect this same recognition system to operate during *mtm* targeting (Wang et al., 2003). Mtm may initially recognize PI(3)P through weak interactions in its phosphoinositide-binding domain and then subsequently interact with resident proteins located at target sites to stabilize its localization. In addition to mediating its localization, cooperative binding of Mtm to both its phosphoinositide substrates and resident membrane proteins may also regulate its catalytic activity. Such a regulatory mechanism would then provide an additional mechanism to limit the PI(3)P pools *mtm* is able to interact with and regulate. Co-immunoprecipitation of Mtm-interacting proteins might aid in the identification of biochemical relationships between Mtm and the cellular components important for its localization and/or activity. Examination of Mtm distribution patterns in cells deficient for identified Mtm-interacting proteins would then confirm the requirement of these factors for Mtm targeting. Cells mutant or deficient for proteins necessary for Mtm localization would be expected to exhibit altered Mtm distribution patterns and possibly decreased puncta formation due to the inability to associate with the proper membrane domains. Given the results suggesting the specificity of *mtm* activity to defined subpools of PI(3)P, a spatial requirement is predicted for *mtm* function. Therefore, we might also expect mutant cells with mislocalized Mtm protein to phenocopy the *mtm* mutant phenotypes.

One likely regulator of Mtm activity is the catalytically inactive myotubularin-related protein, Sbf. Overexpression of tagged Sbf proteins in Kc

cells downregulated PI(3)P levels, as detected by the 2xFYVE reporter, suggesting that the influence of Sbf on cellular processes could occur through PI(3)P. Similar to hemocyte-specific *mtm* depletion, *Sbf* depletion in hemocytes resulted in pharate adult lethality, round hemocyte morphology, and disrupted blood cell distribution. These findings, in conjunction with previous work demonstrating the stimulation of human MTMR2 phosphatase activity with the *Sbf* homolog MTMR13, implicate Sbf as a regulator of Mtm phosphatase activity (Berger et al., 2006). In co-localization experiments performed in Kc cells, Sbf not only colocalized with the same phosphoinositide species and cellular domains as Mtm, but also exhibited extensive colocalization with Mtm itself. This is suggestive of a physical interaction between Mtm and Sbf, and is consistent with earlier work showing that MTMR13 regulation of MTMR2 required the hetero-oligomerization of these two proteins (Robinson and Dixon, 2005). The suspected interaction between Mtm and Sbf can be further verirfied by confirming the biochemical relationship between the two proteins through co-immunoprecipitation experiments. If hetero-oligomerization of these two proteins does occur, a possible consequence of such an interaction (along with the regulation of Mtm's catalytic activity) may be the recruitment of Mtm by Sbf to specific cellular compartments. In fact, work in our lab has demonstrated that *Sbf* loss of function resulted in the partial mislocalization of Mtm from a punctate distribution to a diffusely cytoplasmic one and loss of *mtm* resulted in mislocalization of Sbf from the plasma membrane (S. Jean, A. Kiger, unpublished

work). Therefore, Sbf may target to specific PI(3)P pools and then either recruit Mtm to these domains, or through its ability to stimulate Mtm phosphatase activity, ensure that Mtm is only active at these specific sites. *Sbf* depletion would therefore be expected to disrupt proper cellular *mtm* functions through the mislocalization and/or misregulation of its activity. This model would then explain the similarities between the *Sbf* and *mtm* mutant hemocyte morphology phenotypes.

Concluding remarks

Our work provides evidence that through its regulation of specific PI(3)P pools, *mtm* affects cellular morphogenesis through its integration of cytoskeletal remodeling, endolysosomal membrane/protein trafficking, and membrane remodeling and homeostasis (Fig. 38). Greater clarity to this network utilized by *mtm* to effect cellular morphogenesis can be attained through the exact identification of the mechanisms controlling *mtm* activity as well as the elucidation of all the morphogenesis-related downstream processes influenced by *mtm* phosphatase activity. Identifying both the upstream pathways integrated by *mtm*-related phosphoinositide signaling as well as the downstream networks affected by it may then give us a better understanding of the molecular and cellular bases of *mtm*-related diseases.

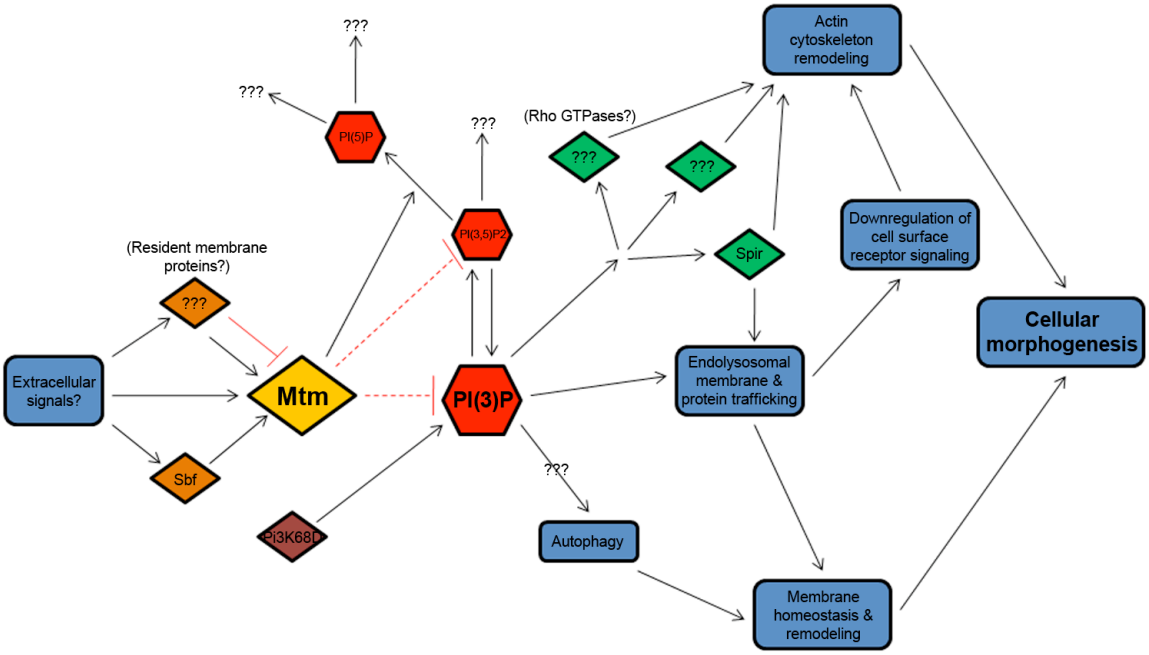

Figure 38: Possible mechanism of *mtm* function in cellular morphogenesis

Mtm may regulate PI(3)P concentrations and distributions to regulate downstream signaling pathways involved in membrane homeostasis and remodeling, endolysosomal membrane and protein trafficking, and actin cytoskeleton remodeling to influence cellular morphogenesis.

REFERENCES

Aderem, A., and Underhill, D.M. (1999). Mechanisms of phagocytosis in macrophages. Annu Rev Immunol *17*, 593-623.

Begley, M.J., and Dixon, J.E. (2005). The structure and regulation of myotubularin phosphatases. Curr Opin Struct Biol *15*, 614-620.

Behnia, R., and Munro, S. (2005). Organelle identity and the signposts for membrane traffic. Nature *438*, 597-604.

Berger, P., Berger, I., Schaffitzel, C., Tersar, K., Volkmer, B., and Suter, U. (2006). Multi-level regulation of myotubularin-related protein-2 phosphatase activity by myotubularin-related protein-13/set-binding factor-2. Hum Mol Genet *15*, 569-579.

Blommaart, E.F., Krause, U., Schellens, J.P., Vreeling-Sindelarova, H., and Meijer, A.J. (1997). The phosphatidylinositol 3-kinase inhibitors wortmannin and LY294002 inhibit autophagy in isolated rat hepatocytes. Eur J Biochem *243*, 240-246.

Bolino, A., Bolis, A., Previtali, S.C., Dina, G., Bussini, S., Dati, G., Amadio, S., Del Carro, U., Mruk, D.D., Feltri, M.L.*, et al.* (2004). Disruption of Mtmr2 produces CMT4B1-like neuropathy with myelin outfolding and impaired spermatogenesis. J Cell Biol *167*, 711-721.

Bolino, A., Muglia, M., Conforti, F.L., LeGuern, E., Salih, M.A., Georgiou, D.M., Christodoulou, K., Hausmanowa-Petrusewicz, I., Mandich, P., Schenone, A.*, et al.* (2000). Charcot-Marie-Tooth type 4B is caused by mutations in the gene encoding myotubularin-related protein-2. Nat Genet *25*, 17-19.

Buj-Bello, A., Laugel, V., Messaddeq, N., Zahreddine, H., Laporte, J., Pellissier, J.F., and Mandel, J.L. (2002). The lipid phosphatase myotubularin is essential for skeletal muscle maintenance but not for myogenesis in mice. Proc Natl Acad Sci U S A *99*, 15060-15065.

Cao, C., Backer, J.M., Laporte, J., Bedrick, E.J., and Wandinger-Ness, A. (2008). Sequential Actions of Myotubularin Lipid Phosphatases Regulate Endosomal PI(3)P and Growth Factor Receptor Trafficking. Mol Biol Cell *19*, 3334-3346.

Clague, M.J., and Lorenzo, O. (2005). The myotubularin family of lipid phosphatases. Traffic *6*, 1063-1069.

Clague, M.J., Thorpe, C., and Jones, A.T. (1995). Phosphatidylinositol 3-kinase regulation of fluid phase endocytosis. FEBS Lett *367*, 272-274.

Crozatier, M., Ubeda, J.M., Vincent, A., and Meister, M. (2004). Cellular immune response to parasitization in Drosophila requires the EBF orthologue collier. PLoS Biol *2*, E196.

Di Paolo, G., and De Camilli, P. (2006). Phosphoinositides in cell regulation and membrane dynamics. Nature *443*, 651-657.

Futter, C.E., Collinson, L.M., Backer, J.M., and Hopkins, C.R. (2001). Human VPS34 is required for internal vesicle formation within multivesicular endosomes. J Cell Biol *155*, 1251-1264.

Gary, J.D., Wurmser, A.E., Bonangelino, C.J., Weisman, L.S., and Emr, S.D. (1998). Fab1p is essential for PtdIns(3)P 5-kinase activity and the maintenance of vacuolar size and membrane homeostasis. J Cell Biol *143*, 65-79.

Gaullier, J.M., Simonsen, A., D'Arrigo, A., Bremnes, B., Stenmark, H., and Aasland, R. (1998). FYVE fingers bind PtdIns(3)P. Nature *394*, 432-433.

Gillooly, D.J., Morrow, I.C., Lindsay, M., Gould, R., Bryant, N.J., Gaullier, J.M., Parton, R.G., and Stenmark, H. (2000). Localization of phosphatidylinositol 3-phosphate in yeast and mammalian cells. Embo J *19*, 4577-4588.

Hartenstein, V. (2006). Blood cells and blood cell development in the animal kingdom. Annu Rev Cell Dev Biol *22*, 677-712.

Huynh, C., Roth, D., Ward, D.M., Kaplan, J., and Andrews, N.W. (2004). Defective lysosomal exocytosis and plasma membrane repair in Chediak-Higashi/beige cells. Proc Natl Acad Sci U S A *101*, 16795-16800.

Ito, N., Yokomizo, T., Sasaki, T., Kurosu, H., Penninger, J., Kanaho, Y., Katada, T., Hanaoka, K., and Shimizu, T. (2002). Requirement of phosphatidylinositol 3-kinase activation and calcium influx for leukotriene B4-induced enzyme release. J Biol Chem *277*, 44898-44904.

Johndrow, J.E., Magie, C.R., and Parkhurst, S.M. (2004). Rho GTPase function in flies: insights from a developmental and organismal perspective. Biochem Cell Biol *82*, 643-657.

Kerkhoff, E., Simpson, J.C., Leberfinger, C.B., Otto, I.M., Doerks, T., Bork, P., Rapp, U.R., Raabe, T., and Pepperkok, R. (2001). The Spir actin organizers are involved in vesicle transport processes. Curr Biol *11*, 1963-1968.

Kim, S.A., Vacratsis, P.O., Firestein, R., Cleary, M.L., and Dixon, J.E. (2003). Regulation of myotubularin-related (MTMR)2 phosphatidylinositol phosphatase

by MTMR5, a catalytically inactive phosphatase. Proc Natl Acad Sci U S A *100*, 4492-4497.

Lanot, R., Zachary, D., Holder, F., and Meister, M. (2001). Postembryonic hematopoiesis in Drosophila. Dev Biol *230*, 243-257.

Laporte, J., Blondeau, F., Gansmuller, A., Lutz, Y., Vonesch, J.L., and Mandel, J.L. (2002). The PtdIns3P phosphatase myotubularin is a cytoplasmic protein that also localizes to Rac1-inducible plasma membrane ruffles. J Cell Sci *115*, 3105-3117.

Laporte, J., Hu, L.J., Kretz, C., Mandel, J.L., Kioschis, P., Coy, J.F., Klauck, S.M., Poustka, A., and Dahl, N. (1996). A gene mutated in X-linked myotubular myopathy defines a new putative tyrosine phosphatase family conserved in yeast. Nat Genet *13*, 175-182.

Lemmon, M.A. (2003). Phosphoinositide recognition domains. Traffic *4*, 201-213.

Lindmo, K., and Stenmark, H. (2006). Regulation of membrane traffic by phosphoinositide 3-kinases. J Cell Sci *119*, 605-614.

Lorenzo, O., Urbe, S., and Clague, M.J. (2006). Systematic analysis of myotubularins: heteromeric interactions, subcellular localisation and endosomerelated functions. J Cell Sci *119*, 2953-2959.

Luo, H., and Dearolf, C.R. (2001). The JAK/STAT pathway and Drosophila development. Bioessays *23*, 1138-1147.

Meister, M., and Lagueux, M. (2003). Drosophila blood cells. Cell Microbiol *5*, 573-580.

Nicot, A.S., and Laporte, J. (2008). Endosomal phosphoinositides and human diseases. Traffic *9*, 1240-1249.

Odorizzi, G., Babst, M., and Emr, S.D. (1998). Fab1p PtdIns(3)P 5-kinase function essential for protein sorting in the multivesicular body. Cell *95*, 847-858.

Oikawa, T., Yamaguchi, H., Itoh, T., Kato, M., Ijuin, T., Yamazaki, D., Suetsugu, S., and Takenawa, T. (2004). PtdIns(3,4,5)P3 binding is necessary for WAVE2-induced formation of lamellipodia. Nat Cell Biol *6*, 420-426.

Otto, I.M., Raabe, T., Rennefahrt, U.E., Bork, P., Rapp, U.R., and Kerkhoff, E. (2000). The p150-Spir protein provides a link between c-Jun N-terminal kinase function and actin reorganization. Curr Biol *10*, 345-348.

Palamidessi, A., Frittoli, E., Garre, M., Faretta, M., Mione, M., Testa, I., Diaspro, A., Lanzetti, L., Scita, G., and Di Fiore, P.P. (2008). Endocytic trafficking of Rac is required for the spatial restriction of signaling in cell migration. Cell *134*, 135-147.

Proux-Gillardeaux, V., Raposo, G., Irinopoulou, T., and Galli, T. (2007). Expression of the Longin domain of TI-VAMP impairs lysosomal secretion and epithelial cell migration. Biol Cell *99*, 261-271.

Quinlan, M.E., Heuser, J.E., Kerkhoff, E., and Mullins, R.D. (2005). Drosophila Spire is an actin nucleation factor. Nature *433*, 382-388.

Ramet, M., Manfruelli, P., Pearson, A., Mathey-Prevot, B., and Ezekowitz, R.A. (2002). Functional genomic analysis of phagocytosis and identification of a Drosophila receptor for E. coli. Nature *416*, 644-648.

Ridley, A.J. (1994). Signal transduction through the GTP-binding proteins Rac and Rho. J Cell Sci Suppl *18*, 127-131.

Robinson, F.L., and Dixon, J.E. (2005). The phosphoinositide-3-phosphatase MTMR2 associates with MTMR13, a membrane-associated pseudophosphatase also mutated in type 4B Charcot-Marie-Tooth disease. J Biol Chem *280*, 31699-31707.

Robinson, F.L., Niesman, I.R., Beiswenger, K.K., and Dixon, J.E. (2008). Loss of the inactive myotubularin-related phosphatase Mtmr13 leads to a Charcot-Marie-Tooth 4B2-like peripheral neuropathy in mice. Proc Natl Acad Sci U S A *105*, 4916-4921.

Rosales-Nieves, A.E., Johndrow, J.E., Keller, L.C., Magie, C.R., Pinto-Santini, D.M., and Parkhurst, S.M. (2006). Coordination of microtubule and microfilament dynamics by Drosophila Rho1, Spire and Cappuccino. Nat Cell Biol *8*, 367-376.

Rusten, T.E., Rodahl, L.M., Pattni, K., Englund, C., Samakovlis, C., Dove, S., Brech, A., and Stenmark, H. (2006). Fab1 phosphatidylinositol 3-phosphate 5-kinase controls trafficking but not silencing of endocytosed receptors. Mol Biol Cell *17*, 3989-4001.

Rutherford, A.C., Traer, C., Wassmer, T., Pattni, K., Bujny, M.V., Carlton, J.G., Stenmark, H., and Cullen, P.J. (2006). The mammalian phosphatidylinositol 3-phosphate 5-kinase (PIKfyve) regulates endosome-to-TGN retrograde transport. J Cell Sci *119*, 3944-3957.

Schaletzky, J., Dove, S.K., Short, B., Lorenzo, O., Clague, M.J., and Barr, F.A. (2003). Phosphatidylinositol-5-phosphate activation and conserved substrate

specificity of the myotubularin phosphatidylinositol 3-phosphatases. Curr Biol *13*, 504-509.

Schulz, C., Kiger, A.A., Tazuke, S.I., Yamashita, Y.M., Pantalena-Filho, L.C., Jones, D.L., Wood, C.G., and Fuller, M.T. (2004). A misexpression screen reveals effects of bag-of-marbles and TGF beta class signaling on the Drosophila male germ-line stem cell lineage. Genetics *167*, 707-723.

Stephens, L., Ellson, C., and Hawkins, P. (2002). Roles of PI3Ks in leukocyte chemotaxis and phagocytosis. Curr Opin Cell Biol *14*, 203-213.

Stewart, S.A., Dykxhoorn, D.M., Palliser, D., Mizuno, H., Yu, E.Y., An, D.S., Sabatini, D.M., Chen, I.S., Hahn, W.C., Sharp, P.A.*, et al.* (2003). Lentivirus-delivered stable gene silencing by RNAi in primary cells. RNA *9*, 493-501.

Suter, U. (2007). Phosphoinositides and Charcot-Marie-tooth disease: new keys to old questions. Cell Mol Life Sci *64*, 3261-3265.

Tanaka, Y., and Hirokawa, N. (2002). Mouse models of Charcot-Marie-Tooth disease. Trends Genet *18*, S39-44.

Taylor, G.S., Maehama, T., and Dixon, J.E. (2000). Inaugural article: myotubularin, a protein tyrosine phosphatase mutated in myotubular myopathy, dephosphorylates the lipid second messenger, phosphatidylinositol 3-phosphate. Proc Natl Acad Sci U S A *97*, 8910-8915.

Tronchere, H., Laporte, J., Pendaries, C., Chaussade, C., Liaubet, L., Pirola, L., Mandel, J.L., and Payrastre, B. (2004). Production of phosphatidylinositol 5-phosphate by the phosphoinositide 3-phosphatase myotubularin in mammalian cells. J Biol Chem *279*, 7304-7312.

Tsujita, K., Itoh, T., Ijuin, T., Yamamoto, A., Shisheva, A., Laporte, J., and Takenawa, T. (2004). Myotubularin regulates the function of the late endosome through the gram domain-phosphatidylinositol 3,5-bisphosphate interaction. J Biol Chem *279*, 13817-13824.

Walker, D.M., Urbe, S., Dove, S.K., Tenza, D., Raposo, G., and Clague, M.J. (2001). Characterization of MTMR3. an inositol lipid 3-phosphatase with novel substrate specificity. Curr Biol *11*, 1600-1605.

Wang, Y.J., Wang, J., Sun, H.Q., Martinez, M., Sun, Y.X., Macia, E., Kirchhausen, T., Albanesi, J.P., Roth, M.G., and Yin, H.L. (2003). Phosphatidylinositol 4 phosphate regulates targeting of clathrin adaptor AP-1 complexes to the Golgi. Cell *114*, 299-310.

Williams, M.J., Habayeb, M.S., and Hultmark, D. (2007). Reciprocal regulation of Rac1 and Rho1 in Drosophila circulating immune surveillance cells. J Cell Sci *120*, 502-511.

Yamamoto, A., DeWald, D.B., Boronenkov, I.V., Anderson, R.A., Emr, S.D., and Koshland, D. (1995). Novel PI(4)P 5-kinase homologue, Fab1p, essential for normal vacuole function and morphology in yeast. Mol Biol Cell *6*, 525-539.